STRUCTURAL, HYDROGEOLOGIC FRAMEWORK, AND TEXTURAL MODEL OF THE RIALTO-COLTON BASIN AND THE CHINO AND NORTH RIVERSIDE AREA

A Thesis

Presented to the faculty of the Department of Geology

California State University, Sacramento

Submitted in partial satisfaction of
the requirements for the degree of

MASTER OF SCIENCE

in

Geology

by

Scott Paulinski

FALL
2012

STRUCTURAL, HYDROGEOLOGIC FRAMEWORK, AND TEXTURAL MODEL OF THE RIALTO-COLTON BASIN AND THE CHINO AND NORTH RIVERSIDE AREA

A Thesis

by

Scott Paulinski

Approved by:

_____, Committee Chair
Dr. Tim Horner

_____, Second Reader
Dr. David Evans

_____, Third Reader
Dr. Linda Woolfenden

_____, Fourth Reader
Dr. Claudia Faunt

_____
Date

Student: Scott Paulinski

I certify that this student has met the requirements for format contained in the University format manual, and that this thesis is suitable for shelving in the Library and credit is to be awarded for the thesis.

_____, Graduate Coordinator_____
Dr. Timothy C. Horner Date

Department of Geology

Abstract

of

STRUCTURAL, HYDROGEOLOGIC FRAMEWORK, AND TEXTURAL MODEL OF THE RIALTO-COLTON BASIN AND THE CHINO AND NORTH RIVERSIDE AREA

by

Scott Paulinski

This study involved constructing a structural, hydrogeologic framework, and textural model of water-bearing units in the Rialto-Colton Basin and parts of the Chino, and North Riverside Basins (referred to as the Chino and North Riverside areas). The models were based on available borehole lithologic and geophysical logs, and water-level data. Data and interpretations from previous structural and geophysical studies were evaluated to update fault locations in the Rialto-Colton Basin. Fault locations were updated based on previous InSAR, gravity, aeromagnetic, and seismic studies.

The hydrogeologic framework model is based on the water-bearing units defined by previous studies (Woolfenden and Kadhim, 1997). Borehole lithologic and geophysical logs were used to determine boundaries between these water-bearing units, which were then interpolated throughout the study area. The boundaries of a perching layer in the Rialto-Colton basin were determined using a similar approach. The resulting framework model indicates that the stratigraphic boundaries of the water-bearing units generally follow the elevation contours of the land surface. The perching layer was determined to extend throughout most of the middle and northwestern part of the Rialto-Colton Basin, and its thickness varies from more than 50 feet in some parts of the basin to areas of minimal thickness around the edges where it pinches out. The

Upper and Lower water-bearing units in the Rialto-Colton Basin generally thicken to the northwest and thicken somewhat to the northeast. The two uppermost water-bearing units in the Chino and North Riverside area, Chino Layer 1 and Chino Layer 2, thicken somewhat to the northeast. Chino Layer 3 thickens to the southwest.

The texture model of the study area simulated the distribution of the percentage of coarse sediment. Borehole lithologic and 16 inch normal resistivity logs were used to estimate the percentage of coarse-grained sediment from each borehole. The percentage of coarse-grained sediment was determined along 10 foot intervals of each borehole. The resulting percent coarse values with depth at each borehole were then interpolated to obtain a three dimensional textural model of the study area using water-bearing unit boundaries and fault boundaries as interpolation boundaries. Coarse sediment distribution in the Rialto-Colton Basin was variable over much of the basin. There was a general trend of finer sediments with depth. The southeast part of the Rialto-Colton Basin contained the highest percentage of fine sediments, with areas in the middle part of the basin containing high percentages of coarse sediments. In Chino and North Riverside area coarse sediments were determined to occur along the northeast boundary between Chino Basin and Rialto-Colton Basin. Fine sediments were determined to occur throughout most of the North Riverside area.

_____, Committee Chair
Dr. Tim Horner

_____
Date

ACKNOWLEDGEMENTS

This research was conducted by the United State Geologic Survey in cooperation with San Bernardino Valley Municipal Water District.

I would like to thank Dr. Tim Horner for his guidance on this project and throughout my graduate education. I would also like to thank Dr. Linda Woolfenden and Dr. Claudia Faunt for the valuable guidance they provided me on my thesis. In addition, I appreciate the support and guidance I received from my entire thesis committee and the Faculty of the Sacramento State Geology Department.

TABLE OF CONTENTS

Page

LIST OF TABLES

Tables Page

LIST OF FIGURES

Figures Page

1 Introduction

Perchlorate is a commercially produced oxidizer used in solid propellants. Perchlorate affects the thyroid functions of persons exposed to it and can lead to birth defects. A perchlorate contamination problem discovered in 1997 in the Rialto-Colton Basin (figure 1) has led to the contamination of 20 water supply wells (U.S. Environmental Protection Agency, 2011) with concentrations above the 2004 California action level of 6 parts per billion (ppb) (California Department of Public Health, 2012). The Rialto-Colton perchlorate plume is one of the densest perchlorate plumes in the United States, with perchlorate levels up to 10,000 ppb (Scott, 2009) near one of the sources. The U.S. Environmental Protection Agency (USEPA) is treating the contaminated area from one of the sources as a superfund site (Superfund site is EPA #: CAN000905945). There are a number of public supply wells in the vicinity of the plume (Figures 2, 3) that provide drinking water to the residents in the Rialto-Colton Basin. The movement of the perchlorate plume is influenced by the types of sediments and faults in the region. A structural, hydrogeologic framework, and textural model of the basin that describe the distribution of fine and coarse sediment as well as the geometry of faults in the area are important first steps in understanding and analyzing the hydrogeology, and hence the movement of the perchlorate plume.

The Rialto-Colton Basin is located in southern California about 60 miles northeast of Los Angeles, California. It is bounded by the San Jacinto fault with the Lytle and Bunker Hill Basins to its northeast, and is bounded by the Rialto-Colton fault with the Chino and North Riverside Basins to the southwest (figure 1). The San Gabriel Mountains form the northwestern boundary of the basin and the Box Springs Mountains form the southeastern boundary. Groundwater generally flows through the Rialto-Colton Basin from the northeast to the southwest.

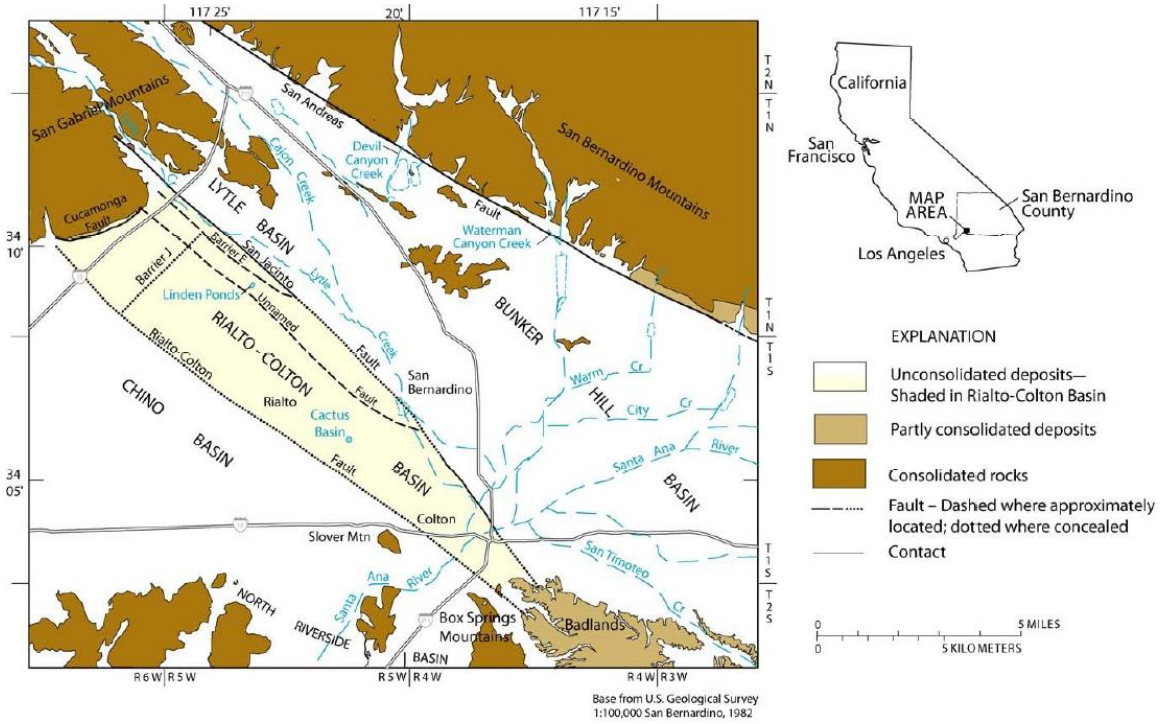

Figure 1: Rialto-Colton study area (modified from Woolfenden and Koczot , 2008)

Thrust, right lateral strike-slip, and normal faulting occur in the vicinity of the study area (Woolfenden and Kadhim, 1997; Dutcher and Garrett, 1963). This region is dominated by right lateral strike-slip faulting (San Andreas and San Jacinto Faults), with bends in these faults causing compressional and extensional stresses (figure 1). The major fault in the vicinity of the Rialto-Colton Basin is an oblique right-lateral strike-slip fault known as the San Jacinto Fault.

The Rialto-Colton Fault is an oblique right lateral strike-slip fault with about 600 meters (m) of vertical normal offset and 2 kilometers (km) of right lateral offset. The San Jacinto Fault is an active right lateral strike-slip fault that is approximately 1.5 million years old (Ma) (Stephenson et al, 2002). It has 25 km of right lateral offset and 1 km of vertical normal offset (Wisely and Schmidt, 2010). San Jacinto Fault is an oblique right-lateral fault in the vicinity of the Rialto-

Colton Basin (Wisely and Schmidt, 2010), which perhaps explains why the Rialto-Colton Fault is also an oblique strike-slip fault (a fault with both normal and strike-slip offset).

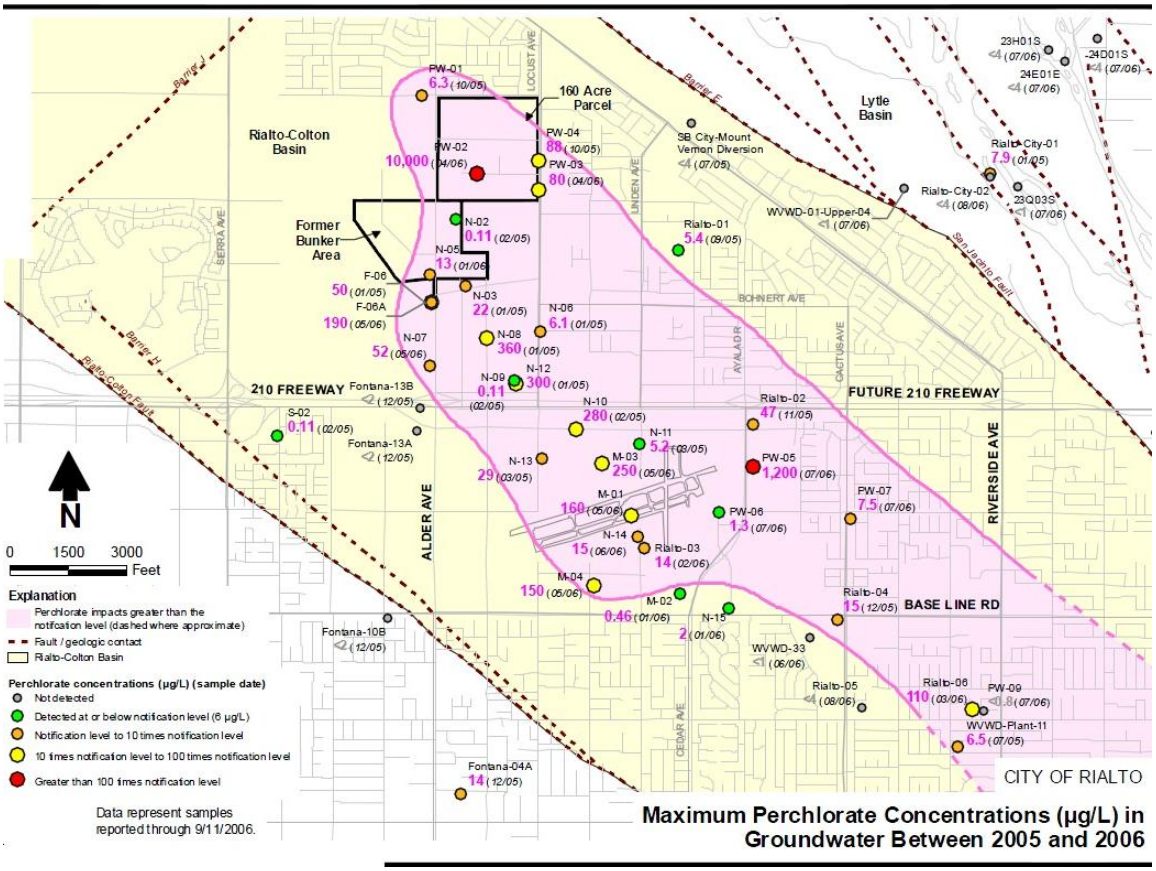

Figure 2: Perchlorate plume in the Rialto-Colton basin (from CH2MHILL 2006)

The Rialto-Colton Basin consists of alluvial and continental deposits throughout much of the basin, with fluvial deposits to the far southeast in the vicinity of the Santa Ana River and Warm Creek and small areas of unconsolidated dune sand (Dutcher and Garret, 1963). The source of the alluvial deposits is the San Gabriel Mountains. The source of the fluvial deposits to the southeast is the Santa Ana River.

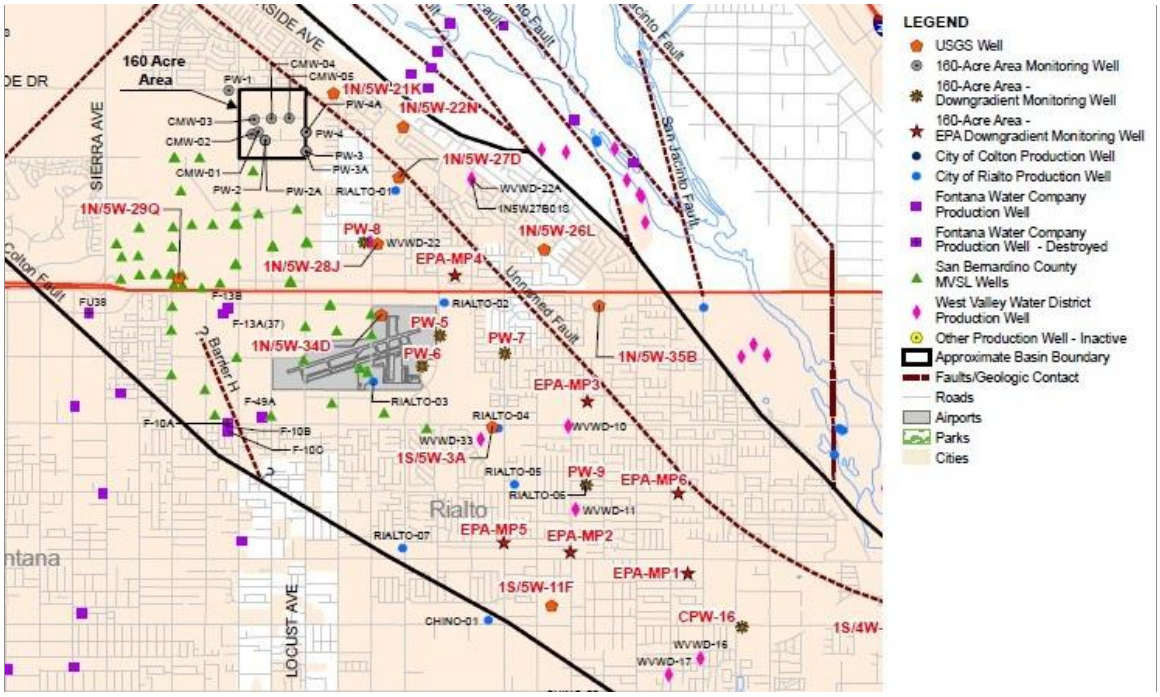

Figure 3: Production and monitoring wells in the Rialto-Colton area 10/7/2009 (CH2MHILL, 2010)

2 Purpose

This purpose of this study is to develop a structural, hydrogeologic framework, and textural model of the Rialto-Colton Basin (figure 4), the eastern part of the Chino Basin (referred to as the Chino area), and the northern part of North Riverside Basin (referred to as the North Riverside area). Two studies, one of the Chino Basin (Wildermuth Environmental, Inc., 2003) and the other of the Rialto-Colton Basin (Woolfenden and Kadhim, 1997) both identified water-bearing units in their respective study areas. A correlation between these two sets of water-bearing units, which are offset by the Rialto-Colton Fault Zone, could not be determined. Therefore the study area was divided into two sections, one consisting of the Rialto-Colton Basin and one consisting of the eastern part of Chino Basin and north Riverside Basin (figure 5).

The structural, hydrogeologic framework, and textural model from this study are intended to be a first step towards a groundwater model of the Rialto-Colton Basin. This study therefore is primarily focused on the Rialto-Colton Basin, with the Chino and North Riverside area of secondary interest.

The following questions are addressed as part of this study:

1) What do recent geologic studies (gravity, aeromagnetic, seismic, InSAR) and geophysical data (lithology, resistivity, spontaneous potential, sonic, water level) indicate about faulting in the study area?
2) What are the dimensions of the water-bearing units the study area?
3) What is the distribution of coarse and fine sediment in the study area?

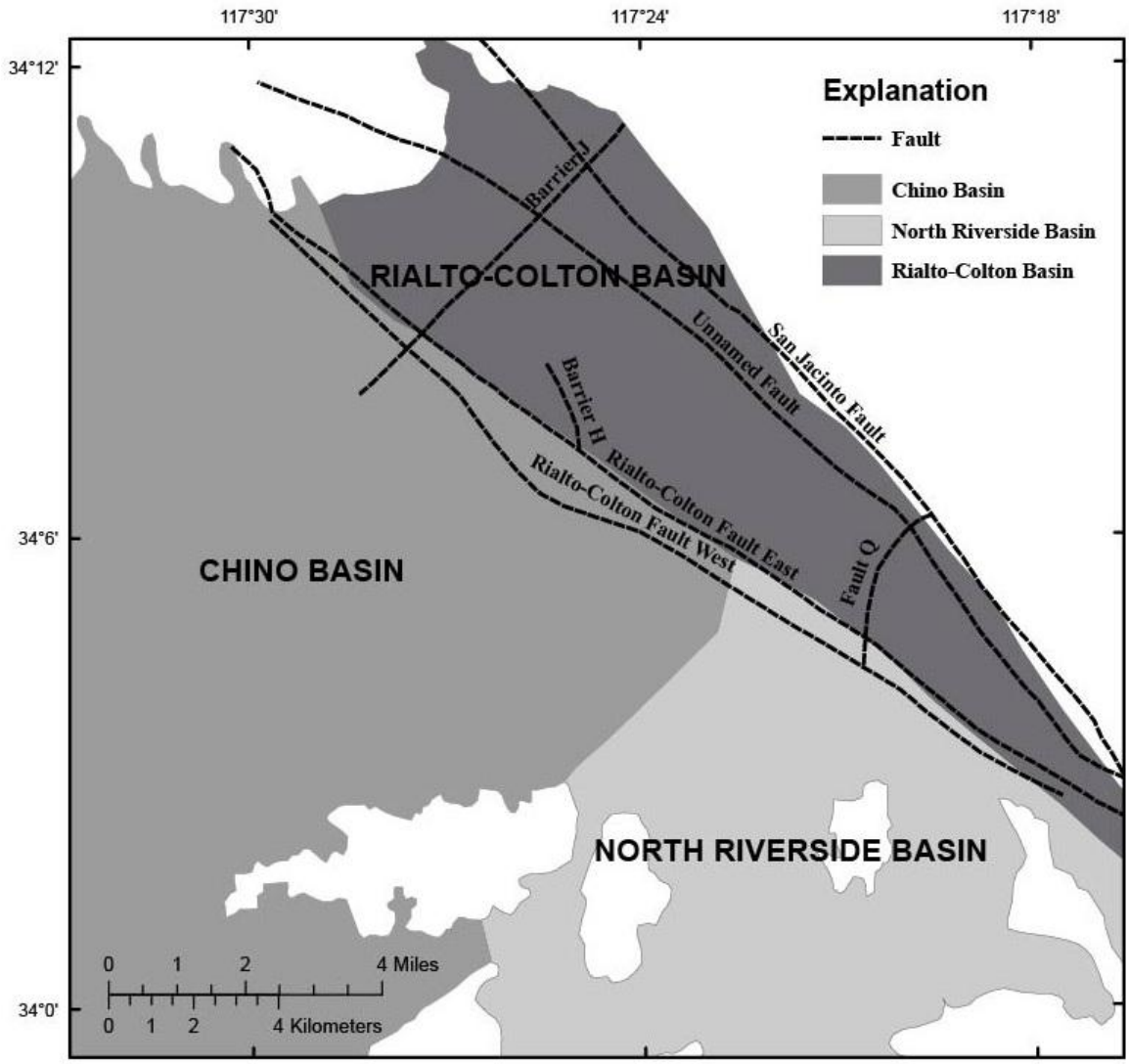

Figure 4: Groundwater Basins in the study area.

This conceptual model includes:

1) A three-dimensional gradational distribution of the coarse and fine sediments throughout the Rialto-Colton Basin and the Chino and North Riverside areas.
2) The location and extent of the faults in the Rialto-Colton Basin.

The conceptual model is supported by borehole lithology logs, borehole resistivity data, water level data, digital elevation data, and maps of existing faults.

3 Overview of Literature and Related Studies

There have been three previous phases in the Rialto-Colton basin studies.

1) Phase 1: Geohydrology and water chemistry study which investigated the ground-water flow and chemistry of the Rialto-Colton Basin using existing borehole data (geophysical and lithologic logs), water level measurements, and chemical analyses of water samples.
2) Phase 2: Develop a finite-difference ground-water flow model using MODFLOW and MODPATH to determine the fate and movement of imported water.
3) Phase 3: Determine the location and extent of Rialto-Colton Fault using gravity, seismic, and aeromagnetic data.

The results of phases 1 and 2 are described in two USGS publications, "Geohydrology and Water Chemistry in the Rialto-Colton Basin, San Bernardino County, California" (Woolfenden and Kadhim,1997) and "Numerical Simulation of Ground-Water Flow and Assessment of the Effects of Artificial Recharge in the Rialto-Colton Basin, San Bernardino County, California" (Woolfenden and Koczot, 2001), respectively. The results of phase 3 are described in Anderson, et al. (2000) and Anderson et al. (2004). A USGS publication describing the recently collected data in the Rialto-Colton Basin also is included in Phase 3 (Brown and Teague, in review).

There are three other studies currently under way that include the Rialto-Colton and adjacent Basins. One of these studies is the Perchlorate Chemistry project, which includes assessing the source, vertical distribution, and fate of perchlorate in the upper Santa Ana River Basin. Another study is the Rialto-Colton Fault Water-Level project which includes assessing the direction of groundwater movement within Rialto-Colton and adjacent basins in the vicinity of the Rialto-Colton Fault. The GAMA (Groundwater Ambient Monitoring Assessment) project, which is a

comprehensive assessment of statewide groundwater quality, includes the Rialto-Colton Basin as one of its study units.

Studies of the structure in the Rialto-Colton basin and adjacent areas include two seismic reflection studies (Stephenson et al., 2001 and Catchings et al., 2008), two vertical deformation studies (Lu, Z,, and Danskin W, 2001, Wisely et al., 2010), and a gravity/aeromagnetic study (Anderson et al, 2004).

Other groundwater studies include a description of the hydrologic features in San Bernardino County by Dutcher and Garrett (1963), a hydrogeologic study of the Rialto-Colton Basin by Fox and Roberts (1995), a groundwater transport model of perchlorate migration in northern Rialto-Colton Basin by GeoLogic Associates in 2007, and a description of the groundwater flow system and flow model of Chino Basin by Wildermuth Environmental, Inc. (2003).

4 Previous Work

This report's structural and hydrogeologic framework models of the study area use and analyze results from previous hydrogeologic, gravity and aeromagnetic, InSAR, seismic, and tectonic studies. These studies include, Dutcher and Garrett (1963), Fox and Roberts (1995), Woolfenden and Kadhim (1997), Anderson et al (2000), Woolfenden and Koczot (2001), Lu and Danskin (2001), Stephenson et al (2002), Wildermuth Environmental, Inc. (2003), Anderson et al (2004), GeoSyntec Consultants (2006), Catchings et al (2008), CH2MHILL (2009), Wisely and Schmidt (2010), and Cook et al (2010).

4.1 Hydrogeologic Studies

Dutcher and Garrett (1963) mapped the geologic and hydrologic features on the San Bernardino area. Original fault locations as defined in Dutcher and Garret (1963) are presented in this study along with updated fault locations from subsequent studies.

Fox and Roberts (1995) analyzed the hydrogeologic features of the Rialto-Colton Fault and Barrier H (figure 17). The study consists of a water quality, water level, and geologic well log analysis of wells near the Rialto-Colton Fault. According to the Fox and Roberts (1995) study Barrier H is only a minor fault segment which extends to the northeast of the Rialto-Colton Fault. The study states that there is no evidence to indicate that this splay continues for more than a short distance and that the area within the splay is in hydraulic continuity with nearby wells located to the north and to the east of the splay. The 1995 study is largely based on water chemistry data.

Woolfenden and Kadhim (1997) analyzed the geohydrology and water chemistry of the Rialto-Colton Basin. The study defined water-bearing units in the Rialto-Colton Basin, which were used by this study. In addition, the study determined the boundaries of these water-bearing units in

eleven boreholes by analyzing borehole geophysical and lithology logs. The water-bearing units defined in Woolfenden and Kadhim (1997) and the subsequent analysis of eleven boreholes form the basis for the hydrogeologic framework model presented in sections 5.3 and 6.1 of this report.

Wildermuth Environmental, Inc., (2003) developed a conceptual and groundwater model for Chino Basin. The study groups the sediment in Chino Basin into three hydrostratigraphic units, Layer 1, Layer 2, and Layer 3, which are referred to in this report as Chino Layer 1, Chino Layer 2, and Chino Layer 3. The study constructs eight cross sections through Chino Basin which delineate Chino Layer 1, Chino Layer 2, and Chino Layer 3. This report (section 6.4) constructs a 3-D model of these hydrostratigraphic units based on the cross sections from Wildermuth Environmental, Inc., (2003) and additional borehole data from the Chino and North Riverside area.

GeoSyntec Consultants (2006) conducted a groundwater investigation in the Rialto-Colton Basin. The report investigates the perched aquifer in Rialto-Colton Basin using water level data from wells screen in the shallow perched aquifer and wells screened in the deeper regional aquifer. The report shows hydraulic heads being significantly (70+ ft) higher in the perched aquifer than in the regional aquifer. Well data from the GeoSyntec Consultants (2006) report was used in this report (section 5.3.3 and 6.2.7) along with sonic, resistivity, and lithologic logs to model the dimensions of the perching layer.

CH2MHILL (2009) published groundwater elevation data in Rialto-Colton Basin for November/December of 2009. These data were used by this report (section 6.1) in the analysis of the Rialto-Colton Fault Zone.

4.2 Gravity and Aeromagnetic Study

Anderson et al (2004) analyzed the structure of the San Bernardino area using gravity and aeromagnetic data. The gravity data were interpreted by Anderson et al (2004) to produce a map of depth to bedrock in the Rialto-Colton Basin and surrounding areas. Interpretation of the depth to bedrock map indicated two major grabens in the vicinity of the Rialto-Colton Basin, the northwest graben and the southeast graben (figure 16). Interpretation of the aeromagnetic data by Anderson et al (2004) indicated stretched magnetic anomalies in the Rialto-Colton Basin (figure 15) which were interpreted by Anderson (2004) as the result of faulting. A magnetic anomaly is a variation in the Earth's magnetic field caused by variations in magnetism or chemistry of rocks. Magnetic anomalies can be stretched by sheering forces such as those present along active strike-slip faults.

The results of the Anderson et al (2004) study are used in the structural interpretation of the Rialto-Colton Basin and the Chino and North Riverside area in section 6.1 and 6.3 of this study. In this study, the depth to bedrock map from Anderson et al (2004) is used in conjunction with results from other studies and borehole data to analyze the structure of the Rialto-Colton Basin. The aeromagnetic map from Anderson et al (2004) is used in section 6.1.4.1 of this study in the analysis of the Rialto-Colton Fault Zone.

4.3 InSAR Studies

Data and interpretations from two InSAR studies (Lu and Danskin, 2001; Wisely and Schmidt, 2010) were used to help determine the location of water barriers in the Rialto-Colton Basin. Since land surface deformation can be caused by changes in water levels, a fault acting as a water barrier can show up on InSAR interferograms (plots of the differences in land surface elevation

between two time periods) as a linear boundary that separates areas with different amounts of ground surface deformation.

Lu and Danskin (2001) used data from the ERS-1 and ERS-2 satellites between the years of 1992 to 1995 to detect the change in groundwater levels using interferograms. A change in groundwater levels is indicative of deformation between the two time periods. The study analyzed InSAR data to determine natural recharge and structure in the San Bernardino area.

The interferograms from the study are used in section 6.1.4.2 of this study to help refine the location of Barrier H and in section 6.1.4.3 of this study to help refine the location of Fault Q.

Wisely and Schmidt (2010) used data from the ERS-1 and ERS-2 satellites to distinguish between deformations caused by change in groundwater levels and deformations caused by interseismic strain between 1995 to 1999. The study processed data using the ROI_PAC software package. The Wisely and Schmidt (2010) study also developed interseimic (between seismic events) deformation models for the San Bernardino area. The interseismic models calculated the expected deformation based on seismic strain data from major active faults in the region.

In addition, Wisely and Schmidt (2010) performed an analysis of fault geometry and motion in the region, and concluded that there were areas of tectonic uplift and subsidence in the vicinity of the Rialto-Colton Basin. Wisely and Schmidt's simple and complex analyses of seismic forces in the region indicate that the eastern portion of the Rialto-Colton Basin is experiencing interseismic deformation causing up to 0.2 mm/year of subsidence (figure 11). The simple analysis involved only major faults in the region while the complex analysis involved both major and minor faults in the region.

The interseismic models from the Wisely and Schmidt (2010) study are used in section 6.1.2 of this study, which compares the interseismic (between seismic events) models from Wisely and Schmidt (2010) to the depth to bedrock map from the Anderson et al (2004) study.

4.4 Seismic Studies

Two seismic studies of the Rialto-Colton Basin and surrounding areas (Stephenson et al, 2002; Catchings et al, 2008) used seismic data to locate faults along seismic transects. The fault locations were used in section 6.1 of this study to constrain the location of faults and fault zones in the Rialto-Colton Basin.

Stephenson et al (2002) includes a cross basin transect through the southeastern part of Rialto-Colton Basin. The study collected continuous, shallow seismic reflection data using a small vibrator source, or Mini-vib, as its seismic source. The study identified two possible faults in the vicinity of the Rialto-Colton Fault and the San Jacinto Fault.

Catchings et al (2008) also included a cross basin transect through the southeastern part of Rialto-Colton Basin. The study used explosions in shallow boreholes as seismic sources. The results of the study indicated six faults in the Rialto-Colton Basin along the 2008 seismic transect. Catchings et al (2008) also reinterpreted the seismic transect from Stephenson et al (2002) and concluded there were additional faults in the Stephenson et al (2002) transect.

4.5 Tectonic Studies

Cook et al (2010) simulated fault activity in the San Bernardino area. The simulation suggests that the amount of tectonic stress on the San Jacinto Fault Zone has been shifting during the last several hundred thousand years.

5 Methods

This study involved collecting data from a variety of sources, building a structural and hydrogeologic framework model of the Rialto-Colton Basin and the Chino and North Riverside area, and building a physical property model based on the fault boundaries, water-bearing unit boundaries, and lithologic and geophysical data.

5.1 Data

The data used in this study includes lithology, resistivity, natural gamma, and spontaneous potential logs, water level data, and digital elevation data. These data come from a variety of sources including borehole drillers' logs and geophysical logs (California Department of Water Resources and local water districts, unpublished data, various years), lithologic and borehole geophysical logs for USGS sites, annual Watermaster reports for the San Bernardino Valley (Water Master Support Services, 2009), the USGS NWIS database (http://waterdata.usgs.gov/usa/nwis/, accessed 2011), and the U.S. Geological Survey 1999 National Elevation Dataset (U.S. Geological Survey, 1999). All data were digitized and imported into several databases. All data were stored in Microsoft Access or Microsoft Excel based formats.

Additional data include fault maps, InSAR data, seismic data, gravity data, and magnetic data (as mentioned in the "Previous works" section). In many cases the interpreted results from studies containing these data also were used.

5.1.0 Borehole Data Compilation

Borehole data were compiled from drillers' logs and geophysical logs and stored in a Rockworks database and Excel spreadsheets. Borehole data included borehole location, lithology logs,

geophysical logs (16-inch normal resistivity, natural gamma, and spontaneous potential), and water level data. Available borehole data in the study area is shown in figure 5.

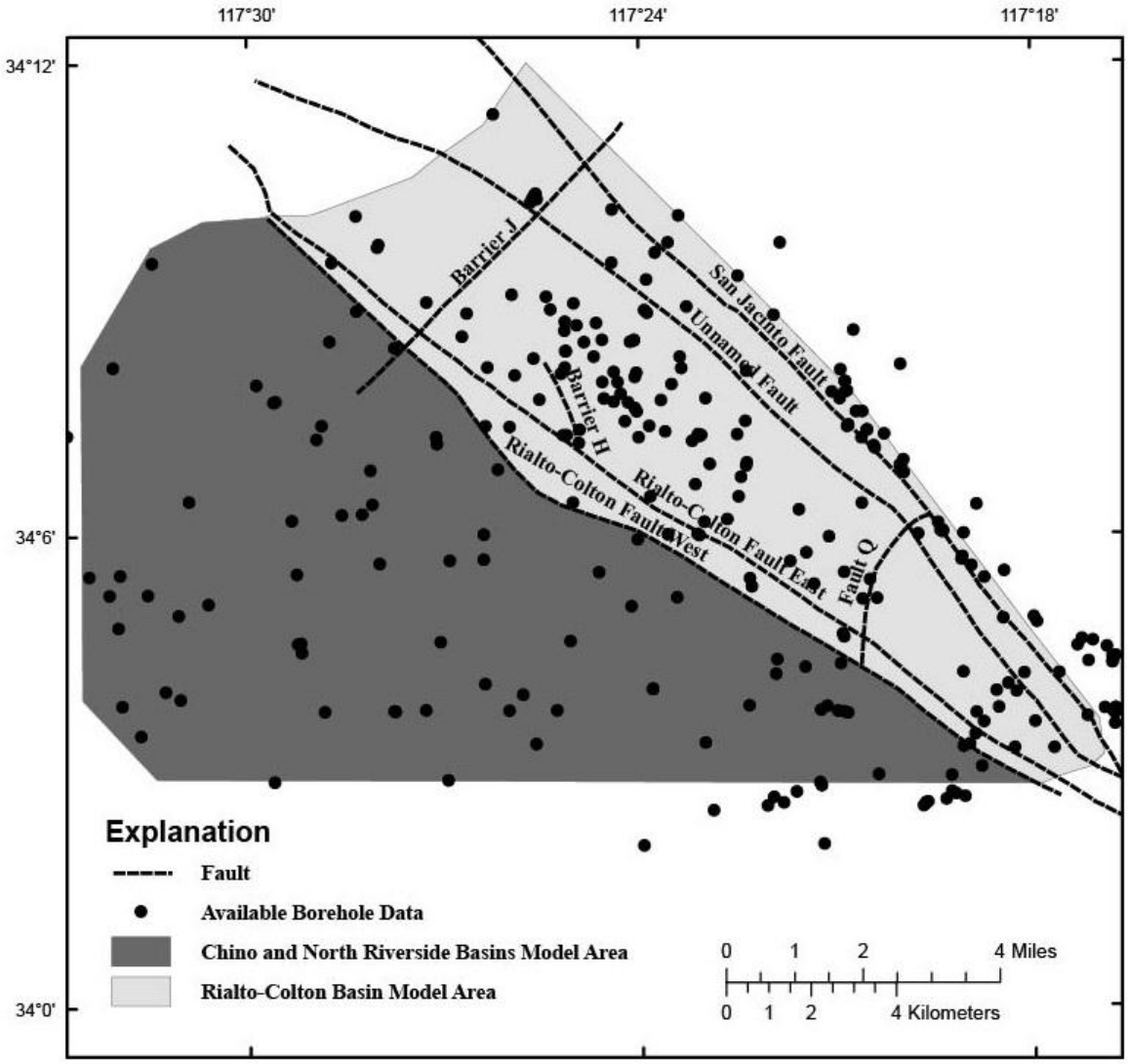

Figure 5: Available borehole data in the study area.

5.1.0.1 Borehole Location

The quality of borehole location information provided in drillers' logs varied from borehole to borehole. Location information consisted of one or more of types listed in table 1, listed from most to least precise.

The precision of the borehole locations varied from within several feet for newer boreholes with coordinates determined utilizing high precision GPS, to within ~400 feet for older boreholes where distances were given to the nearest 0.05 mile.

Table 1: Borehole location information provided by drillers' logs

Location Type	**Description**
Latitude/Longitude Coordinates	Latitude and Longitude coordinates were provided in the drillers' log. In this case the coordinates were converted to State Plan Coordinates using NOAA's Geodetic Toolkit (http://www.ngs.noaa.gov/TOOLS/spc.shtml).
Distance from cross street	The location of the well was given as two perpendicular distances from a cross street (usually North/South and East/West distances). Most of the drillers' logs recorded distance in 100 ft intervals. Other drillers' logs recorded distances in a variety of increments including to the nearest 0.05 mile. In some cases accuracy of well location was improved by using elevation data for the well to narrow down its location.
Township/range information	Township/range information was given. The level of detail of this information varied from the tract level to intervals as small as a 16^{th} of a tract. If township/range information was given in addition to the above data, it was used to verify the location of a well and/or further confine the well's location.

5.1.0.2 Borehole Lithology

Borehole drillers' logs were used to determine lithology types along the specified intervals. These lithology types for 266 boreholes were entered into Rockworks. Comments were added with details about lithologies for each interval. Table 2 lists the lithology types from the drillers' logs along with the interpretation of each lithology type used in this study.

5.1.0.3 Geophysical logs

Geophysical logs including resistivity (16-inch normal), natural gamma, spontaneous potential, and sonic were used to interpret changes in stratigraphic units and lithologies. Many of these geophysical logs were scanned from hard copy and then digitized into numeric values using

Engauge Digitizer Version 4.1. The digitized data were imported into Microsoft Excel for graphing and interpretation.

Table 2: Lithology types

Drillers' Log Lithology Type	**Interpretation of Lithology Type**
Altered Granite	Bedrock
Clay	Mostly clay with less than 15% gravel, sand, or silt.
Clay/Gravel	Mostly clay with at least 15% gravel
Clay/Sand	Mostly clay with at least 15% sand
Clay/Sand/Gravel	Mostly clay with at least 15% sand and 15% gravel
Cobbles/Boulders	Mostly cobbles and/or boulders
Concrete	Cemented alluvium
Conglomerate	Conglomerate rock
Gravel	Mostly gravel with less than 15% sand, silt, or clay.
Gravel/Clay	Mostly gravel with at least 15% clay
Gravel/Sand	Mostly gravel with at least 15% sand
Gravel/Silt	Mostly gravel with at least 15% silt
Limestone	Carbonate rock
Sand	Mostly sand with less that 15% gravel, silt, or clay
Sand/Clay	Mostly sand with at least 15% clay
Sand/Gravel	Mostly sand with at least 15% gravel
Sand/Gravel/Clay	Mostly sand with at least 15% gravel and 15% clay
Sand/Silt	Mostly sand with at least 15% silt
Sand/Silt/Clay	Mostly sand with at least 15% silt and 15% clay
Sandstone	Sandstone rock
Shale	Shale rock
Silt	Mostly silt with less than 15% gravel, sand, or clay
Silt/Clay	Mostly silt with at least 15% clay
Silt/Gravel	Mostly silt with at least 15% gravel
Silt/Sand	Mostly silt with at least 15% sand

5.1.0.4 Borehole Data Quality

Lithologic logs were divided into three groups based on data quality. Table 3 describes how the lithologic logs were grouped.

Borehole data (lithologic and geophysical data) were then scored into seven categories according to data quality, numbered zero through six, with six being the highest quality boreholes (table 4). These categories were based on the lithology data quality and the existence of geophysical data.

These categories were one factor in determining if and how the borehole data were used in the stratigraphic and percent coarse interpolation of the study area. Many of the lowest quality boreholes were not used in the stratigraphic and percent coarse interpolations.

Table 3: Lithology data quality categories

Quality	**Description**
Good Data	The lithological descriptions were very detailed. Intervals where lithogies were recorded were on average fairly short (under 30 ft intervals).
Average Data	At least some adjectives were used to describe the lithology. Intervals averaged under 50 ft.
Poor Data	Very brief descriptions of lithologies were given with few if any qualifying adjectives (ex: "Sand" instead of "Fine sand with streaks of clay") or intervals averaged greater than 50 ft.

Table 4: Borehole data quality categories

Borehole Quality (0-6)	**Lithology Log**	**Geophysical Log(s) Present**
0	Poor	No
1	Average	No
2	Good	No
3	No Lithology Log	Yes
4	Poor	Yes
5	Average	Yes
6	Good	Yes

5.1.0.5 Water Level Data

Water level data were used in the interpretation of borehole geophysical logs. Resistivity logs often recorded a sharp change in resistivity around the water table. Water level data were used to avoid falsely interpreting these sharp resistivity changes. Information used to calculate water level elevations and evaluate their usefulness included the following:

- Well location (easting and northing)
- Land surface elevation
- Depth to bottom of the well
- Screened interval of well (depth)

- Sample date
- Water level elevation

5.1.1 DEM Data

The National Elevation Dataset from a digital elevation model (DEM) developed by the U.S. Geological Survey in 1999 was used to define the surface elevation of the stratigraphic and percent coarse model and to more precisely define the elevation of some of the old agricultural wells with only approximate elevations given in their drillers' logs. The DEM data are in raster format with cells 10-meters (~31 feet) by 10-meters.

5.2 Structural Model of Study Area

An understanding of the structure of the study area and the seismic forces acting in the region was a prerequisite to updating the existing fault maps and stratigraphic model in the study area. Results from seismic, gravity, magnetic, and InSAR studies were analyzed to develop a general structural model for the study area. Cross sections including boreholes with high quality data were constructed.

5.2.1 Evaluation of Seismic Stress in the Rialto-Colton Basin

An analysis of these seismic forces (Catchings et al, 2008) along with bedrock depth data (Anderson et al, 2004) was used by this study to identify possible areas of uplift and subsidence in the basin. Areas of uplift and subsidence were compared with basement elevations in the Rialto-Colton Basin. In addition, modeled uplift or subsidence due to bends in the San Jacinto and San Andreas Faults were compared with water-bearing unit thickness where thicker units may indicate subsidence and thinner units may indicate uplift.

In addition, there is a possibility that seismic forces may have changed during the deposition of alluvium in the Rialto-Colton Basin. Results from a study by Cook et al, (2010) suggests that the amount of right lateral strain handled by the San Jacinto and San Andreas faults have changed over the last several hundred thousand years. A change in right lateral strain in the area is significant since there are a number of currently inactive traces of the San Jacinto fault in the Rialto-Colton Basin that may have been active during times of increased right lateral strain.

5.2.2 Evaluating Fault Locations

Fault locations were evaluated for the Rialto-Colton Fault, Barrier H, and the Unnamed Fault. The locations for these faults were based on results from fault studies, seismic studies, InSAR studies, gravity and magnetic studies, water level data, and geophysical borehole data. Evidence is presented to support the locations of these faults used in this study. In addition, the possibility of the existence of previously unmapped faults in the Rialto-Colton Basin was considered for this study.

5.3 Hydrogeologic Framework Model of Study Area

The hydrogeologic framework model of this study area focused on modeling the dimensions of stratigraphic units defined in Woolfenden and Kadhim (1997). The dimensions of a perching layer in the Rialto-Colton Basin were also modeled. Stratigraphic units were modeled by using stratigraphic boundary interpretations from boreholes and interpolating these interpretations throughout the study area.

5.3.1 Stratigraphic Interpretations of Selected High Quality Borehole Data

This study reevaluated stratigraphic interpretations from eleven boreholes in Rialto-Colton Basin given in (Woolfenden and Kadhim, 1997) and, in some cases, minor changes to the stratigraphic boundaries were made.

Also, this study evaluated lithologic and geophysical logs from thirty-one additional boreholes (Appendix A). Boreholes were selected for a detailed stratigraphic analysis based on:

1) The quality of data for that borehole (table 4)
2) The depth of the borehole, with deeper boreholes being preferable
3) The nearness of the borehole to a cross-section (figure 77)
4) The availability of geophysical logs for that borehole (resistivity, gamma, and spontaneous potential logs)

Stratigraphic boundaries used consisted of the top of each stratigraphic unit and the bottom of the bottom-most stratigraphic unit. Each borehole was evaluated to determine the elevation of each stratigraphic boundary that the borehole passed through (when enough geophysical and lithologic data were available to make the determination). All boreholes were assumed to be vertical.

For the purposes of a groundwater flow model, the major stratigraphic boundaries of interest are the boundaries between the river deposits and the upper unit, the upper unit and the middle unit, the middle unit and the lower unit, and the lower unit and the base of the aquifer (the base of the aquifer is either consolidated deposits or basement rock). These boundaries are most important because they define the major boundaries between the different water-bearing units (the upper, middle, and lower units do not generally pinch out in the Rialto-Colton Basin which makes defining additional boundaries unnecessary).

Wildermuth Environmental, Inc., (2003) defined stratigraphic units for Chino Basin which could not be correlated with the stratigraphic units defined in the Rialto-Colton Basin (Woolfenden and Kadhim, 1997). Therefore, stratigraphic units were defined separately for the Rialto-Colton Basin and the Chino and North Riverside area. The stratigraphic water-bearing units used for the

Rialto-Colton Basin were based on those used in Woolfenden and Kadhim (1997). These units and the units that form the base of the aquifer are listed in table 5 in stratigraphic order from top (most recent) to bottom (older). The Chino and North Riverside area stratigraphic water-bearing units were determined from a previous hydrology study of the Chino Basin (Wildermuth, 2003). These units are listed in table 6.

Table 5: Stratigraphic units of the Rialto-Colton Basin

Stratigraphic Layer	**Description**
River Deposits	The upper-most stratigraphic layer in the model. The river deposits layer was found to only exist in the southeastern most portion of the Rialto-Colton Basin. The river deposits layer consists of Quaternary alluvium.
Upper Water-Bearing Unit	The upper-most stratigraphic layer in most of the Rialto-Colton Basin except in the southeastern part (where it underlies River Deposits). This stratigraphic unit consists of Quaternary alluvium.
Middle Water-Bearing Unit	The middle stratigraphic layer occurs throughout the Rialto-Colton Basin. This stratigraphic unit consists of Quaternary to Tertiary deposits in the Rialto-Colton basin and underlies the Upper Water-Bearing Unit (Woolfenden and Koczot, 2001).
Lower Water-Bearing Unit	The lower water-bearing stratigraphic layer occurs throughout the Rialto-Colton Basin and underlies the Middle Water-Bearing Unit. This stratigraphic unit consists of Tertiary deposits in the Rialto-Colton Basin.
Consolidated Deposits	Consolidated deposits were found below the lower water-bearing unit in much of the Rialto-Colton Basin. The top of the consolidated deposits defines the bottom of the Rialto-Colton aquifer, where Consolidated Deposits are found.
Bedrock	Granitic rock underlying the alluvium and sedimentary rocks in Rialto-Colton Basin.

Additional unit boundaries were defined to delineate the confining layer for a perched aquifer in the northwestern part of the Rialto-Colton Basin southeast of Barrier J (figure 29). The confining layer of the perched aquifer occurs inside the middle water-bearing unit, splitting the middle water-bearing unit into two sub-units.

In addition previous studies were used as a guide in this analysis. These previous stratigraphic studies were:

1) Geologic and Hydrologic Features of the San Bernardino Area California, Geological Survey Water-Supply Paper 1419, L.C. Dutcher and A.A. Garrett, 1963
2) Numerical Simulation of Ground-Water Flow and Assessment of the Effects of Artificial Recharge in the Rialto-Colton Basin, San Bernardino County, California, Woolfenden and Koczot, 2001
3) Optimum Basin Management Program Chino Basin Dry-Year Yield Program Modeling Report, Wildermuth Environmental, Inc., July 2003

Table 6: Stratigraphic units in the Chino and North Riverside area.

Stratigraphic Layer	**Description**
Chino Layer 1	The upper-most stratigraphic layer in the Chino and North Riverside area. This stratigraphic unit consists of Quaternary alluvium.
Chino Layer 2	The middle stratigraphic layer in most of the study area. This stratigraphic unit consists of Quaternary deposits in the Chino and North Riverside area.
Chino Layer 3	The lower stratigraphic layer in most of the study area. This stratigraphic unit consists of Quaternary deposits in the Chino and North Riverside area.
Consolidated Deposits	Consolidated deposits are found below the lower water-bearing unit in some areas of the Chino and North Riverside area.
Bedrock	Granitic rock underlying the alluvium and sedimentary rocks in the Chino and North Riverside area.

5.3.2 Stratigraphic Interpretations of Lower Quality Borehole Data

The lower quality boreholes, most of which contain an incomplete set of geophysical logs, were evaluated last. There were 65 lower quality boreholes in Rialto-Colton Basin and 78 lower quality boreholes in the Chino and North Riverside area. Stratigraphic boundaries were

determined using the available data for each borehole. These data were interpreted in conjunction with nearby boreholes having more complete data sets.

The following procedure was used for the lower quality boreholes:

1) Find all nearby boreholes with good quality lithology and geophysical data.
2) Determine a range of likely boundary elevations of stratigraphic layers for the borehole being analyzed based on nearby boreholes and faults.
3) Determine the stratigraphic boundaries at that borehole based on the range of likely boundary elevations, the borehole lithology logs, and any available geophysical data.
4) If poor-quality borehole data is inconsistent with an interpolation of surrounding borehole stratigraphy, either reconsider the surrounding borehole stratigraphy or reconsider faults in the area. If borehole data still is irreconcilable and borehole data is of much poorer quality than the data from nearby boreholes, eliminate the borehole with poorer quality data from the stratigraphic analysis.

5.3.3 Perching Layer

A perched aquifer in middle northwestern part of the Rialto-Colton Basin has been identified in a previous study (GeoSyntec Consultants, 2006) which analyzed water level data from different depths to show the presence of a perched aquifer. The fine-grained perching layer was modeled as a separate stratigraphic unit for this study. This was done by determining the upper and lower boundaries of the perching layer from the lithologic and sonic logs of each borehole located in the area of the basin where the perching layer occurs and from previous studies. The following procedure was followed in defining the boundaries of the perched aquifer.

1) Identify boreholes where an approximate depth range of the perching layer can be determined by sonic logs or water level data.
2) Select a single borehole with sonic or water level data indicating a perched aquifer. Look at the lithology, resistivity, and sonic logs to determine if a specific interval of fine-grained sediments is likely the confining layer of the perched aquifer. This is indicated by a layer of fine-grained sediments that is at approximately the correct depth.
3) Examine nearby boreholes to determine if there are fine-grained sediments at similar depths. When fine-grained sediments are found at similar depths of all nearby boreholes, record the top and bottom of the perching layer at each nearby borehole.
4) Continue steps 2-3 for each borehole with sonic or flow logs, first selecting the boreholes closest to the last set of boreholes analyzed, and then selecting boreholes at distances from the original borehole until the entire perched aquifer has been delineated.
5) Build a grid of points for the top and bottom elevations of the boundaries of the perching layer based on the data points defined in steps 1-5.
6) Using the minimum tension interpolation in EarthVision, produce a top and bottom grid bounding the perched layer from these points.
7) Interpolate percent coarse property data within the perching layer. Confirm that the interpolation produces fine sediments (below 50 percent coarse) within the perching layer.

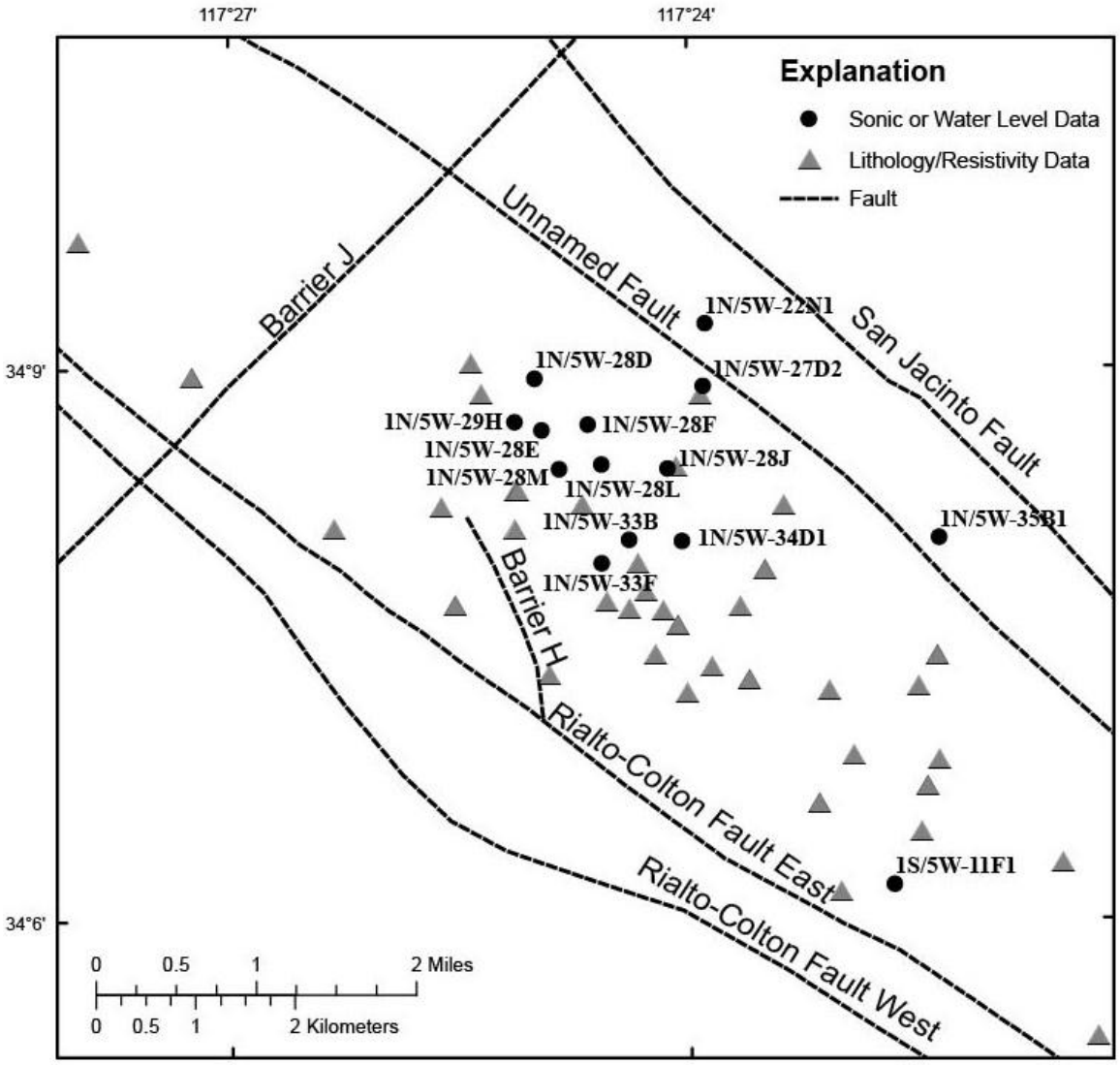

Figure 6: Boreholes used in interpolation of perching layer.

Boreholes used in the interpolation of the perching layer are shown in figure 6. Boreholes with sonic logs and water level data were mostly confined to the area between Barrier H and the San Jacinto Fault with the notable exception of 1S/5W-11F1, which is over two miles to the southeast of the other sonic log and water level data. Boreholes with lithology and resistivity data were distributed more uniformly throughout the basin.

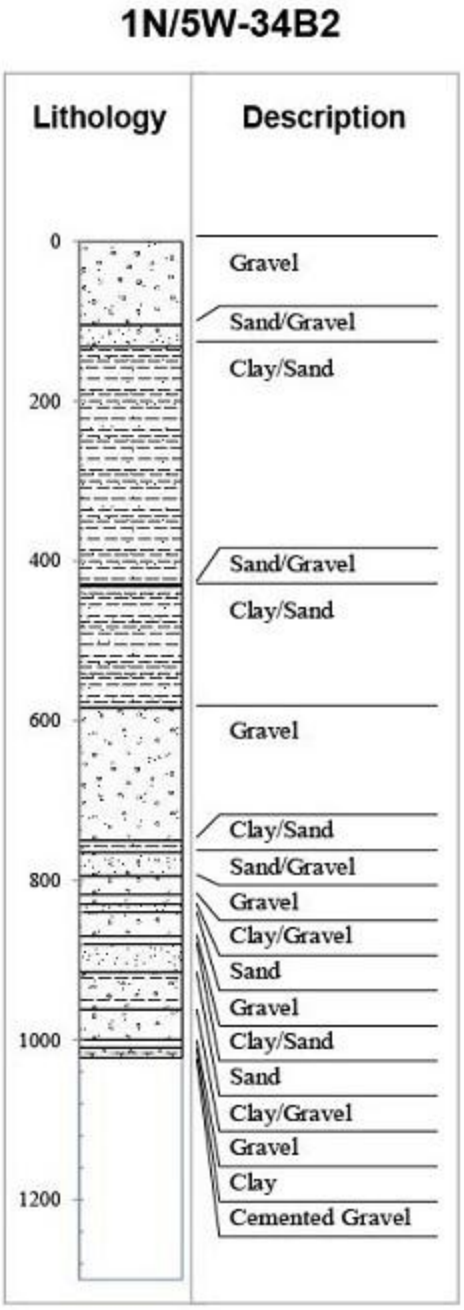

Figure 7: Lithology of borehole 1N/5W-34B2

Data points that could not be resolved with the rest of the data were not used in the stratigraphic interpolation. For example, one data point of note was borehole 1N/5W-34B2. The lithologic log for this borehole has a nearly continuous interval of fine-grained sediments totaling 452 feet thick

(figure 7). Nearby boreholes have far thinner intervals of fine sediment (less than 200 feet thick). An increase in thickness of the perching layer by over 200 feet was not justified based on one data point of average quality. Furthermore, 238 ft of the continuous fine grained layer logged in 1N/5W-34B2 was logged as a single entry, "Sandy, brown clay". This is the only borehole in the area that was logged as having a large continuous interval of clay. This suggests there may be more detail in the drill cuttings obtained during drilling of this well than were included in the lithologic log. As a result 1N/5W-34B2 was not used.

5.3.4 General Parameters 3-D Stratigraphic and Textural Model

A 3-D model of water-bearing unit stratigraphy and distribution of the percent of coarse-grained sediments was constructed using EarthVision™ 8.1. EarthVision is a software package for spatial analysis and geologic modeling. It can be used for interpolation or extrapolation of stratigraphic boundaries, faults, and aquifer properties. Modeling can be done using surfaces (such as faults and stratigraphic boundaries) as interpolation barriers. Interpolation barriers are 2-D surfaces that block or limit data points on one side of the surface from influencing the interpolation on the other side of the surface. As discussed previously, the stratigraphic boundaries were based on analysis of the borehole data and the distribution of the percent of coarse-grained sediments. The stratigraphic boundaries and faults were considered interpolation barriers in Rialto-Colton Basin and the Chino and North Riverside area models. This model was completed using the general model parameters in table 7. More specific parameters are presented in each subsection.

Table 7: EarthVision general parameters

EarthVision Parameter Name	**Setting**
Coordinate System Name	State Plane Coordinates
Full Coordinate System	NAD83 / Lambert California State Planes, Zone V (405), US feet
Model Rotation	45 degrees counterclockwise
Model Pivot Point	6741973 Easting, 1804175 Northing, -110 Elevation
Model Dimensions	57988 ft by 81008 ft, by 2200 ft

The model dimensions were chosen to include both the Rialto-Colton Basin and the Chino and North Riverside area out to Interstate 15 (figure 8). The model grid was rotated 45 degrees to align it with the general direction of deposition, major faulting and groundwater flow in the Rialto-Colton Basin.

5.3.5 Stratigraphic Interpolation

Two separate stratigraphic interpolations were done, one for the Rialto-Colton Basin, the other for the Chino and North Riverside area. Stratigraphic interpolations were done by importing the stratigraphic boundaries determined in each borehole (sections 5.3.1 – 5.3.3) into EarthVision. Faults were also imported into EarthVision and used as interpolation barriers.

For the interpolation of the Chino and North Riverside area additional vertical faults were used. These vertical faults were defined based on gravity data and borehole data, and were used to constrain the interpolation in areas where basement rock is near the surface and the bottom stratigraphic units have pinched out into the basement rock.

Stratigraphic boundary values for each stratigraphic layer were imported into EarthVision as scattered point data. The stratigraphic horizons were then interpolated between the points using EarthVision's 3-D minimum tension algorithm using faults as interpolation barriers.

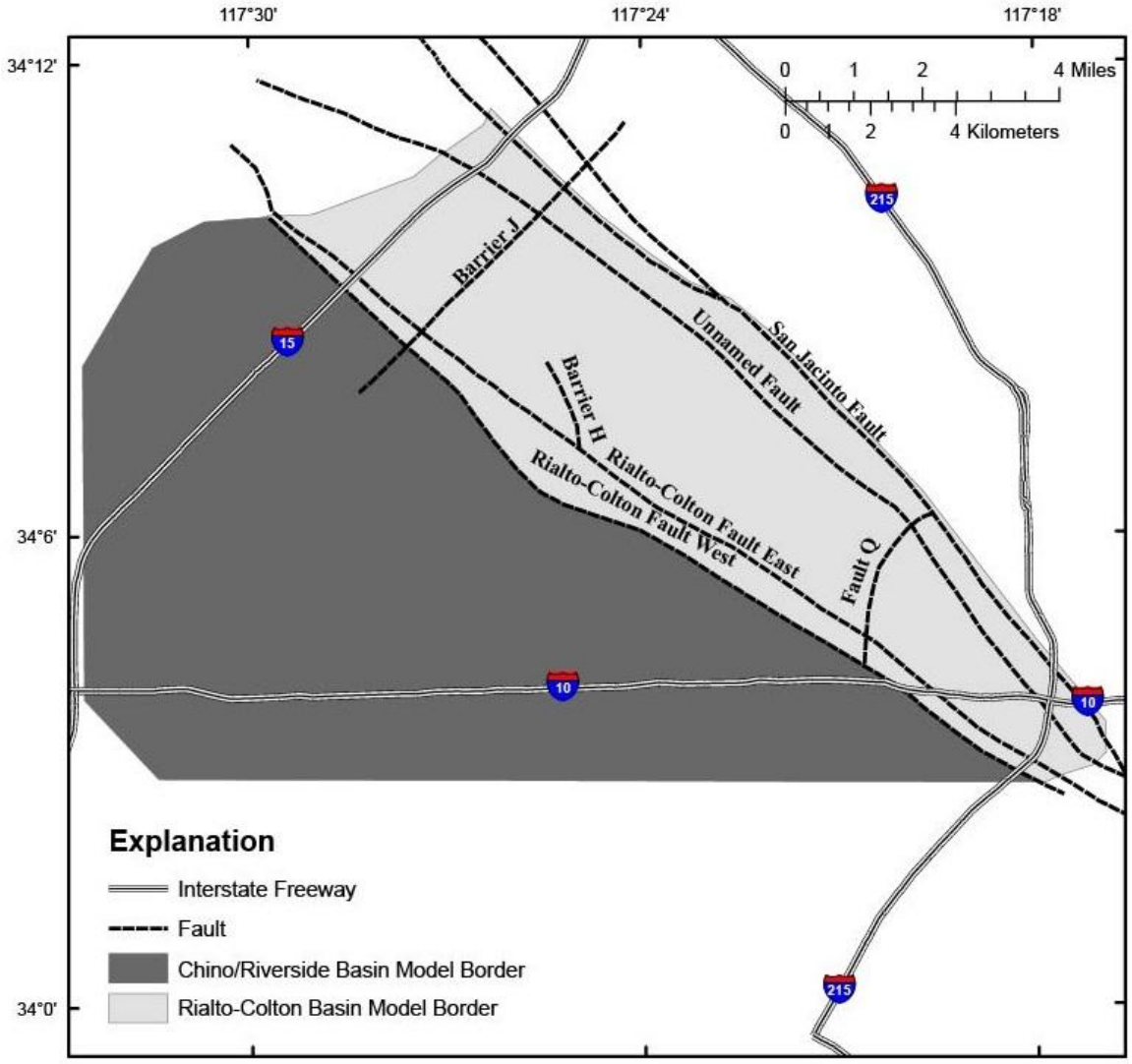

Figure 8: Model area in the Rialto-Colton Basin and in the Chino and North Riverside area.

Table 8: Wells removed from stratigraphic and property interpolations

Well	Basin	Reason Well Data Removed
1N/5W-7H1	Rialto-Colton	4
1N/5W-17G1	Rialto-Colton	1
1N/5W-28J1	Rialto-Colton	1
1N/5W-30G1	Rialto-Colton	1
1N/6W-24C1	Rialto-Colton	1
1S/4W-16L1	Rialto-Colton	3
1S/4W-18G1	Rialto-Colton	1
1S/4W-29A2	Rialto-Colton	1
1S/4W-29H1	North Riverside	2
1S/4W-32B1	North Riverside	1
1S/4W-32E9	North Riverside	1
1S/4W-32G1	North Riverside	1
1S/5W-3A1	Rialto-Colton	1
1S/5W-4D2	Rialto-Colton	1
1S/5W-24M2	North Riverside	1
1S/5W-24Q1	North Riverside	1
1S/5W-29K1	Chino	1
1S/6W-1M1	Chino	1
1S/6W-17P1	Chino	1
1S/6W-18D1	Chino	1
1S/6W-20B1	Chino	1

1 Poor quality data that does not significantly increase coverage
2 Within 800 ft of better quality data
3 Poor data quality and close to fault boundary (the exact location of the fault is not known precisely enough to accurately determine which side of the fault the data point is on)
4 On other side of Cucamonga Fault on border of study area

Some poor quality data points were removed from the stratigraphic and percent coarse interpolations. Removal of well logs with poor quality data for percent coarse modeling is suggested in "Groundwater Availability of the Central Valley Aquifer, California" (Faunt et al, 2009). Table 8 and 9 summarizes the borehole data removed from the stratigraphic interpolation and the reasons for their removal. Most data were removed due to the data being low quality data. In addition, several virtual points were added to the stratigraphic interpolation at the edges of the model where a lack of data points was causing the 3-D minimum tension algorithm to

intersect with neighboring stratigraphic boundaries (mostly for the boundaries of the lower and base units). These virtual points were added to keep extrapolations of straigraphic boundaries from intersecting with stratigraphic boundaries above or below. Figure 9 shows where data was removed and added.

Table 9: Individual stratigraphic points removed from stratigraphic interpolation

Well	**Basin**	**Horizon**	**Reason Removed**
1N/5W-17K1	Rialto-Colton	Base	Conflicts with 1N/5W-17K2. Both same quality data, but K2 is a smoother fit to the model.
1N/5W-17K1	Rialto-Colton	Middle	Conflicts with well 1N/5W-17L1 which is higher data quality.
1N/5W-17K2	Rialto-Colton	Middle	Conflicts with well 1N/5W-17L1 which is higher data quality.

Table 10: Virtual stratigraphic points added to prevent intersections with neighboring stratigraphic boundaries

Horizon	**Northing**	**Easting**	**Depth**
Base	6734794	1884898	634
Base	6764779	1859405	109.6
Base	6743766	1878965	579.8
Base	6751502	1871926	411
Base	6750781	1870964	450
Base	6769847	1844696	117
Base	6769760	1845233	99
Middle	6762346	1856422	820
Middle	6761159	1852164	820
Lower	6741129	1884377	1092

The 3-D minimum tension interpolation in EarthVision was used to interpolate the stratigraphic unit surfaces from the stratigraphic point data that are based on the borehole drillers' logs. This same technique was used to interpolate the percent coarse distribution from coarse/fine data. EarthVision uses a bicubic spline technique (Dynamic Graphics, 2009) for its minimum tension interpolation. The algorithm has a two-step approach which first generates an initial estimate

using an inverse-distance weighting function. It then uses biharmonic iterations to smooth out the data (Dynamic Graphics, 2009). This technique was used since the model area is heavily faulted and EarthVision's minimum tension interpolation supports the use of faults as interpolation boundaries.

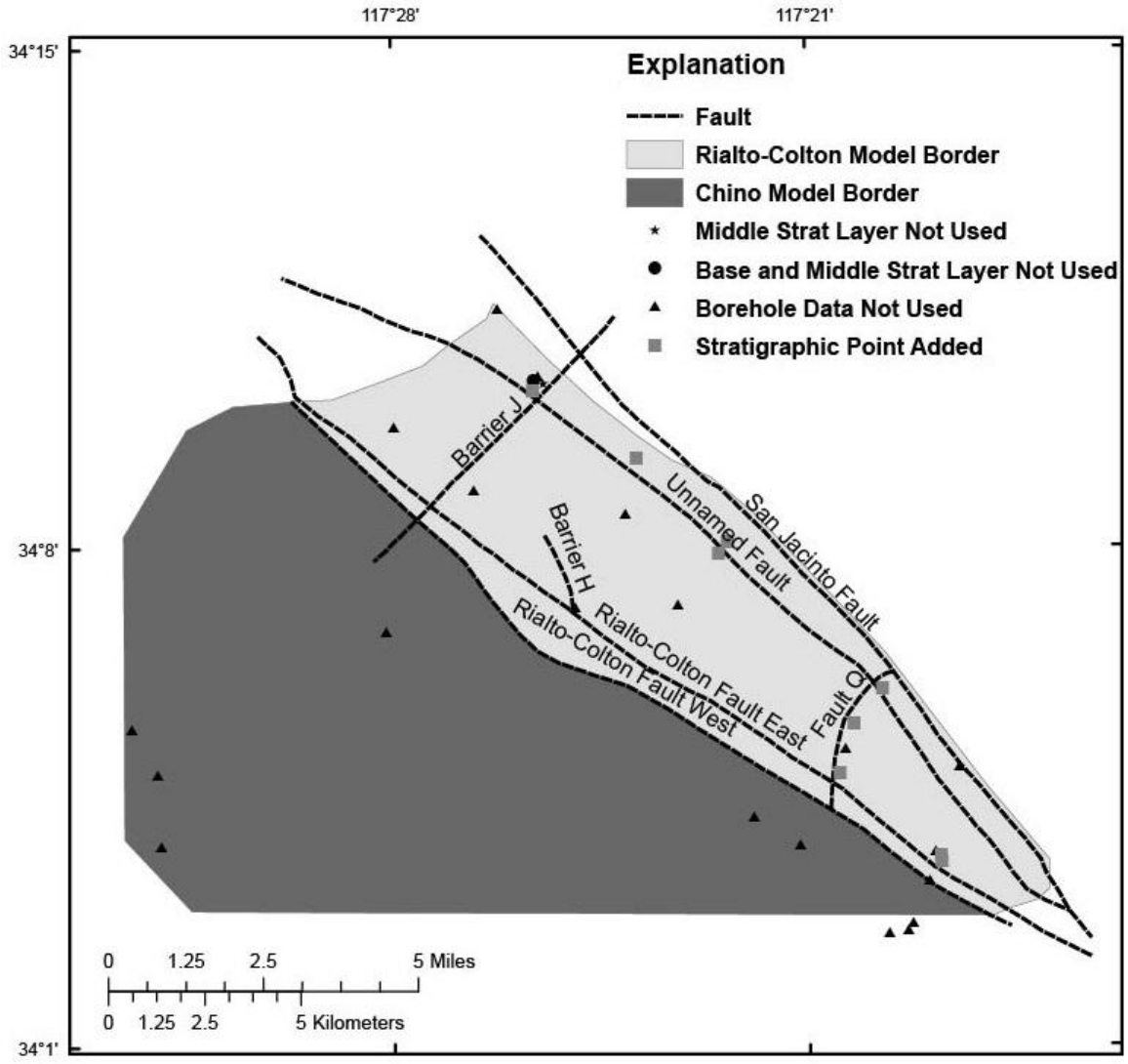

Figure 9: Poor quality data removed and virtual stratigraphic points added.

5.3.6 Rialto-Colton Basin Stratigraphic Units

Boundaries for the stratigraphic water-bearing units were determined from the geophysical analysis done on forty two boreholes in and around the basin. Boreholes containing lithology data and little or no geophysical data were used to aid in the interpolation of these data.

The EarthVision settings used for each of the stratigraphic boundaries are presented in table 11.

Table 11: Stratigraphic horizons defined in EarthVision for the Rialto-Colton Basin.

Boundary	**Operation**	**Cut By Faults**
DEM	Channel Erosion	No
Upper Boundary of River Deposits	Deposition	No
Upper Boundary of Upper Water-Bearing Unit	Deposition	No
Upper Boundary of Middle Water-Bearing Unit	Deposition	No
Upper Boundary of Perching Layer	Unconformity	Yes
Lower Boundary of Perching Layer	Deposition	Yes
Lower Boundary of Lower Water-Bearing Unit	Deposition	Yes
Upper Boundary of Aquifer Base	Deposition	Yes

All stratigraphic boundaries were reference horizons, which allowed the definition of the shape of each boundary based on the data from that boundary instead of defining the shape based primarily on adjacent boundaries. Borehole data were input into EarthVision as the points used in the interpolation of boundaries. The channel erosion operation in EarthVision was used to define the DEM boundary because it can truncate any part of underlying stratigraphic boundaries that are interpolated or extrapolated above it. The rest of the stratigraphic boundaries, with the exception of Perched Upper were defined using the deposition operation to avoid truncating underlying stratigraphic boundaries. The unconformity operation in EarthVision, which allows deposition to occur above a stratigraphic boundary, but prevents any stratigraphic unit below from both existing above and below the boundary, was used to define the Perched Upper stratigraphic

boundary. This allowed for the pinching out of the perched aquifer when the elevation of the Perched Lower stratigraphic boundary was greater than the elevation of the Perched Upper stratigraphic boundary.

Table 12 summarizes the EarthVision settings used in the interpolation of stratigraphic boundaries. Settings were chosen to minimize unrealistic trending of interpolations and extrapolations. Grid spacing was chosen to meet the expected requirements of a hydrogeologic model of this basin.

Table 12: Stratigraphic interpolation parameters used in EarthVision.

EarthVision Parameter Name	**Parameter Value**
Stratigraphic boundaries using vertical faults	Middle, Perched Upper, Perched Lower, Lower, Base
Extrapolation limits	None
Smoothing factor	0
Extrapolation factor	0
Grid spacing	400 ft by 400 ft
Smoothing	0
Extrapolation factor	0
Adj. data extrapolation factor	0
Faces files accuracy	5.5 ft

5.3.7 Cross Sections

Eleven cross sections were constructed throughout the study area with an emphasis on the Rialto-Colton Basin (Appendix B). These cross sections were constructed using EarthVision and were based on EarthVision's 3-D stratigraphic interpolation. Four cross-sections were oriented northwest to southeast along the axis of the basin and seven cross-sections were oriented southwest to northeast across the basin. One of the axial cross sections, H-H', was drawn adjacent to the Rialto-Colton Fault in the Rialto-Colton Fault Zone that divides the Rialto-Colton Basin from the Chino and North Riverside area. Cross sections were selected for coverage of the

Rialto-Colton Basin and the Rialto-Colton Fault Zone in locations where high quality borehole data were available.

5.3.8 Rialto-Colton Basin Faults

Five faults were used to divide the Rialto-Colton Basin into six fault blocks, the eastern and western traces of the Rialto-Colton Fault, the Unnamed Fault, Barrier J, and the San Jacinto Fault. Each block was interpolated separately for the stratigraphic and property (percent coarse) data.

The eastern trace of the Rialto-Colton Fault and the San Jacinto Fault are both oblique strike-slip faults with both normal and strike-slip offset. Normal offset causes a change in stratigraphic boundary depth across the fault. Due to this change in stratigraphic boundary depth, stratigraphic boundaries were modeled separately in each of the six fault blocks.

A 2-D grid of each fault was generated based on data that indicate the surface expression, the general dip angles, and dip directions of the faults. Where dip angles differed at both ends of the fault, the dip angles were linearly interpolated across the length of the fault.

Dip angles were based on previous studies and general structural information of the region (table 13). The Rialto-Colton fault dip angles were calculated in this study based on cross sections from a seismic study (Stephenson et al, 2002) on the southeastern end and were taken directly from a trench study on the northwestern end (Geophysics Unit of Menlo Park CA, 2012). The San Jacinto Fault and Unnamed Fault dip angles were calculated in this study based on Stephenson et al (2002). Since little is known about Barrier J (figure 7), the dip angle was left as near vertical.

Table 13: Fault dip directions and angles used for major faults in the Rialto-Colton Basin

Fault name	**Dip Direction**	**Dip Angle(s)**
Eastern Rialto-Colton	North-East	NW end – 53 Degrees SE end – 45 Degrees
Western Rialto-Colton	North-East	NW end – 53 Degrees SE end – 45 Degrees
San Jacinto	North-East	62 Degrees
Unnamed Fault	North-East	60 Degrees
Barrier J	North	85 Degrees

EarthVision interpolates fault boundaries based on point data points provided for each fault. For each fault data points were provided to EarthVision by:

1) Using a fault map (figure 7) to determine where the fault intersects with land surface. The intersection of each fault with land surface, the fault trace, forms a line (figure 7), but EarthVision requires point data to describe the fault. Therefore points were used along the fault trace along all bends in the fault trace.
2) For each point along the fault trace, additional points below land surface were extrapolated using the approximate dip angle and direction of the fault. The additional extrapolated points were calculated at 100 ft intervals along the dip of the fault. These extrapolated points were calculated using an Excel Spreadsheet macro written for this task.
3) Faults were interpolated from these points by EarthVision using 2-D minimum tension interpolation with trend control, a smoothing factor of 0 (0 – 1), and an extrapolation factor of 0 (0 – 1).

Barrier H and Fault Q were used as vertical fault interpolation barriers. Vertical fault interpolation barriers limit the effect that point data on one side of the boundary has on the interpolation of the other side of the boundary. The West Rialto-Colton Fault was treated as a

block bounding fault that divides the model area up between the Rialto-Colton stratigraphic units and the Chino and North Riverside stratigraphic units. Figure 7 shows the faults used to constrain the stratigraphic and percent coarse interpolation of the Rialto-Colton Basin.

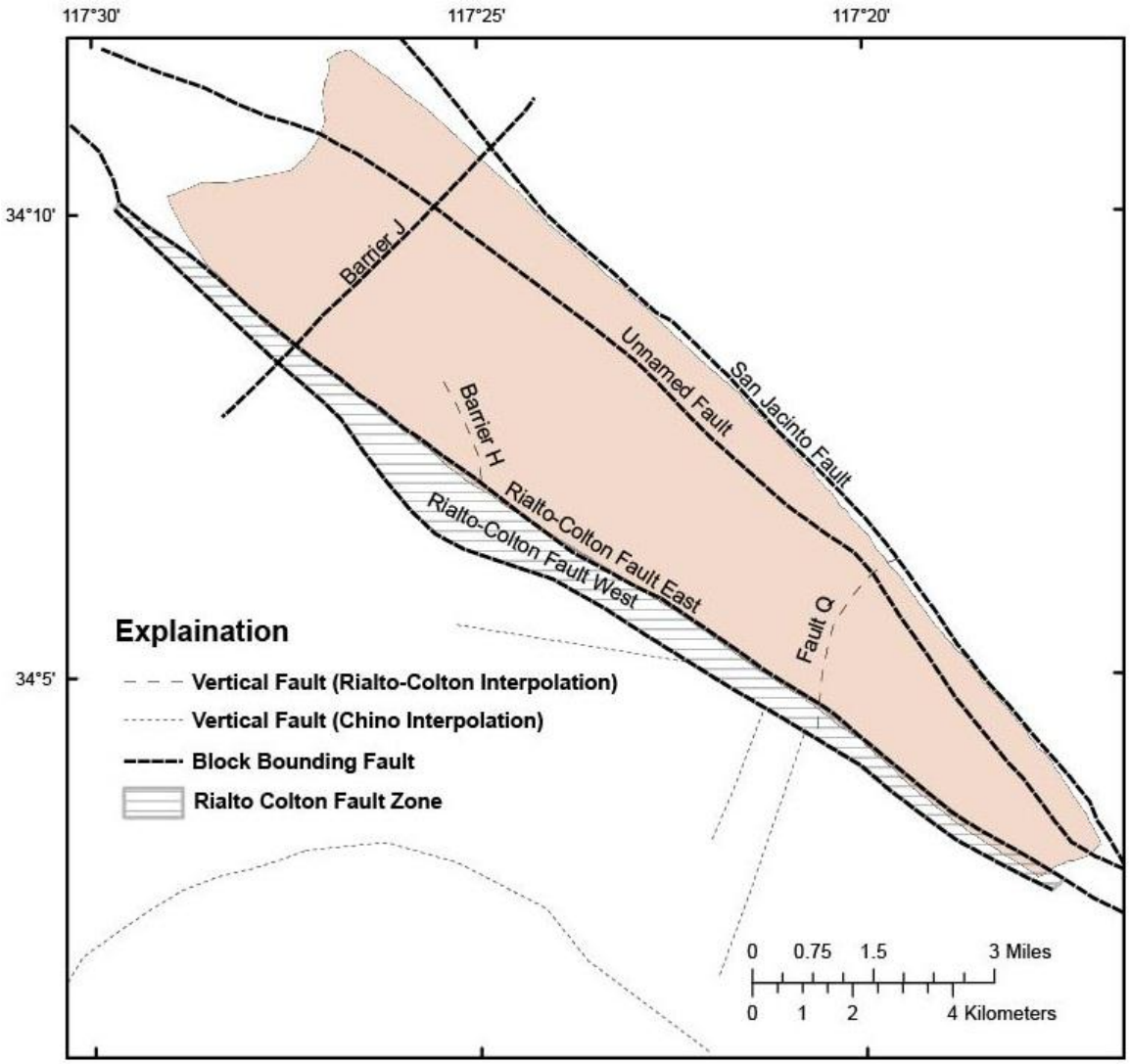

Figure 10: Faults used to bound the stratigraphic interpolation of the Rialto-Colton Basin and the Chino and North Riverside area.

5.3.9 Chino and North Riverside Stratigraphic Units

The boundaries of the stratigraphic units in the Chino and North Riverside area were determined primarily from a previous groundwater study (Wildermuth Environmental, Inc., 2003). Borehole data available in the Chino and North Riverside area consisted mostly of lithology logs with only a few geophysical logs. As a result boundaries of the stratigraphic units were largely based on previous studies. Borehole data were used mostly to refine the interpolation of data points from previous studies. The stratigraphic horizons for the Chino and North Riverside area used in EarthVision are shown in table 14.

Table 14: Stratigraphic horizons defined in EarthVision for the Chino and North Riverside area.

Horizon	**Horizon Type**	**Operation**	**Cut By Faults**
DEM	Reference	Channel Erosion	No
Chino Layer 1	Reference	Deposition	No
Chino Layer 2	Reference	Deposition	No
Chino Layer 3	Reference	Deposition	Yes
Base	Reference	Deposition	Yes

5.3.10 Chino Section Faults

The Rialto-Colton Fault West (western side of the Rialto-Colton Fault Zone) was used as a boundary separating the Chino and North Riverside area stratigraphic units from Rialto-Colton stratigraphic units (figure 8). In addition, four unnamed faults in the North Riverside area were used as stratigraphic interpolation boundaries. These vertical faults do not correspond to faults cited in any previous studies and were used to control the pinching out of the lower stratigraphic units (Chino Layer 3) with bedrock in areas of near-surface bedrock. The faults used in the Chino and North Riverside area stratigraphic interpolation are shown as dotted lines in figure 7.

5.4 Percent Coarse Determination for each Borehole

Percent coarse values were determined using both resistivity logs and lithology logs. Borehole texture/lithology were classified into Boolean values (coarse (1) or fine (0)) of texture at one foot intervals along the borehole starting at the topmost elevation. The top of each coarse interval was determined from the land surface elevation and the depth to the top of the interval. The easting and northing coordinates were determined from the mapped location of the boreholes. All boreholes were assumed to be vertical.

Coarse grained intervals were assigned a value of 1 (100% coarse material) and fine-grained intervals were assigned a value of 0 (0% coarse material). These point values were then interpolated by EarthVision to generate a distribution of percent coarse values ranging from 0 to 1.

5.4.1 Percent Coarse Determination Using Lithologic Logs

For many boreholes only lithologic logs were available. In this case lithologic logs were exclusively used in the determination of percent coarse values.

Table 15: Primary textures and corresponding lithologies

Primary Texture	**Corresponding Lithologies**
Altered Granite	Altered Granite
Clay	Clay, Clay/Sand, Clay/Gravel, Clay/Sand/Gravel
Cobbles	Cobbles/Boulders
Concrete	Concrete
Conglomerate	Conglomerate
Gravel	Gravel, Gravel/Clay, Gravel/Sand, Gravel/Silt
Limestone	Limestone
Sand	Sand, Sand/Clay, Sand/Gravel, Sand/Gravel/Clay, Sand/Silt, Sand/Silt/Clay
Sandstone	Sandstone
Shale	Shale
Silt	Silt, Silt/Clay, Silt/Gravel, Silt/Sand

Table 16: Texture modifiers and corresponding lithologies

Texture Modifier	**Corresponding Lithologies**
Bouldery	Cobbles/Boulders
Clayey	Gravel/Clay, Sand/Clay, Sand/Gravel/Clay, Sand/Silt/Clay
Gravelly	Clay/Gravel, Clay/Sand/Gravel, Sand/Gravel, Sand/Gravel/Clay, Silt/Gravel
Sandy	Clay/Sand, Clay/Sand/Gravel, Gravel/Sand, Silt/Sand
Silty	Gravel/Silt, Sand/Silt, Sand/Silt/Clay

Lithology descriptions (lithology types and comments) stored in Rockworks were used to determine percent coarse values. The lithologic descriptions (lithology type and comments) in the drillers' logs were converted into textures, texture modifiers, and texture qualifiers as given in tables 15-17. These texture fields were then converted by a Microsoft Access application (written by the USGS) into coarse/fine Boolean values based on the algorithm defined below.

Table 17: Texture qualifiers extracted from drillers' log descriptions

Texture Qualifier Keyword
Brittle
Cemented
Coarse
Coarse-Cem.
Consolidated
Fine
Fine to medium
Hard
Joint
Loose
Medium
Medium to coarse
Packed
Semi-consolidated
Set
Small
Soft
Tight
Very Fine
Very Coarse

An interval was determined to be either coarse or fine based on the primary texture, texture modifiers, and texture qualifiers of that interval. The following textures were always considered coarse:

- Cobbles
- Conglomerate

The following textures were always considered fine:

- Altered Granite
- Clay
- Concrete
- Limestone
- Sandstone
- Shale
- Silt

The following rules were used to determine coarse/fine values for the textures not defined above.

1) Gravel was considered coarse unless it had one or more of the texture modifiers cemented, clayey, or silty, in which case it was considered fine.
2) Sand was considered coarse unless had one or more of the texture modifiers clayey or silty, or the texture qualifier cemented, consolidated, or hard, in which case it was considered fine.

5.4.2 Percent Coarse Determination Using Resistivity Data

A resistivity log percent coarse calculator, an Excel application designed by the USGS, was used to determine fine or coarse Boolean values for the available resistivity logs. The resistivity log

percent coarse calculator allows for the division of the resistivity log into up to four sections based on depth. For each section a dividing value is assigned so that every resistivity reading above that dividing value is considered coarse sediment and every resistivity reading below the dividing value is considered fine sediment. The resistivity log percent coarse calculator then generates a coarse or fine value for every resistivity value in the resistivity log.

The resistivity logs also were interpreted in conjunction with water-level and lithology logs. The resistivity logs were broken into separate sections by depth based on water levels and lithology logs, if available. The dividing values of each vertical section (resistivity values above the dividing value indicated coarse sediment and resistivity values below the dividing value indicated fine sediment) were chosen so that the resistivity log generated similar coarse or fine Boolean values to the lithology log. When only resistivity data were available for a borehole, the resistivity logs were interpreted in conjunction with surrounding borehole lithology and water level data. The coarse and fine Boolean values for boreholes with resistivity data were then combined with the coarse and fine Boolean values for boreholes with only lithology logs.

5.4.3 Percent Coarse Interpolation

A 3-D minimum tension interpolation algorithm was used to interpolate percent coarse data. Interpolation was done using both faults and stratigraphic unit boundaries as interpolation boundaries. The same boundaries and interpolation settings from the stratigraphic boundary interpolation were also used in the percent coarse interpolation. Two separate percent coarse models were used, one for the Rialto-Colton Basin, the other for the Chino and North Riverside area (figure 4). The western edge of the Rialto-Colton Fault Zone was used as a dividing line between these two models.

Faults were used as interpolation boundaries of the percent coarse interpolation because the percent coarse values on one side of a fault are not necessarily representative of the percent coarse values on the other side of a fault.

The 3-D minimum tension algorithm gives weight to data points based on their distance from the point being interpolated. The percent coarse value of an interpolated point is influenced more by a nearby data point than a distant data point. If faults were not used as interpolation boundaries a data point on one side of a fault would have a significant influence on a nearby interpolation point on the other side of the fault. This can be problematic since the sediment on one side of a fault may not have been deposited adjacently to the sediment on the other side of the fault due to the sediment deposits being offset by the fault.

There is about 600 meters (m) of vertical normal offset and 2 kilometers (km) of right lateral offset on the Rialto-Colton Fault and 25 km of right lateral offset and 1 km of vertical normal offset on the San Jacinto Fault (Wisely and Schmidt, 2010). The Rialto-Colton Basin is about 10 miles long and varies between 3.5 and 1.5 miles in width (Woolfenden and Koczot, 2001). The offset on the Rialto-Colton Fault is therefore about 12 percent of the length of the basin and the offset on the San Jacinto Fault is about 155 percent of the length of the basin.

Sediment on either side of the Rialto-Colton or San Jacinto fault is offset by miles. The percent coarse of the sediment on one side of the fault therefore is not necessarily a good indicator of the percent coarse of the sediment on the other side. Therefore these faults were used as interpolation boundaries so that the data points on one side of the fault do not influence the interpolation on the other side of the fault.

Additionally, the Unnamed Fault and Barrier J were used as interpolation boundaries. While no information was available for this study on the offset of these faults, it is known that these faults act as water barriers (Woolfenden and Koczot, 2001), and therefore must offset the alluvium where they act as water barriers. Given this, and given the offset of the nearby Rialto-Colton fault and San Jacinto fault, it was decided to use these faults as interpolation boundaries.

Table 18: Percent Coarse interpolation parameters used in EarthVision.

EarthVision Parameter Name	**Setting Using**
Gridding Method	3-D Minimum Tension
Property range	None
Vertical Influence	0
Modeling Domain	In Situ (Actual)
Grid spacing	400 ft by 400 ft by 10 ft
Property isosurface interval	0.05
Vertical influence	0
Trend degree	1
Modeling domain	Actual

6 Results

6.1 Structure of the Rialto-Colton Basin

Borehole geophysical and lithology logs were analyzed and gravity, magnetic, seismic, and InSAR data from previous studies were used and analyzed to determine the structural components of this conceptual model. The geophysical and lithology logs were analyzed to locate the boundaries of water-bearing units. The gravity, magnetic, seismic, and InSAR data were used and analyzed in evaluating fault locations.

6.1.1 Aquifer Base

The base of the aquifer in the Rialto-Colton Basin is the uppermost surface of the consolidated Tertiary continental deposits. Below the consolidated deposits is bedrock (Woolfenden and Kadhim, 1997).

6.1.2 Northeastern Basin Subsidence

Analysis of data for this study indicates Quaternary subsidence in this area. Evidence of subsidence in this region can be seen in this study's cross sections of the Rialto-Colton Basin. A gradual thickening of the Upper and Middle Water-Bearing Units in the cross sections C-C' J-J', and D-D' from southwest to northeast suggests that this area may have been recently subsiding (Appendix B, Figures 81, 82, and 87).

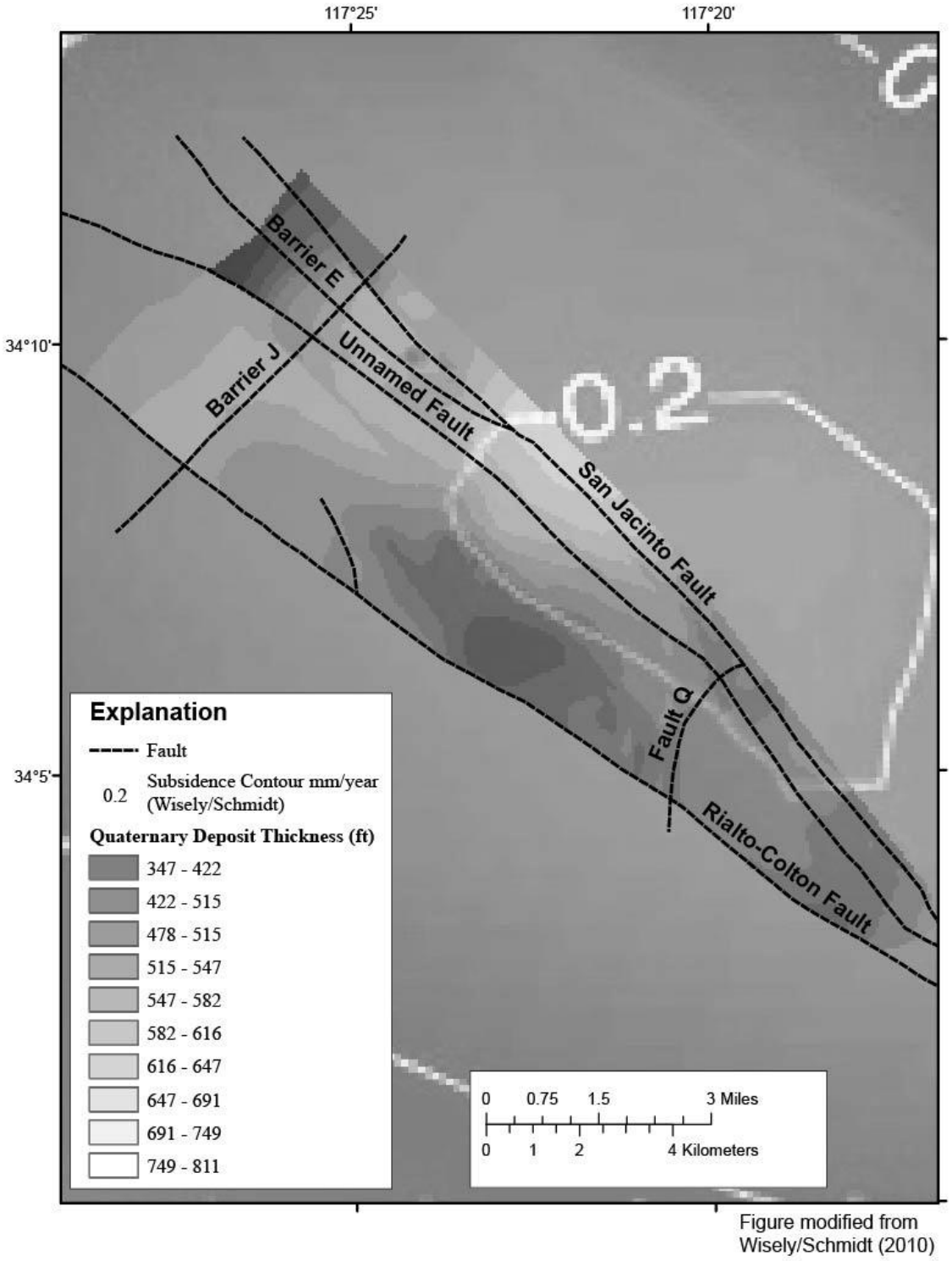

Figure 11: Thickness of selected Quaternary deposit (River Deposits, Upper, and Middle Water-Bearing Units) and calculated subsidence from Wisely and Schmidt (2010).

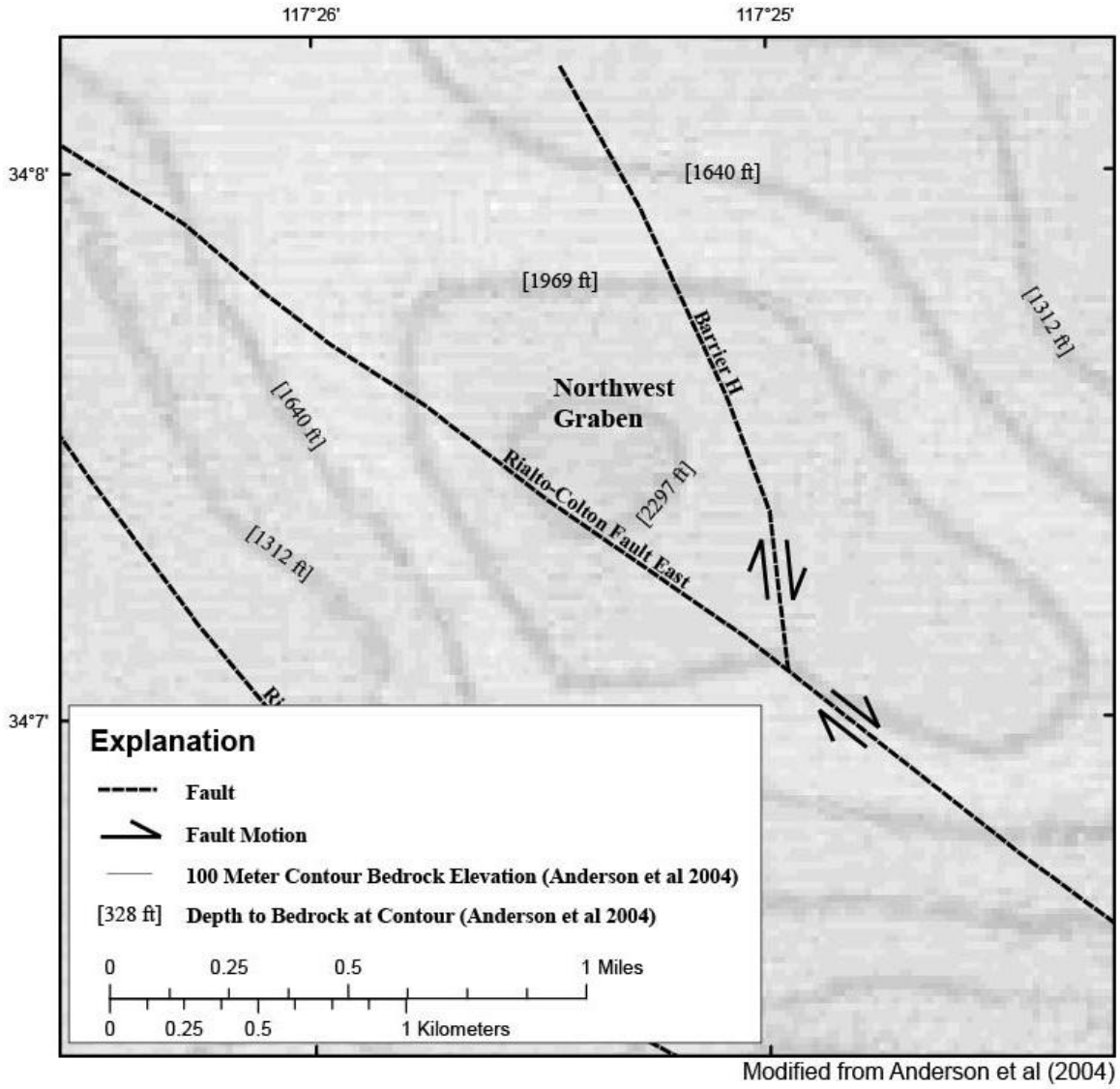

Figure 12: Releasing bend at intersection of Rialto-Colton Fault and Barrier H with bedrock elevation contours superimposed.

The stratigraphic interpolation of the upper and middle water bearing units (section 5.3.5) was used in figure 11 to plot the combined thickness of the top two water-bearing units throughout the Rialto-Colton Basin. The combined thickness of the top two water-bearing units increases to the northeast (Figure 11). This is in agreement with Wisely and Schmidt (2010), that concluded that

there were areas of tectonic uplift and subsidence in the vicinity of the Rialto-Colton Basin (figure 11).

6.1.1 Tertiary Subsidence near Barrier H

Past subsidence and uplift in this area can be inferred from gravity data. Gravity data (Anderson et al, 2004) indicates there is a graben between Barrier H and the Rialto-Colton Fault (figure 12). If Barrier H is an inactive splay of the Rialto-Colton Fault, the right lateral offset of Barrier H and the Rialto-Colton Fault could have acted as a releasing bend. Releasing bends generally lead to subsidence, which is consistent with the graben in this area (figure 12).

Cross section J-J' shows a thicker Lower Water-Bearing Unit between the Rialto-Colton Fault and Barrier H (figure 87). Subsidence in this area could explain the increased thickness of this unit. The Lower Water-Bearing Unit contains mostly tertiary deposits, suggesting that the graben may have formed in the Tertiary period.

6.1.2 Fault Locations

The location and extent of the Rialto-Colton Fault and Barrier H have not been mapped consistently in previous studies (figure 17). These studies include Dutcher and Garrett (1963), Fox and Roberts (1995), Woolfenden and Kadhim (1997), Anderson et al (2004), and Wisely and Schmidt (2010). Also, a number of previously unmapped faults in the Rialto-Colton Basin have been suggested based on seismic and gravity data. A seismic study of the San Bernardino area describes a seismic transect in the southeast part of the Rialto-Colton Basin (Stephenson et al, 2002). The results of the study indicate only two faults in the Rialto-Colton Basin area along this transect, the Rialto-Colton Fault and the San Jacinto Fault. In 2008 a seismic study describes another seismic transect in the southeast part of the Rialto-Colton Basin (Catchings et al, 2008). The study indicated that there are six faults in this area. The 2008 study refers to a Rialto-Colton

Fault Zone containing multiple faults. Results from a gravity and aeromagnetic study by Anderson et al (2004) indicate that the middle portion of the Rialto-Colton Fault differs from the previously mapped location delineated in Dutcher and Garrett (1967). Results described in a USGS open file report (Anderson et al, 2000) indicate that the middle and northern portions of the fault are a fault zone. Figure 13 shows the different interpreted locations of the Rialto-Colton Fault with water-level data from CH2MHILL (2009).

For this study, the location and extent of the faults in the conceptual model of the basin are based on available data and information and include only those that were determined to be barriers to groundwater flow. The location and extent of faults for this study have four main differences from the mapped faults delineated in Woolfenden and Kadhim (1997) (figure 19).

1. The Rialto-Colton Fault is a fault zone that includes two main traces.
2. Barrier H is shorter and splays from the Rialto-Colton Fault at a greater angle.
3. Fault Q is mapped as a fault bounding a buried sediment-filled graben.
4. The Unnamed Fault splays from the San Jacinto Fault further to the southeast in the Rialto-Colton Basin.

6.1.2.1 Rialto-Colton Fault Location and the Rialto-Colton and San Jacinto Fault Zones

The seismic data (Catchings et al, 2008) shown in figure 13 shows that the southeastern part of the Rialto-Colton Basin is highly faulted and that these faults are contained in a single fault zone. However, seismic data in the northwestern part of the Rialto-Colton Basin are not available; hence the extent of these faults to the northwest is unknown.

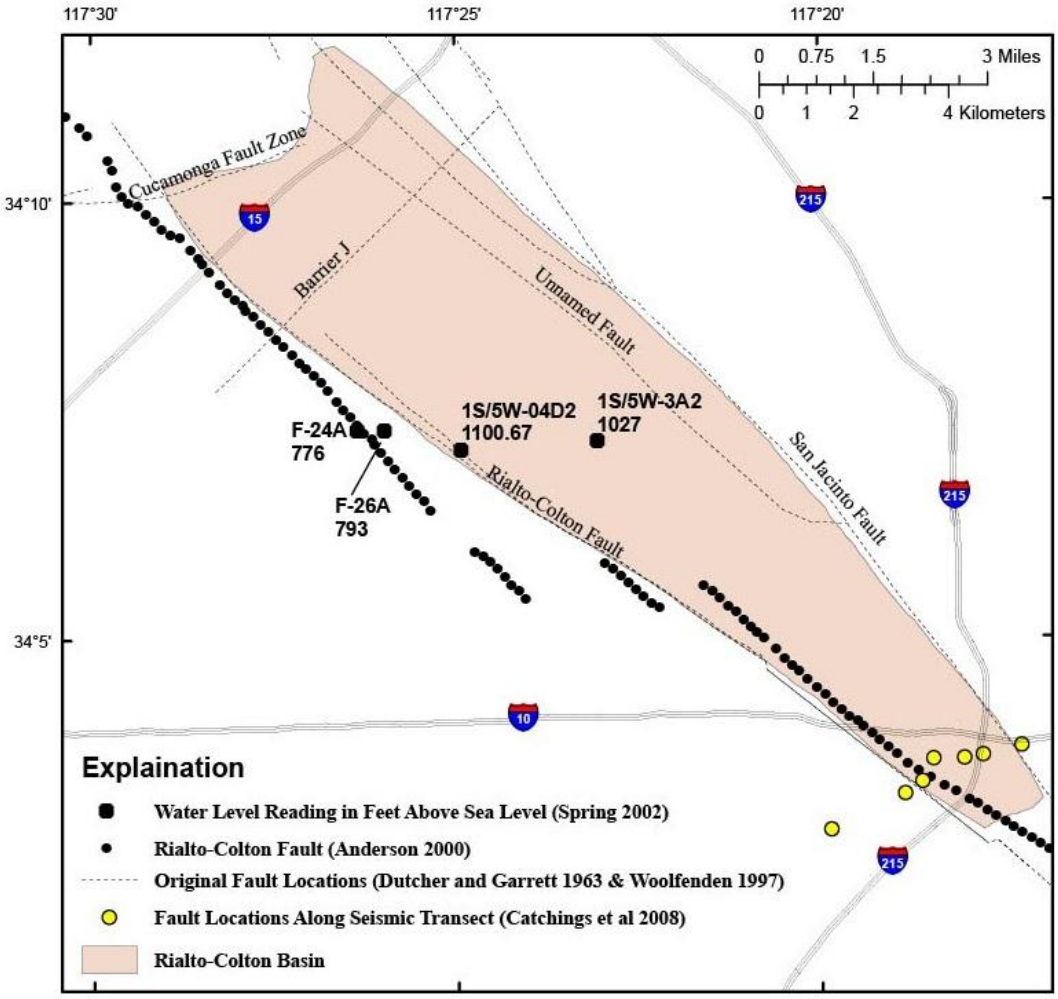

Figure 13: Rialto-Colton Fault location from Anderson et al. (2000), historic Rialto-Colton Fault location from Dutcher and Garrett (1967), fault locations from seismic data (Catchings et al, 2008), and water level data (CH2MHILL, 2009)

The Rialto-Colton Fault has been described as a water barrier in the northwestern part of the basin in previous work (Woolfenden and Koczot, 2001). The water-level data shown in figure 13 supports the barrier effect of the historic location of the Rialto-Colton Fault while the Rialto-Colton Fault mapped by Anderson et al. (2004) does not. Water levels in the vicinity of the Anderson et al. (2004) mapped fault near Barrier H do not change significantly from one side of the fault to the other (figure 13). The interpreted fault locations from

Catchings et al (2008 indicate that the main trace of the Rialto-Colton Fault likely lies between the fault trace mapped by Anderson et al (2004) and the historic fault location (figure 13).

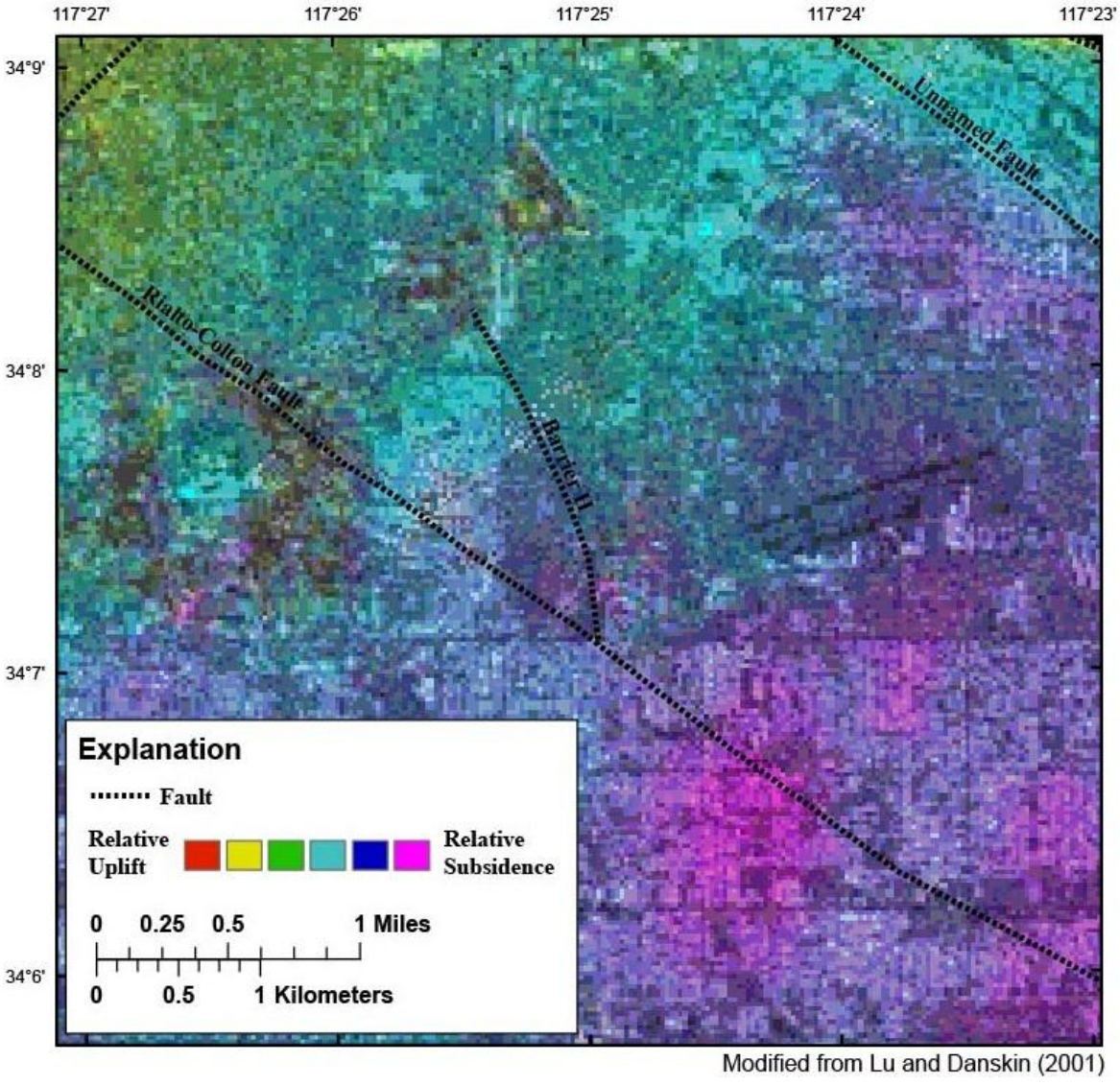

Figure 14: InSAR interferogram of Northwest Rialto-Colton Basin 12/25/1992 to 8/27/1993. Concentric color patterns indicate relative uplift and subsidence.

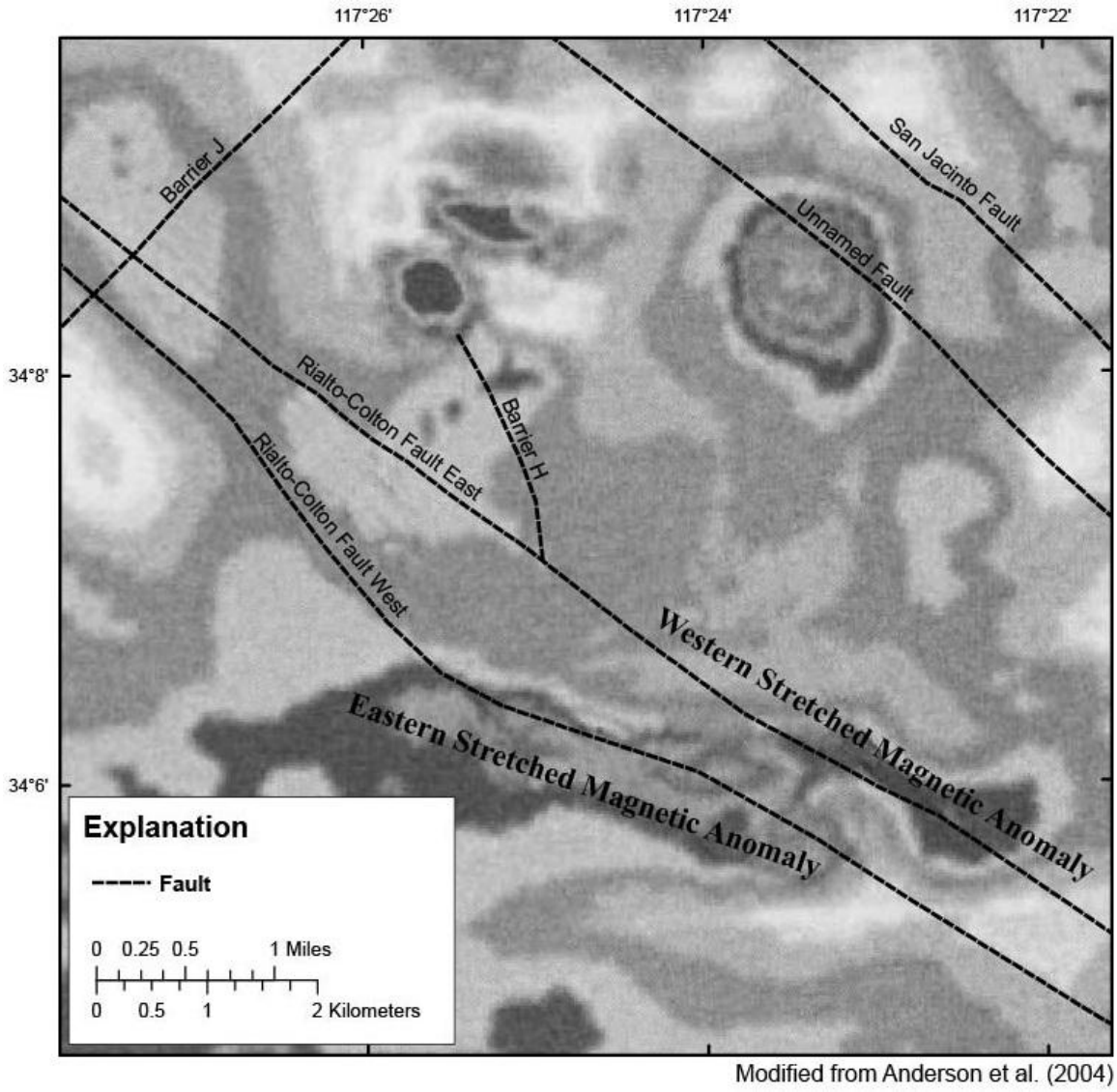

Figure 15: Aeromagnetic data showing eastern and western magnetic anomalies.

The results of the studies by Anderson et al (2004) and Catchings et al (2008) suggest that the Rialto-Colton Fault is a zone containing multiple faults. Given this, both the Anderson et al (2004) and historic locations of the Rialto-Colton Fault could be a realistic configuration, with the historic location being the main water barrier on the northeastern side of the Rialto-Colton Fault Zone, and the Rialto-Colton Fault from Anderson et al (2004) being the main barrier on the southwestern side of the Rialto-Colton Fault Zone (figure 16).

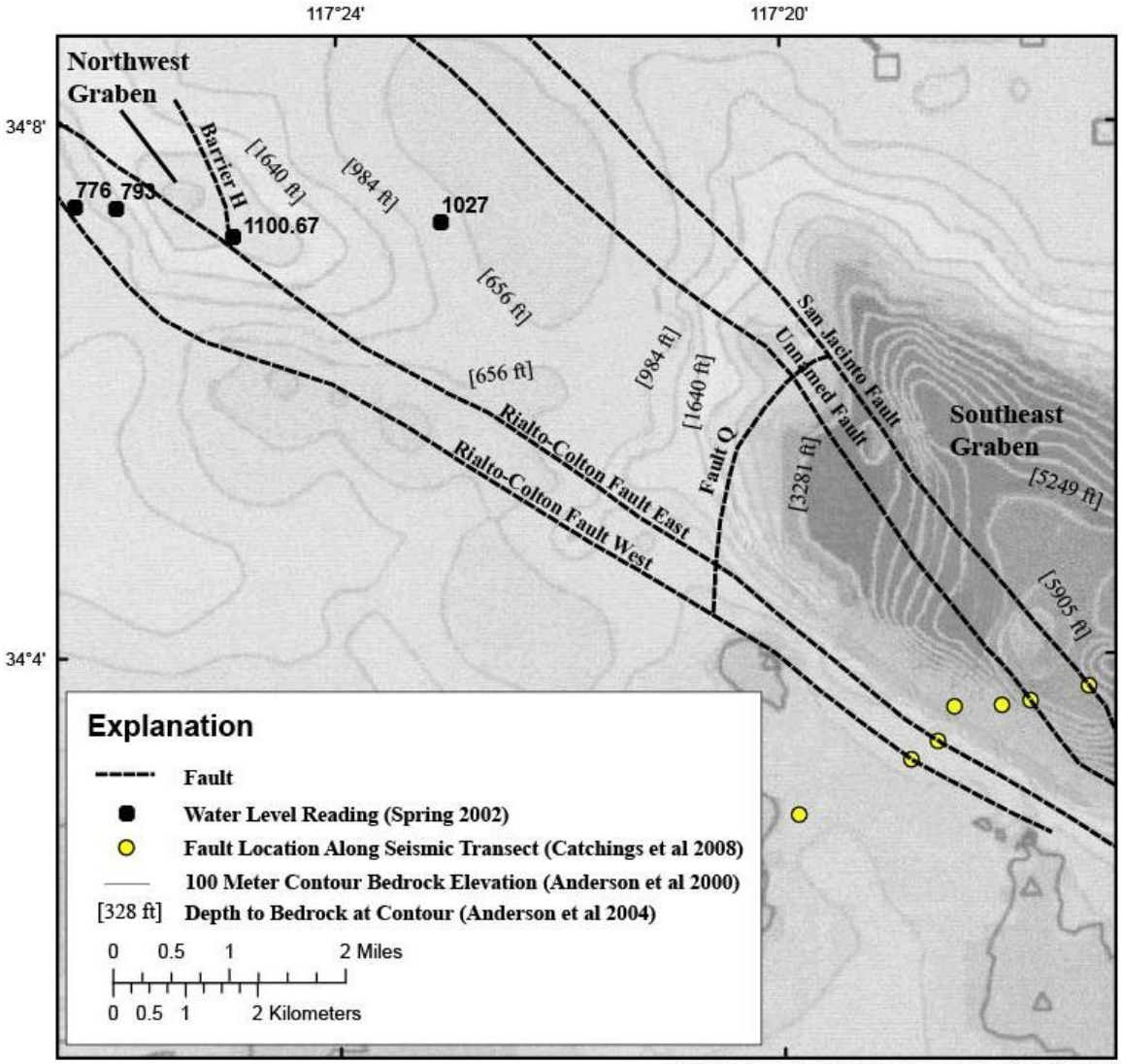

Figure 16: Seismic fault location data (Catchings et al, 2008), gravity data (Anderson et al 2004), and water level location data.

InSAR data from Lu and Danskin (2001) supports the existence of an eastern Rialto-Colton Fault (figure 14). The Eastern Rialto-Colton Fault divides regions with differing amounts of uplift/subsidence, suggesting it may be acting as a water barrier in this region. Magnetic data from Anderson et al (2004) supports the existence of a western Rialto-Colton Fault (figure 15).

A magnetic anomaly is a region where there are significantly different aeromagnetic readings. If an anomaly is highly linear, it may be interpreted as having been stretched from a circular shape as the result of faulting. In figure 15 there are two magnetic anomalies that are stretched, suggesting there might be strike-slip motion. If movement along the Rialto-Colton Fault was responsible for the western stretched magnetic anomaly (figure 15), the Rialto-Colton Fault would have to trend more to the west in this area in order to bisect the magnetic anomaly.

If movement along the Rialto-Colton Fault was responsible for the eastern portion of the stretched anomaly the Rialto-Colton Fault would have to trend more to the east in order to bisect the anomaly. A Rialto-Colton Fault Zone, containing both western and eastern traces of the Rialto-Colton Fault could account for the east and west stretched anomalies.

On the basis of the data and information presented here, the Rialto-Colton Fault Zone (RCFZ) in this study is bounded by a main trace on the eastern side of the zone (Rialto-Colton Fault East) and another main trace on the western side of the zone (Rialto-Colton Fault West). A RCFZ with an east and a west Rialto-Colton Fault is consistent with the InSAR, magnetic, seismic, and water level data. These two faults also are indicated in the seismic studies in the southeast and can be extended to the northwest in a way that is consistent with the InSAR, magnetic, gravity, and water level studies. The Rialto-Colton Fault East is the main water barrier with the Rialto-Colton Fault West bisecting most of the stretched magnetic anomaly.

6.1.2.2 Barrier H Fault Existence/Location

The existence of Barrier H is based on water-level differences found on either side of the barrier (Fox and Roberts, 1995). The location and extent of Barrier H is not consistent in previous work. It is mapped in some studies (Dutcher and Garrett, 1963; Woolfenden and Kadhim, 1997; Lu and Danskin, 2001; GeoSyntec Consultants, 2006; Wisely and Schmidt, 2010) as a long narrow fault

closely paralleling the Rialto-Colton Fault while it is mapped in other studies (Fox and Roberts, 1995; Woolfenden and Koczot, 2001; CH2MHILL, 2010; CH2MHILL, 2012) as a shorter fault splaying at a greater angle from the Rialto-Colton Fault (figure 17).

According to a study of the Rialto-Colton Fault by Fox and Roberts (1995), Barrier H is a minor fault which extends to the northeast from its junction with the Rialto-Colton Fault. The study states that there is no evidence to indicate that this splay continues for more than a short distance and that the area within the splay is in hydraulic continuity with nearby wells located to the north and to the east of the splay. This suggests that Barrier H may not be a barrier to groundwater flow.

The 1995 study is based primarily on water level and water chemistry data. While differences in water level support the existence of a Barrier H, water chemistry data shows that the areas on either side of Barrier H are in continuity.

Based on data from an InSAR study (2001), differences in ground displacement show the possibility of a water barrier near where the shorter Barrier H splaying at a higher angle has been postulated (figure 14). Furthermore, gravity data indicates there is a several hundred-foot deep graben located between the Rialto-Colton Fault and the shorter Barrier H splaying at a higher angle (figure 16).

In addition, cross section J – J’ (figure 87) shows a significant thickening of the Lower Water-Bearing Unit (Tertiary deposits) between well F-10B on the west side of Barrier H and F-49A on the east side. These wells are less than 500 feet apart.

Given this evidence, Barrier H was drawn as a shorter fault than that originally mapped by Dutcher and Garrett, that protrudes from the Rialto-Colton Fault at a greater angle (figure 17).

This orientation of Barrier H separates areas of different vertical displacement indicated in the InSAR data (figure 14) and is consistent with the location of the graben from the gravity study (figure 16) between Barrier H and the Rialto-Colton fault.

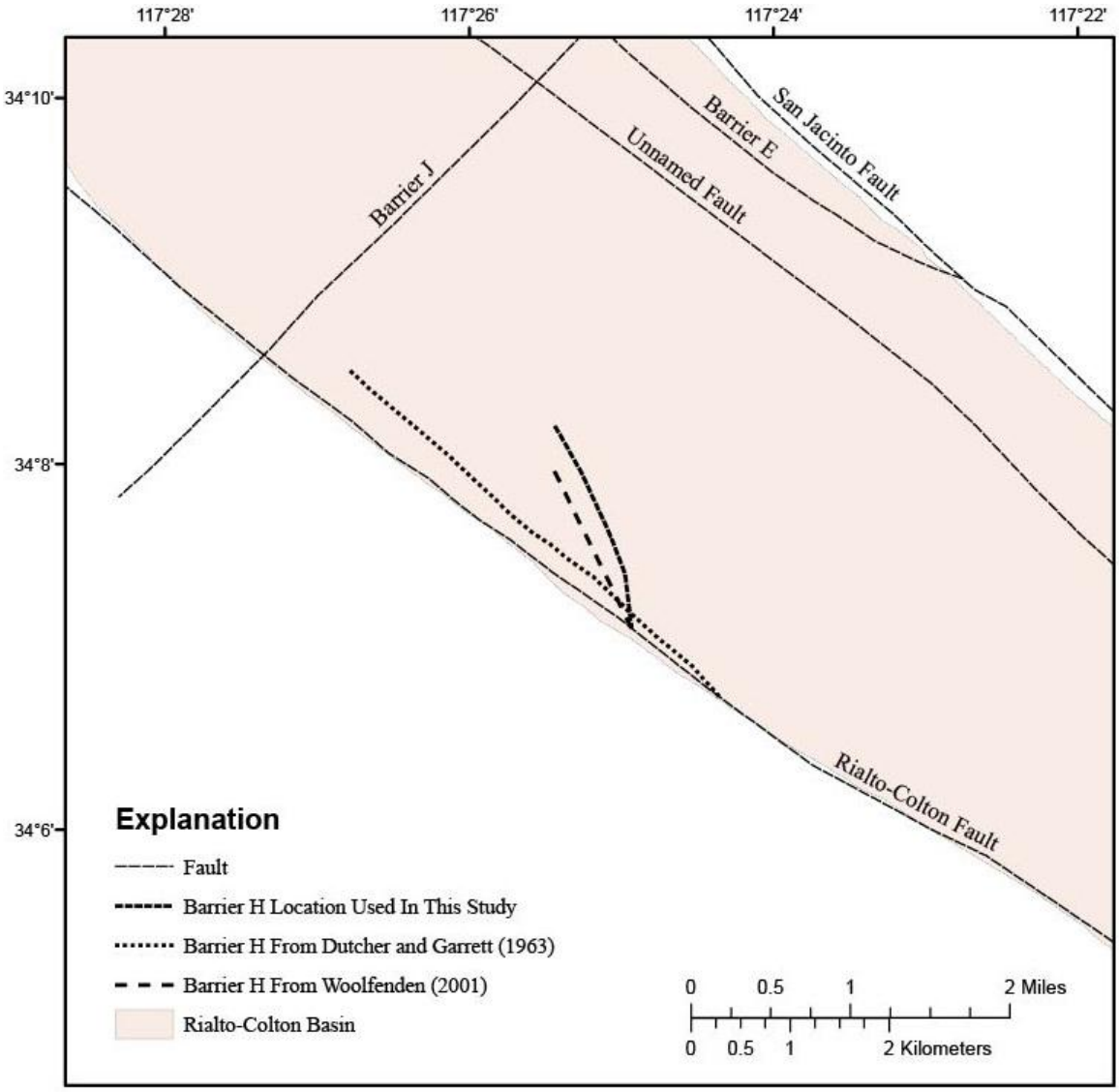

Figure 17: Different locations Barrier H has been drawn in previous studies.

6.1.2.3 Fault Q Location and Extent

Fault Q bounds the northwestern side of a sediment filled graben described by Anderson et al (2004) in a gravity and aeromagnetic study (figure 16). In addition to the gravity study, InSAR data from Lu and Danskin (2001) suggests that a water barrier might be in the vicinity of the proposed Fault Q (figure 18). Sufficient borehole and water-level logs immediately southeast of Fault Q were not available to determine if Fault Q is a barrier to groundwater flow. However, two different water levels studies (Woolfenden and Koczot, 2001; CH2MHILL, 2009) show groundwater flow direction changing from northwest to southeast flow on the northwest side of Fault Q to northeast to southwest flow on the southeast side of Fault Q.

6.1.2.4 The Unnamed Fault and Additional Northwest to Southeast Striking Faults

As previously mentioned, a recent seismic study (Catchings et al, 2008) indicates that the southeastern end of the Rialto-Colton basin is heavily faulted (figure 13). The results from the seismic study associated these faults with the Rialto-Colton Fault Zone (RCFZ) and San Jacinto Fault Zone (SJFZ), suggesting that they run parallel to the Rialto-Colton and San Jacinto Faults. This recent seismic study also indicates there is a fault along a seismic profile just south-west of the intersection of the I-10 and I-215 freeways (figure 17 of the study). If the mapped location of the unnamed fault is extended south along the basin, it intersects one of the faults indicated along this seismic profile (figure 16). It is therefore possible that the unnamed fault extends southeast and runs the entire length of the Rialto-Colton Basin. InSAR data provides additional evidence that the unnamed fault may extend further to the southeast than mapped in previous studies. InSAR data shown in figure 18 suggest that a southern extension of the unnamed fault may act as a barrier to groundwater flow in some locations.

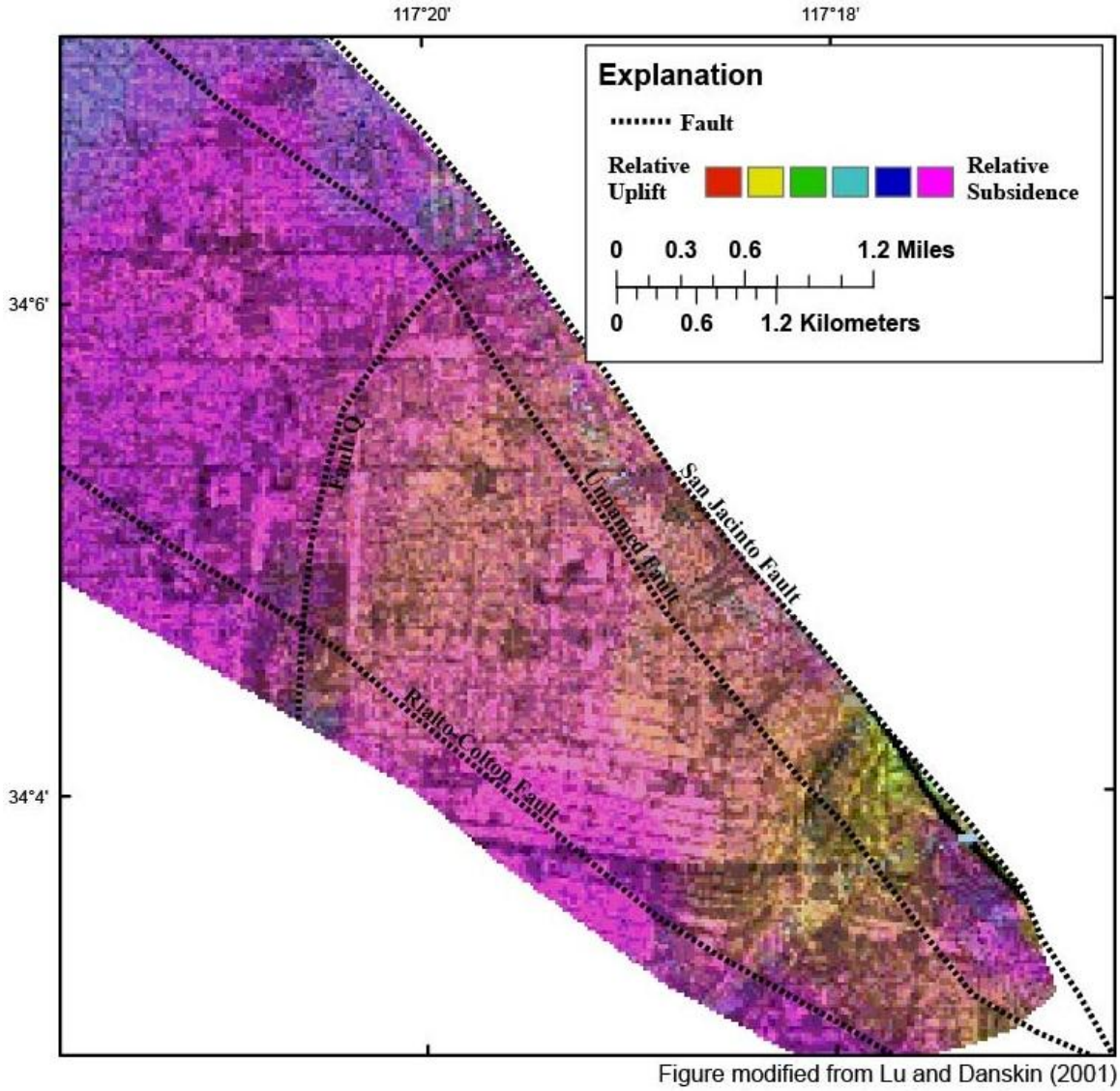

Figure 18: InSAR interferogram of southeast Rialto-Colton Basin 12/25/1992 to 8/27/1993 (Lu and Danskin, 2001).

Extending the unnamed fault further to the southeastern part of the basin may not significantly change its effectiveness as a barrier to groundwater flow. Fault Q intersects the San Jacinto Fault where previous studies have the unnamed fault splaying off of the San Jacinto Fault (figure 18). Fault Q therefore might act as a barrier to groundwater flow in the area that is bounded by the unnamed fault in the southeast and the San Jacinto Fault in the northwest.

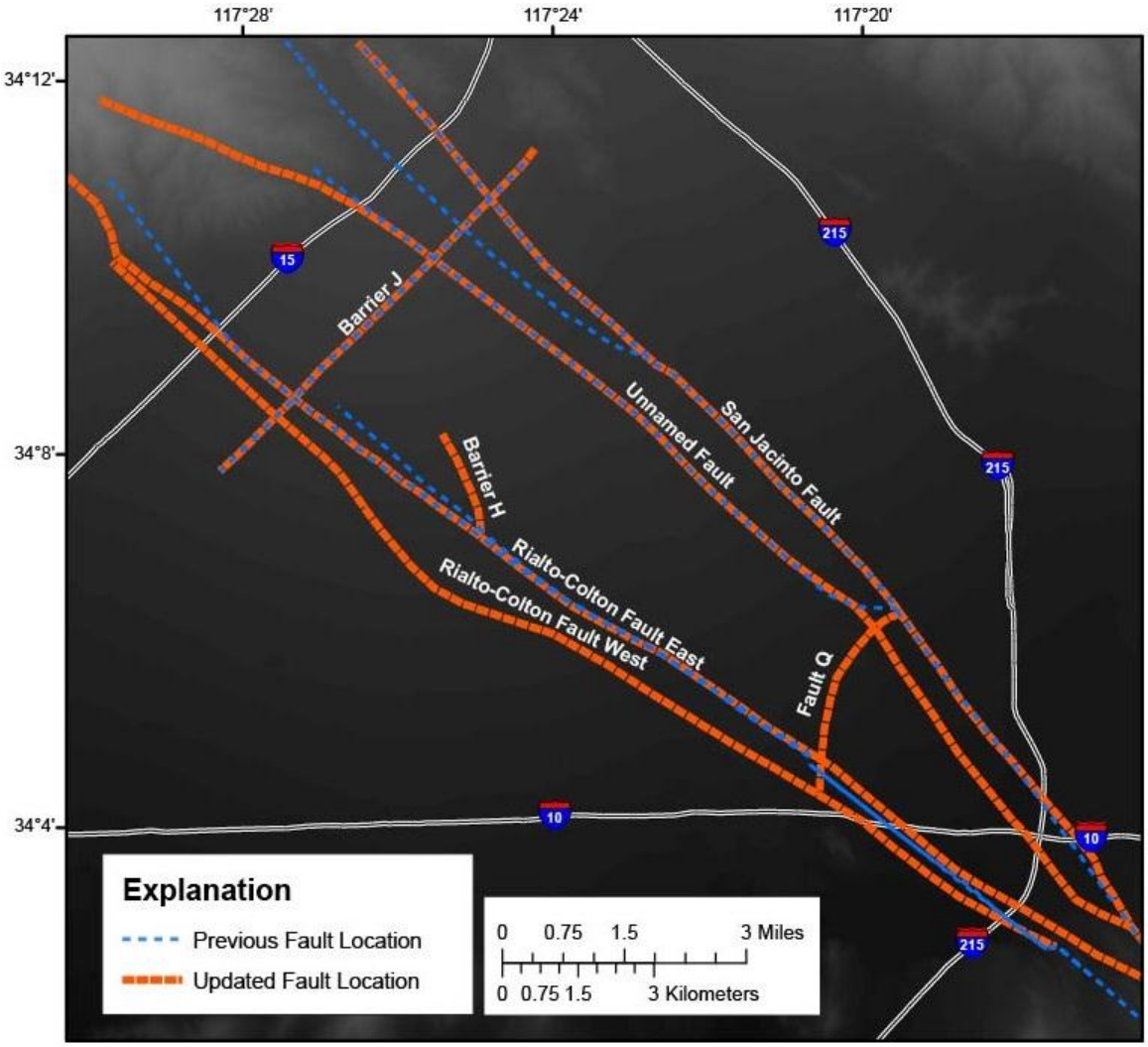

Figure 19: Previous fault locations and updated fault locations used in this study.

The interpreted data (Catchings et al, 2008) along the seismic transect (figure 16) indicates that there may be two more faults between the unnamed fault and the Rialto-Colton Fault in the southeastern part of the Rialto-Colton Basin. Additional data for the extension of these faults to the northwest of their locations on the seismic transect were not available for this study. Therefore, these possible faults were not included in this study.

6.2 Hydrogeologic Framework Model of the Rialto-Colton Basin

Results from the interpolation of water-bearing unit boundaries from borehole logs are presented in this section. Data used in the three dimensional stratigraphic model of the Rialto-Colton Basin are shown in figures 22-25. This model consists of spatial representations of the top elevation and thickness for each water-bearing unit and the perching layer generated from EarthVision.

The top elevations for all stratigraphic layers in the model generally follow the contours of the land surface. Layer thickness varies from minimal thickness where layers such as the river deposits pinch out to several hundred feet thick in areas of the upper, middle, and lower water-bearing units.

6.2.1 Analysis of Selected Boreholes

A total of forty two boreholes were initially analyzed for stratigraphic boundaries. Of these boreholes, eleven already had been analyzed in a previous study (Woolfenden and Kadhim, 1997). Re-analysis of these boreholes along with additional information not available at the time of the 1997 study resulted in minor changes in the depths of the stratigraphic boundaries. Table 19 summarizes these changes.

Stratigraphic boundary elevations were based on interpretations of borehole geophysical and lithology logs. Two borehole logs with stratigraphic boundary interpretations are shown in figures 20 and 21. Figure 20 shows a borehole log in the northwestern part of Rialto-Colton Basin near the San Gabriel Mountains. Figure 21 shows a borehole log in the southeastern part of the Rialto-Colton Basin near the Santa Ana River. The interpretations of the stratigraphic boundaries for all the wells used in this analysis are given in Appendix A.

Table 19: Changes in depth to water-bearing units from Woolfenden and Kadhim (1997)

Borehole	Stratigraphic Boundary	Depth Changed From (ft)	Depth Changed To (ft)	Reason for the Change
1N/5W-22N1	Middle - Lower	620	610	The gamma and resistivity logs both decrease to lower values at around 610 ft.
1N/5W-34D1	Middle-Lower	680	580	Gamma, resistivity, and spontaneous potential logs from additional nearby wells (PW5, PW6, and PW8) indicate the Middle Water-Bearing Unit does not extend as deep in this area.
1N/5W-34D1	Lower – Consolidated	923	NE	Resistivity and gamma logs usually decrease to lower values for the consolidated deposits. This trend is not clearly evident in the geophysical logs for 1N/5W-34D1. Borehole logs (F-49A) indicates that the depth of consolidated layer is below 1000 ft in this part of the basin.
1S/4W-08E1	Upper-Middle	218	270	The sharp decrease in resistivity from 190 ft – 220 ft is likely due to a change from unsaturated to saturated conditions (water level ~193 ft). The stratigraphic boundary was set at 270 ft depth, where there is a change in lithologies from Sand/Gravel/Clay to Sand/Clay (with an increase in clay content) and there was also an increase in gamma variability and a decrease in spontaneous potential.
1S/4W-08E1	Middle-Lower	485	525	Recent resistivity and gamma logs from CEH 17 indicate the bottom of the Middle Water-Bearing Unit is around 475 ft in this area. This change also is more consistent with Resistivity and Gamma logs of 1S/4W-08E1.
1S/4W-08E1	Lower-Consolidated	839	950	The gamma and SP logs for 1S/4W-8E1 indicate that the boundary between these units likely occurs at 950 ft where there is a more pronounced decrease in the logs.

Borehole	Stratigraphic Boundary	Depth Changed From (ft)	Depth Changed To (ft)	Reason for the Change
1S/4W-20H1	Lower-Consolidated	750	860	Resistivity and SP logs from 1S/4W-21L4 indicate that the Lower Water-Bearing Unit extends deeper in this area. A deeper extension of the Lower Water-Bearing Unit is still consistent with the resistivity, gamma, and SP logs of 1S/4W-20H1.

*NE – Not encountered

The analysis of lithologic and geophysical logs from 31 boreholes drilled after 1996 added to the number of locations where the elevation of each stratigraphic boundary had previously been determined. The number of locations where stratigraphic boundaries were determined from borehole logs for this study and Woolfenden and Kadhim (1997) is given in table 20.

Table 20: Number of data points defining the stratigraphic surfaces

Stratigraphic Surface of Water-Bearing Unit	Stratigraphic Boundary Data Points
River Deposits Bottom	5
Upper Top*	5
Upper Bottom	41
Middle Top	41
Middle Bottom	39
Lower Top	38
Lower Bottom	21
Consolidated Deposits Top	19
Consolidated Deposits Bottom	3
Basement Top	6

* The top of the upper unit where it is underlies river deposits

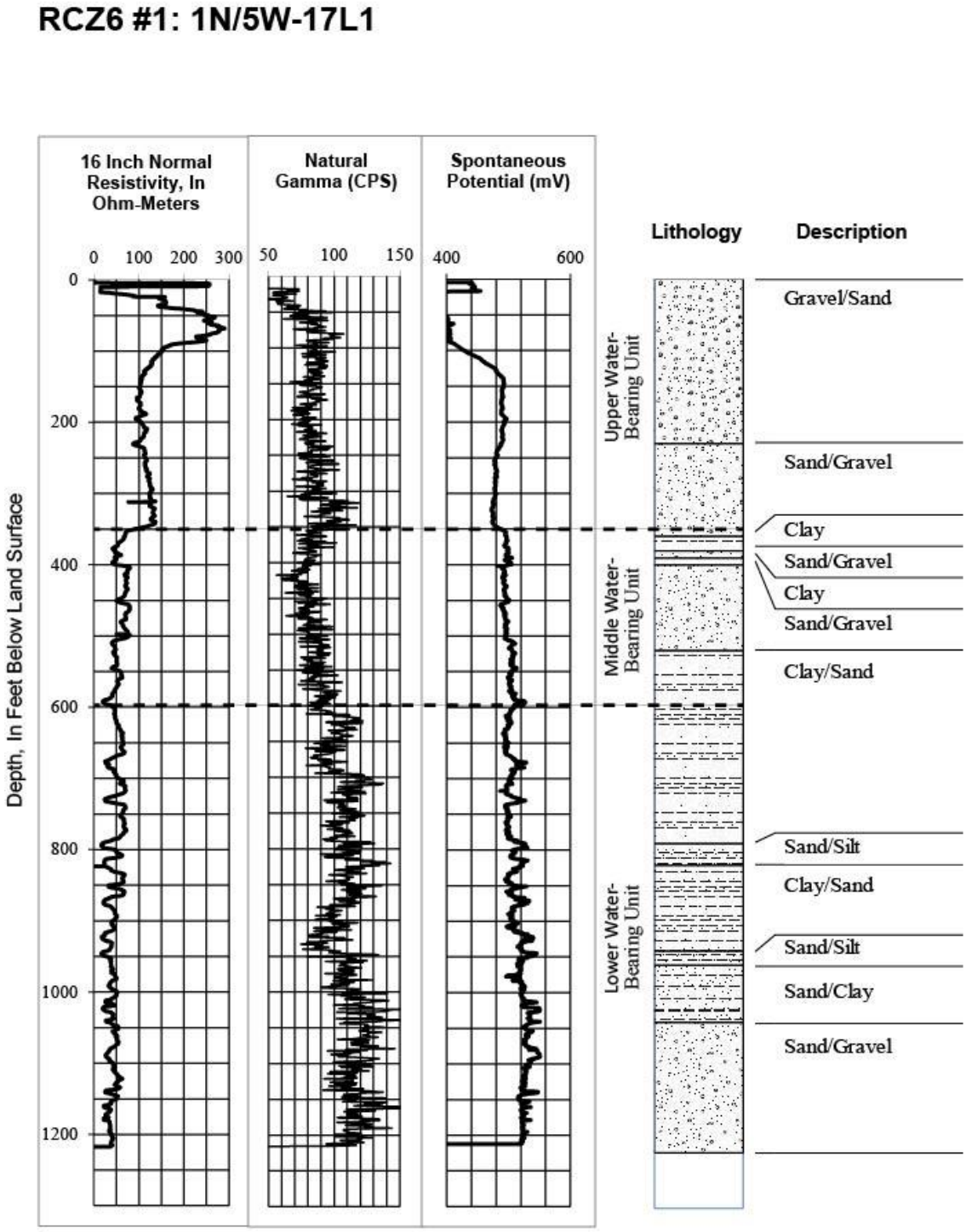

Figure 20: Borehole geophysical and lithologic logs and water-bearing unit boundaries for USGS observation site 1N/5W-17L1.

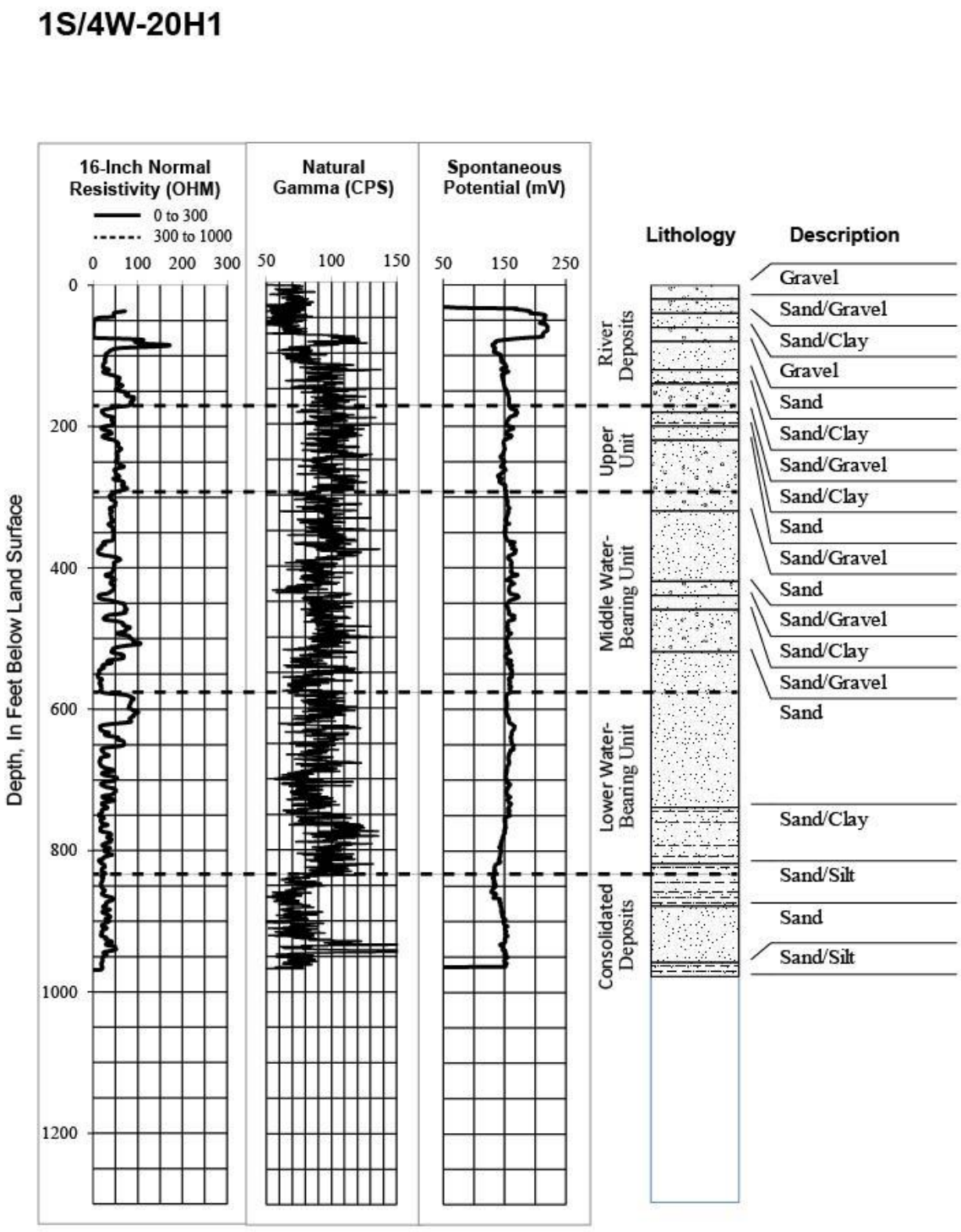

Figure 21: Borehole geophysical and lithologic logs and water-bearing unit boundaries for USGS observation site 1S/4W-20H1.

The distribution of data points for these major stratigraphic boundaries is shown in figures 22 through 25. Data are scarce immediately southeast of Barrier J, immediately southeast of Fault Q, and in the northwestern-most part of the basin. The full extent of the river deposits is unknown due to a general scarcity of available data in the southeastern part of the basin (figure 22). Also, data are scarce north and east of Barrier H (figure 25) for the boundary between the Lower Water-Bearing Unit and the base of the aquifer.

6.2.2 Analysis of Boreholes for Perched Aquifer Conditions

The occurrence of a perched aquifer in the northeastern half of the Rialto-Colton Basin has been delineated previously by GeoSyntec Consultants (2006). GeoSyntec Consultants (2006) delineation included well locations where the existence of the perched aquifer was inferred, but did not include the depth of thickness of the perching layer. The delineation of the perched aquifer for this study was determined from sonic logs; water-level differences in wells at the same location with one screened interval in the perched aquifer and the other in the main aquifer, and (or) by water levels within the perched aquifer in conjunction with an extrapolation of the water level in the main aquifer from nearby wells (showing that the perched water level was higher than that of the water level in the main aquifer).

Table 21 summarizes the locations where perching conditions have been observed or inferred (locations shown in figure 6), constraints on the minimum and maximum range of elevations of the perching layer, and the inferred location of the perching layer based on lithology and/or resistivity logs. Borehole lithology and resistivity logs were used to determine areas of coarse and fine sediments in each borehole. The dimensions of the perching layer were then confined to areas of fine sediment.

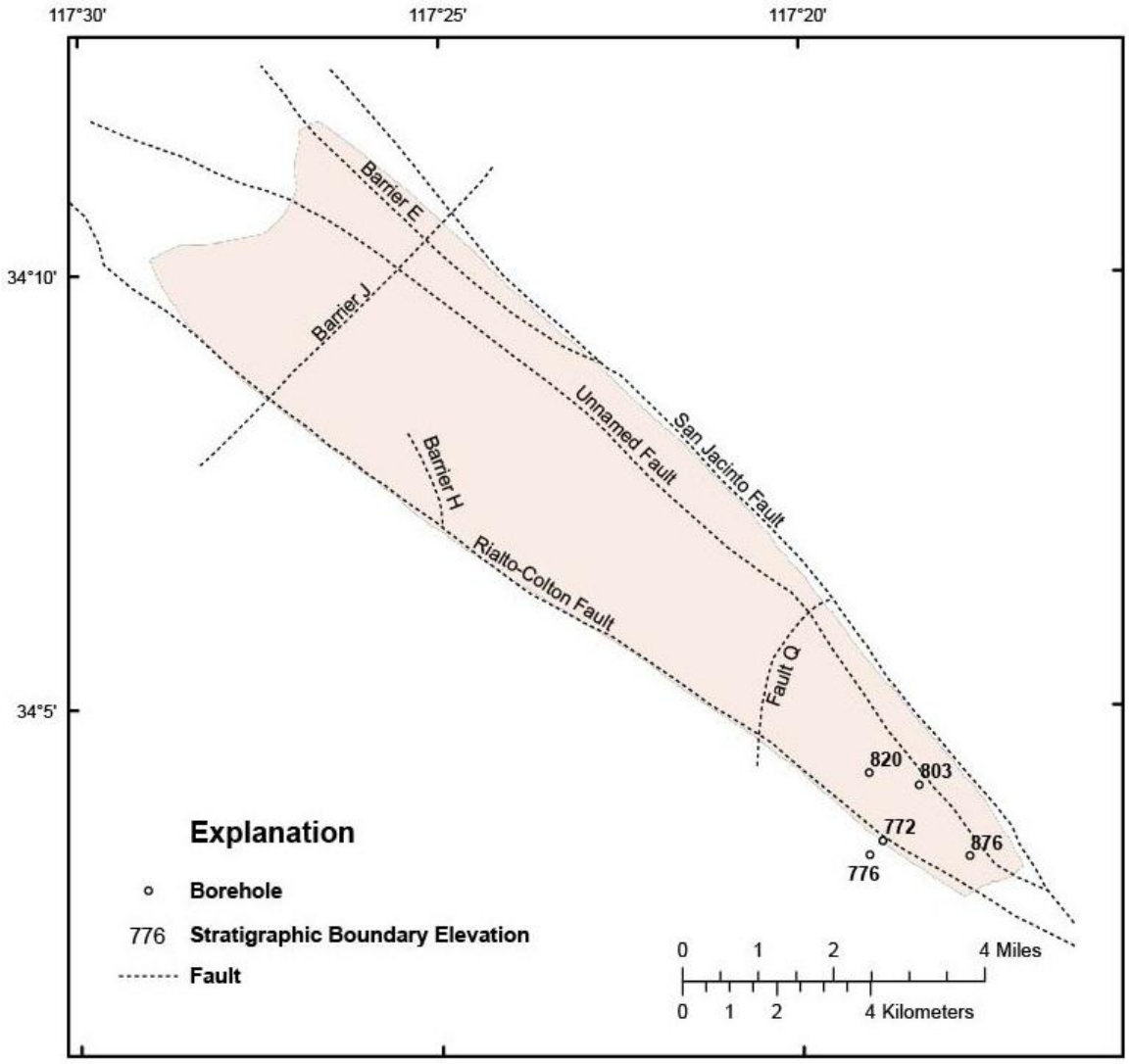

Figure 22: Elevation of the boundary between the River Deposits and the Upper Water-Bearing Unit

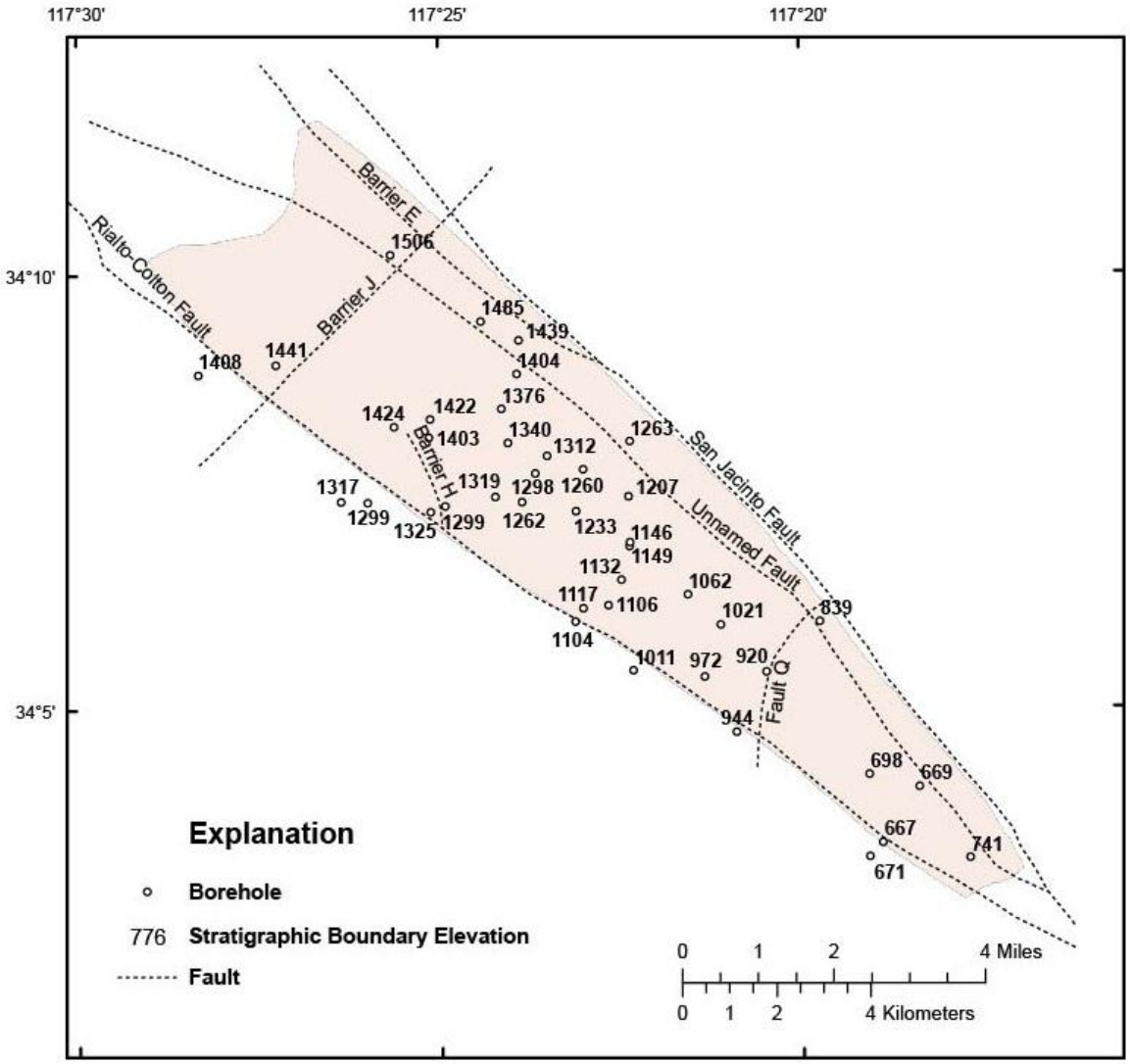

Figure 23: Elevation of the boundary between the Upper Water-Bearing Unit and the Middle Water-Bearing Unit

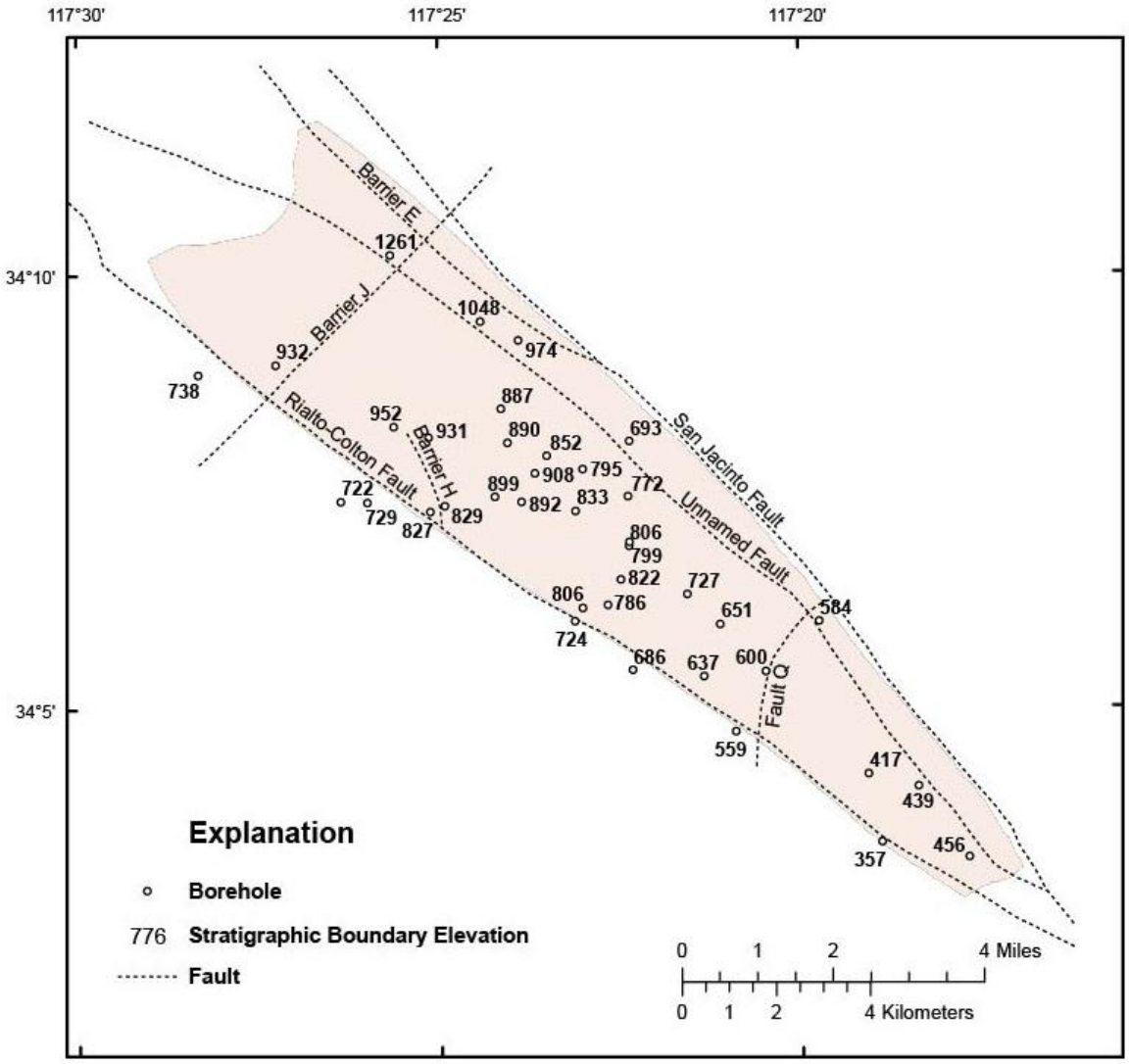

Figure 24: Elevation of the boundary between the Middle Water-Bearing Unit and the Lower Water-Bearing Unit

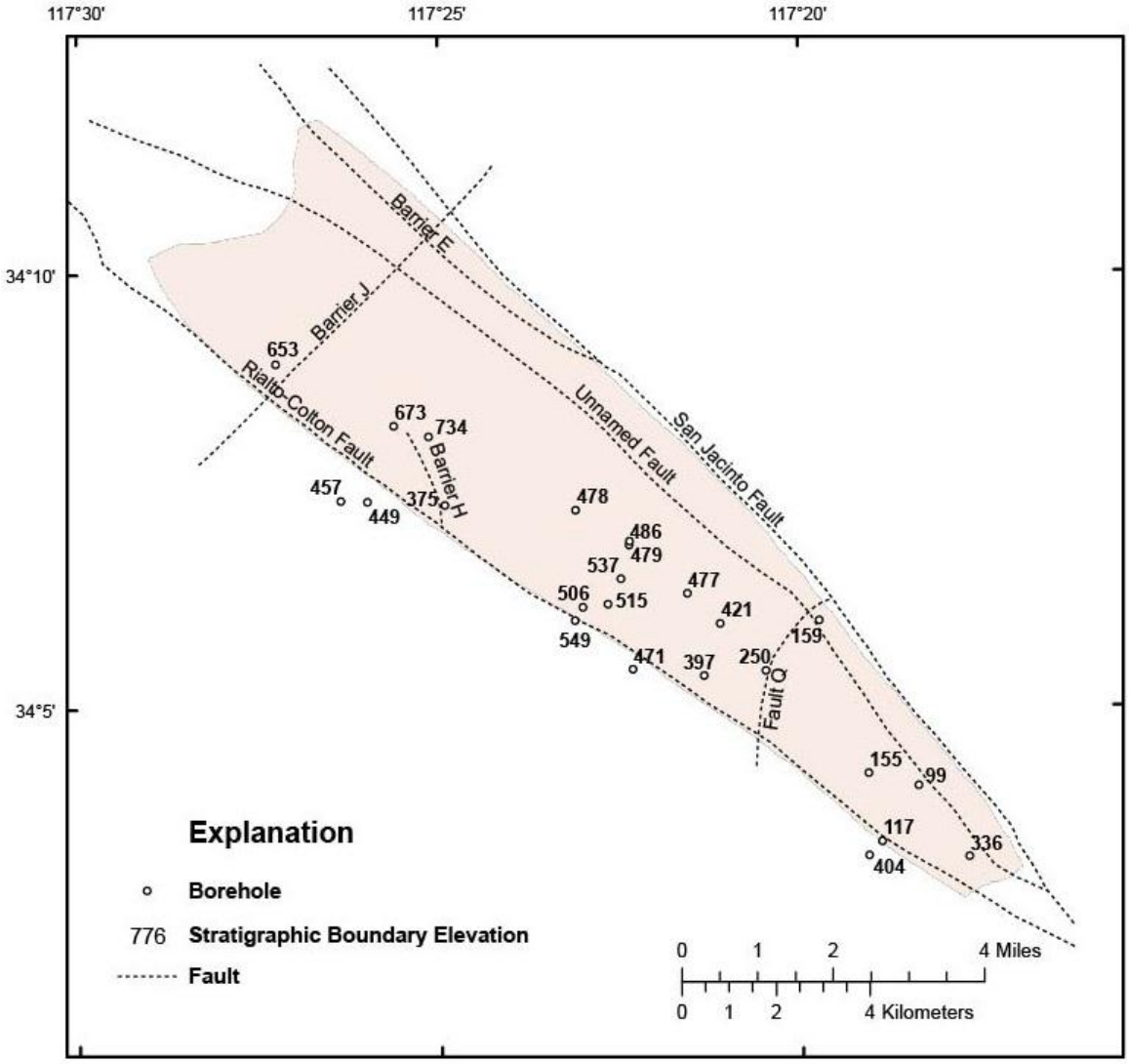

Figure 25: Elevation of the boundary between the Lower Water-Bearing Unit and the Base of the Aquifer

Table 21: Data used to determine the location and extent of the perched aquifer in the Rialto-Colton Basin.

Borehole	**Data Used in Interpretation of Perched Aquifer**	**Data Source**	**Perching Layer Elevation Range (ft)**
1N/5W-27D2 1N/5W-27D4	Water-level difference in monitoring wells at different screened intervals	USGS water level measurements	1092 – 1100
1N/5W-35B1 - B4	Water-level difference in monitoring wells at different screened intervals	USGS water level measurements	1175 – 1183
1N/5W-22N1 - N6	Water level difference in monitoring wells at different screened intervals	USGS water level measurements	1425 – 1432
1S/5W-11F1	Sonic log	USGS Sonic Logs	956 – 983
1N/5W-34D1	Sonic log	USGS Sonic Logs	975 – 984
PW-8	Water-level difference in monitoring wells at different screened intervals	GeoSyntec Consultants Report (October 2006)	1080 – 1100
N-1	Single water level measurement in perched aquifer	GeoSyntec Consultants Report (October 2006)	1065 – 1103
N-2	Single water level measurement in perched aquifer	GeoSyntec Consultants Report (October 2006)	1073 – 1145
N-3	Single water level measurement in perched aquifer	GeoSyntec Consultants Report (October 2006)	1040 – 1086
N-5	Single water level measurement in perched aquifer	GeoSyntec Consultants Report (October 2006)	1053 – 1099
N-6	Single water level measurement in perched aquifer	GeoSyntec Consultants Report (October 2006)	1022 – 1070
N-8	Single water level measurement in perched aquifer	GeoSyntec Consultants Report (October 2006)	1038 – 1062
N-10	Water level difference among monitoring wells at different screened intervals	GeoSyntec Consultants Report (October 2006)	1033 – 1036
N-13	Water level difference among monitoring wells at different screened intervals	GeoSyntec Consultants Report (October 2006)	1011 – 1024

6.2.3 Analysis of Cross Sections

Eleven cross-sections were constructed throughout the Rialto-Colton Basin using the results of the stratigraphic interpolation. The locations of these sections are given in Figure 77, Appendix B. The cross-sections are given in figures 78-88, Appendix B.

The cross-sections reveal several trends in the Rialto-Colton Basin. First, there is a general thickening trend of the water-bearing units thickening up basin (to the northwest). This thickening trend can be observed in cross sections A-A', B-B', and G-G'. The general thickening trend is less prevalent but still present in the vicinity of the Rialto-Colton Fault Zone on cross section H-H'. This general thickening trend is likely due to increased deposition near the San Gabriel Mountains, which is the source of these sediments.

Cross section A-A' in this report covers roughly the same transect as cross section A-A' in Woolfenden and Kadhim (1997). The thickening trend to the northwest is present in both cross sections up to Barrier J. In Woolfenden and Kadhim the water bearing units decrease from about 900 ft total thickness just to the southwest of Barrier J down to about 300 ft thick just to the northeast of Barrier J, and continue at approximately 300 ft thick to the northwest of Barrier J. In this report the water bearing units decrease from 1100 ft thick just to the southeast of Barrier J to 1000 ft thick just to the northwest of Barrier J, and then continue increasing in thickness to the northeast of Barrier J (Figure 78).

There also is thickening of the upper and middle water-bearing units to the northeast. Woolfenden and Kadhim (1997) cross sections C-C' and D-D' show this general thickening trend. This trend is present mostly in the middle part of the basin, as indicated by cross sections C-C', J-J', and D-D' of this report (figures 81, 82, and 87, Appendix B), and extends to the San Jacinto Fault. Though these cross sections are in general oriented from southwest to northeast,

they do not form perfectly straight lines in this direction (their shape is due to the arrangement of available boreholes with geophysical logs). It is therefore not conclusive from these cross sections alone that a southwest to northeast thickening trend exists. Therefore, an interpolation of sediment thickness was plotted to verify that this trend exists (section 6.1.2, figure 11). This interpolation clearly shows both the cross basin (to the northeast) and up basin (to the northwest) thickening trends. The sediments in figure 11 vary from 347 ft thick near the Rialto-Colton Fault Zone between Barrier H and Fault Q, to 811 ft thick near the junction of Barrier E and the San Jacinto Fault. This general thickening trend is consistent with an area of subsidence (Wisely and Schmidt, 2010) shown in Figure 11.

There also may be a general thickening of the water-bearing units to the southeast around Fault Q (cross sections A-A', B-B', G-G'). However, the availability of borehole logs is insufficient in the southeastern part of the Rialto-Colton Basin to confirm that this is not just a result of the interpolation technique used. Woolfenden and Kadhim (1997) cross sections A-A' and B-B' do not show any thickening trend in this area. However, gravity data suggest that there is a graben in this area (figure 16), which could be related to this possible general thickening trend.

Other trends based on the available data are:

- A thicker Lower Water-Bearing Unit between Rialto-Colton Fault and Barrier H (cross section J-J')
- A thinning of lower units and bedrock encountered mid-basin in the Rialto-Colton Fault Zone (cross section H-H' around 1S/5W-10H02)

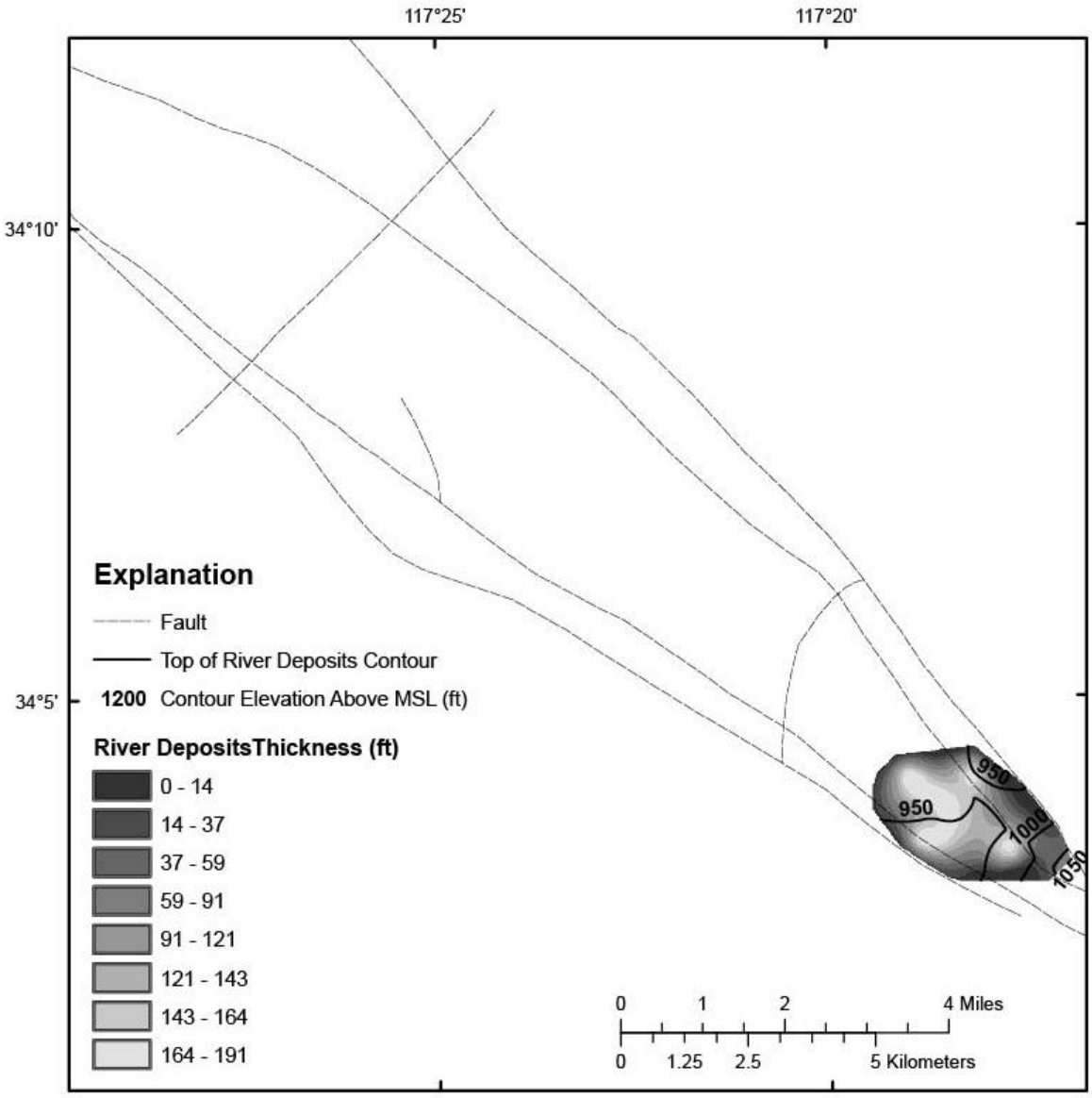

Figure 26: Top elevation and thickness of River Deposits.

6.2.4 River Deposits

The River Deposits occur in the southeastern part of the Rialto-Colton Basin (figure 26). Data were not available to determine the full extent of the river deposits. The River Deposits are generally thicker where they underlie the Santa Ana River and Warm Creek and thin out with distance from these streams. The River Deposits range in thickness from around 190 ft thick to 0

ft thick (where they pinch out) in the study area. In Woolfenden and Kadhim (1997) the River Deposits range from about 170 ft to 0 ft thick and cover roughly the same area as in this report.

6.2.5 Upper Water-Bearing Unit

The Upper Water-Bearing Unit extends throughout the Rialto-Colton Basin. It ranges from approximately 550 feet thick near the San Gabriel Mountains to less than 100 ft thick near Barrier H (figure 27). The top elevation of the Upper Water-Bearing Unit follows the contours of the land surface, decreasing in elevation from the northwest to the southeast. The Upper Water-Bearing Unit is thickest in the northwestern part of the basin adjacent to the San Gabriel Mountains. It is thinnest near Barrier H and under the River Deposits.

The largest difference between the Upper Water-Bearing Unit in this report and that of Woolfenden and Kadhim (1997) is the thickness of the unit near the San Gabriel Mountains. In this report the Upper Water-Bearing Unit is up to 550 feet thick near the San Gabriel Mountains while in Woolfenden and Kadhim (1997) it is less than 50 feet thick.

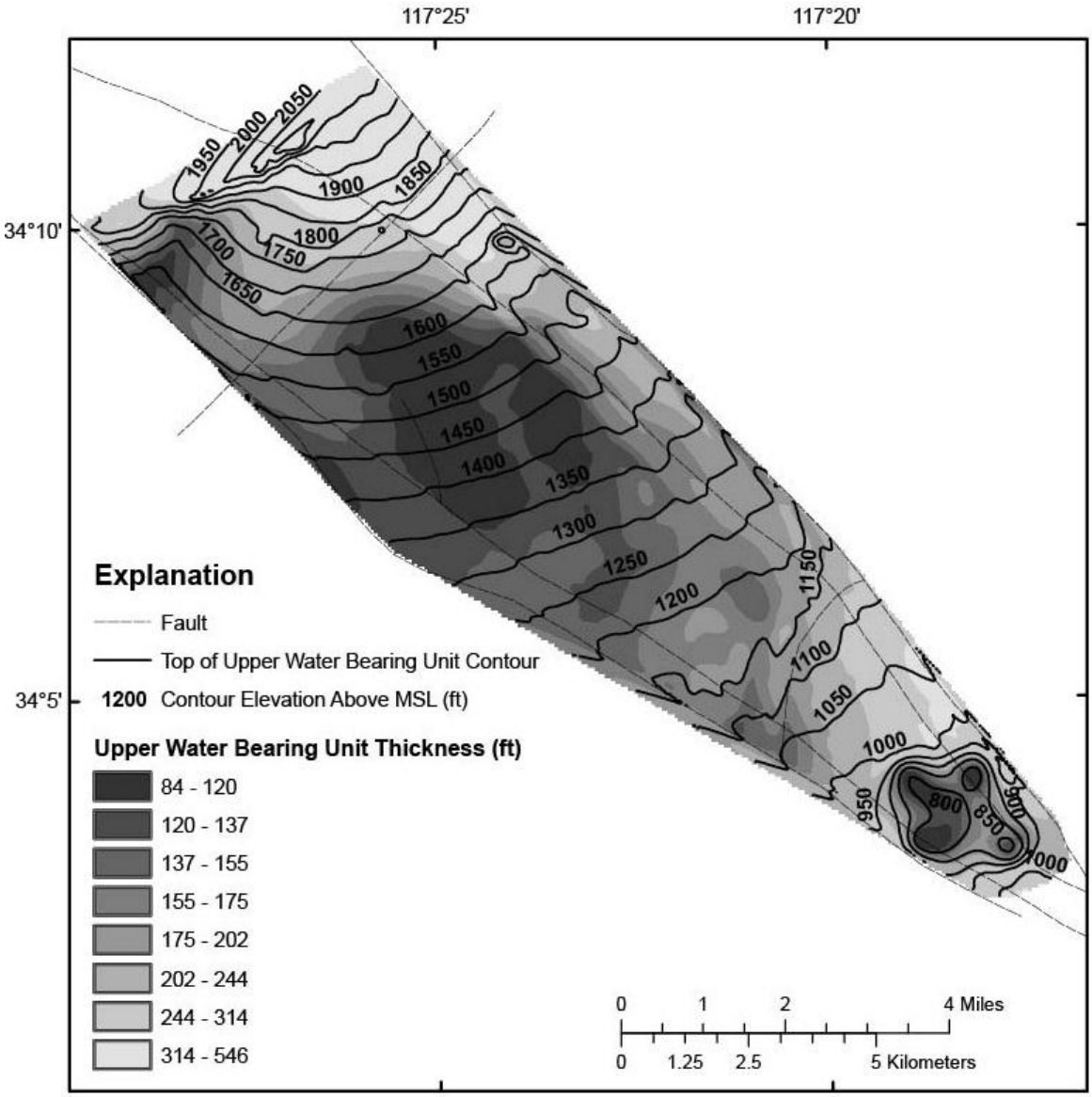

Figure 27: Top elevation and thickness for the Upper Water-Bearing Unit.

6.2.6 Middle Water-Bearing Unit

The Middle Water-Bearing Unit extends throughout the Rialto-Colton Basin. The thickness of this unit generally decreases from the northwest to southeast, with the exception of the northernmost part of Rialto-Colton Basin where the Middle Water-Bearing Unit may be thinnest.

The top elevation of the Middle Water-Bearing Unit roughly parallels the contours of the land surface.

The Middle Water-Bearing Unit ranges in thickness from up to 677 ft thick near the Rialto-Colton Fault northwest of Barrier H, to as little as 240 ft on the southeastern side of the basin (figure 28). This unit is even thinner in the northeast corner of the basin near the San Gabriel Mountains. Data were not available for interpolation in this area and the layer elevation was extrapolated from 1N/5W-17L1, 1N/5W-17K1, 1N/5W-17K1, and 1N/5W-17G2.

The Middle Water-Bearing Unit in this report follows the same trends as in Woolfenden and Kadhim (1997) with the exception of the thickening trend near the San Gabriel Mountains, where in Woolfenden and Kadhim (1997) the Middle Water-Bearing Unit thins to less than 100 ft northwest of Barrier J.

6.2.7 Perching Layer

The perching layer extends through the Rialto-Colton Basin from the San Gabriel Mountains down to about half way between Barrier J and the Santa Ana River, and extends from the San Jacinto Fault to the Rialto-Colton Fault East. This layer is discontinuous between the San Jacinto Fault and the unnamed fault around Barrier J, between Barrier H and the Rialto-Colton Fault East, and to the south of Barrier H near the Rialto-Colton Fault East. Its thickness varies from over 50 feet thick in parts of the central basin to as little as a few feet at the edges of the basin (figure 29). The elevation of the perching layer trends consistently with the land-surface elevation, decreasing from northwest to southeast. However, in the northeastern part of the basin, the elevation increases relative to the land surface.

The perching layer has been identified in a previous study (GeoSyntec Consultants, 2006) which analyzed water level data to confirm the existence of the perching layer and to define the depth and thickness of the perching layer at a few selected boreholes. Since 9 out of 14 main data points used in this study (table 21) were from data provided from GeoSyntec Consultants (2006), this study is in agreement with the results of the previous study. However, an additional 5 data points not present in the GeoSyntec Consultants (2006) study extend the perching layer to the southeast down to 1S/5W-11F1 and to the northeast of the Unnamed Fault based on 1N/5W-22B1 and 1N/5W-35N1 (figure 6). In addition, the perching layer was extended out to the northwest of Barrier J based on lithology logs from 1N/6W-25A1 and 1N/6W-24C1.

6.2.8 Lower Water-Bearing Unit

The Lower Water-Bearing Unit extends throughout the Rialto-Colton Basin. The elevation of the top boundary of the lower water-bearing unit generally follows the trend of the land surface, decreasing from northwest to southeast. The Lower Water-Bearing Unit is thickest adjacent to the San Gabriel Mountains and in southeastern Rialto-Colton Basin around where the Santa Ana River crosses the San Jacinto Fault. Data for the contact between the Lower Water-Bearing Unit and underlying consolidated deposits or bedrock were not available in the northeastern part of the basin (figure 25). Hence, the model results for this part of the basin were extrapolated from F-15A, F-13B, and 1N/5W-29Q1 (figure 46).

The Lower Water-Bearing Unit is approximately 150 feet thick above Barrier J in Woolfenden and Kadhim (1997), while it ranges from 150 feet to over 900 feet thick in this report. In this report the Lower Water-Bearing Unit follows the same trends and is roughly the same thickness as Woolfenden and Kadhim (1997) southeast of Barrier J.

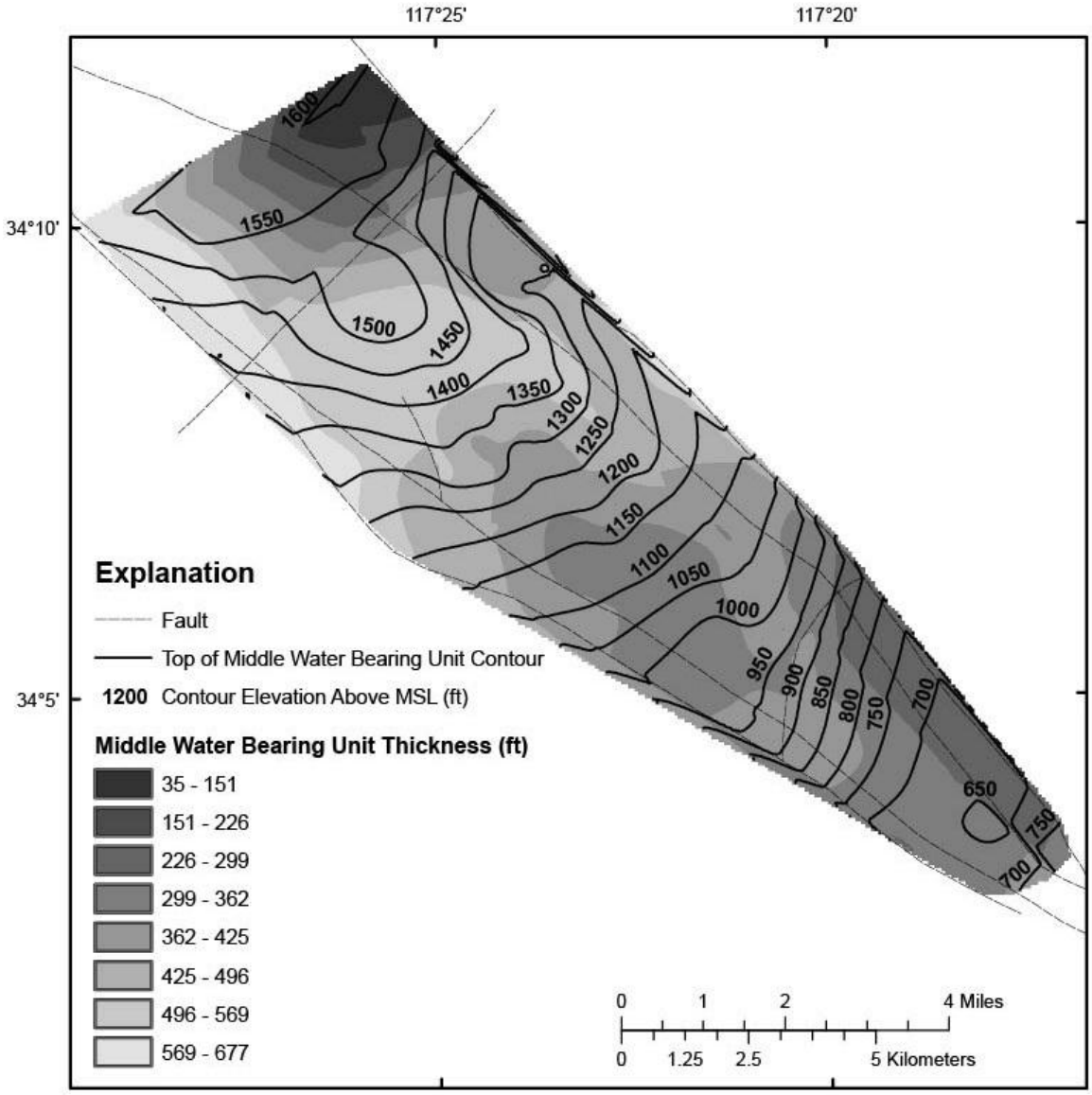

Figure 28: Top elevation and thickness of the Middle Water-Bearing Unit.

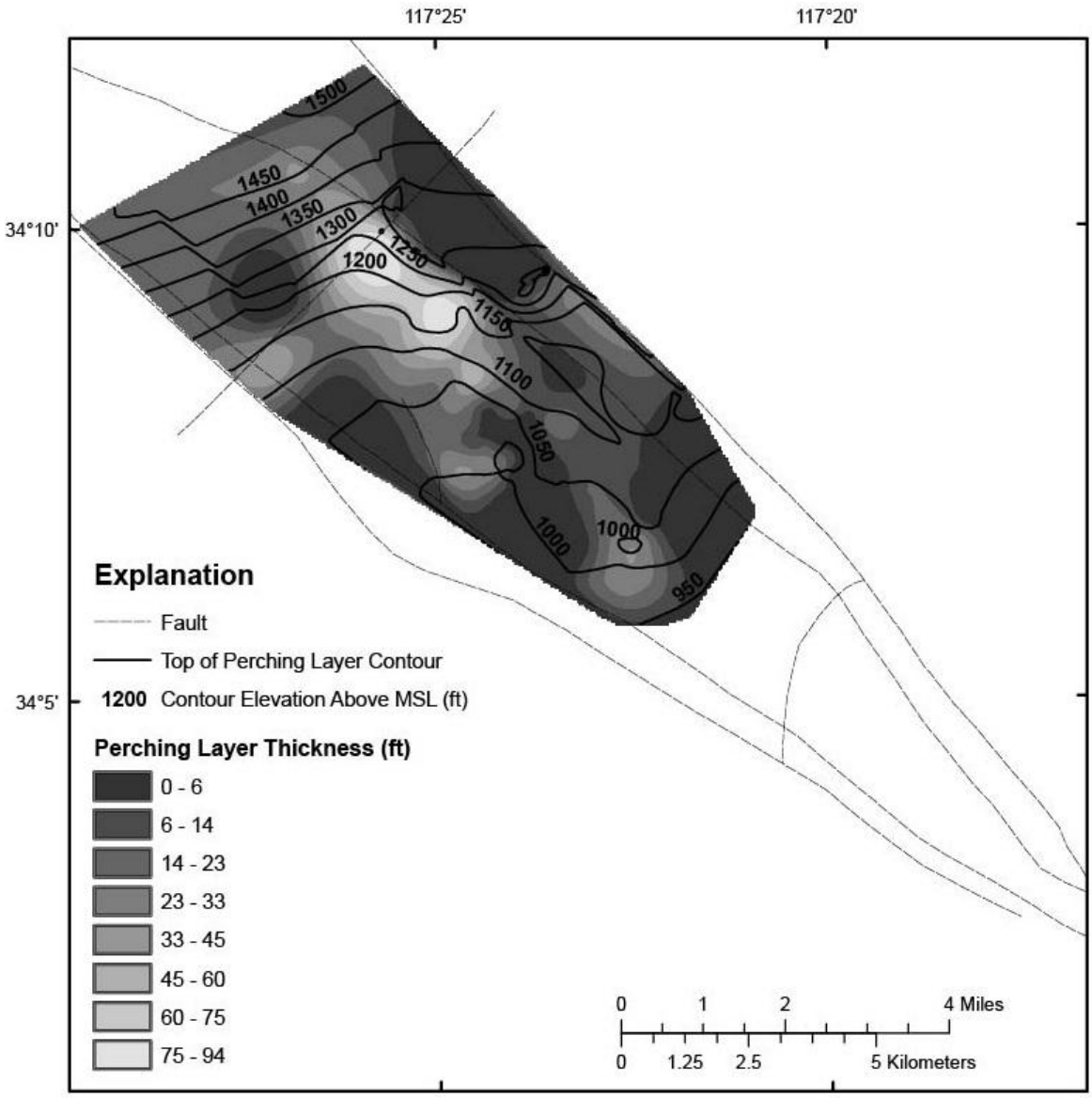

Figure 29: Top elevation and thickness of the Perching Layer.

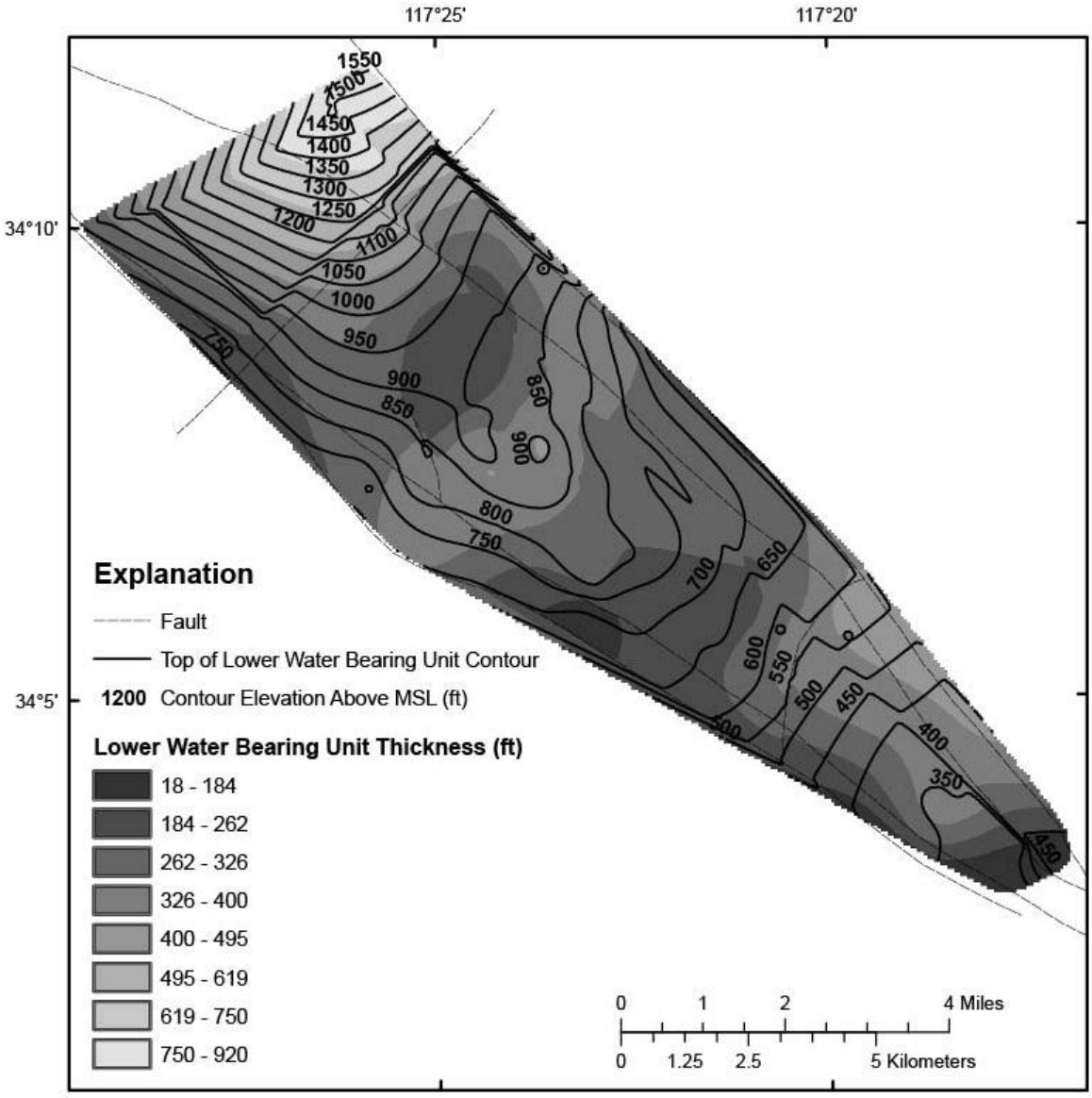

Figure 30: Top elevation and thickness of the Lower Water-Bearing Unit.

6.3 Structure of Southeast Chino and North Riverside Area

6.3.1 Aquifer Base

The base of the aquifer in the southeastern Chino and North Riverside area differs from the base of the aquifer in the Rialto-Colton Basin. The base of the aquifer throughout most of the Rialto-Colton Basin is the top of the consolidated deposits. In southeastern Chino and North Riverside

area, the base of the aquifer primarily is the top of the bedrock and, in places, the top of shale and limestone formations. In addition, the North Riverside area has shallow depth to bedrock, from approximately 40 to 1800 feet, compared to the Rialto-Colton Basin, from approximately 900 to 6000 feet (figure 31). Hence, there were more available borehole logs with bedrock in the Chino and North Riverside area.

Several discrepancies were determined between basement elevations obtained from borehole drillers' logs and basement elevations from the gravity study by Anderson et al (2004). These discrepancies occur in the North Riverside area in boreholes with thick sequences of shale, limestone, and consolidated deposits less than 1000 feet below land surface (figure 31). The drillers' logs from boreholes 1S/4W-18N1 and 1S/5W-25B1 both record greater depth to bedrock than Anderson's study (table 22). The drillers' logs from both of these boreholes also record thick sequences of higher density lithified and consolidated deposits.

These discrepancies can be explained in part by the shale, limestone and consolidated deposits in this area. These deposits are higher density than the alluvium found throughout the basin. Anderson et al (2004) assumed that the density of the basin fill in the Riverside area is 2120 kg/m^3 from 0 to 984 ft in depth and 2240 kg/m^3 from 984 ft to 4265 ft in depth, and the density of the underlying bedrock is 2680 – 2790 kg/m^3.

Shale, limestone, and sandstone have average densities around 2500 kg/m^3, 2700 kg/m^3, and 2650 kg/m^3 respectively (Hilchie, 1978). In addition the average density of conglomerate is 2600 kg/m^3 based on a pebble density of 2700 kg/m^3 with cemented sands and silts ranging from 2500 kg/m^3 to 2650 kg/m^3.

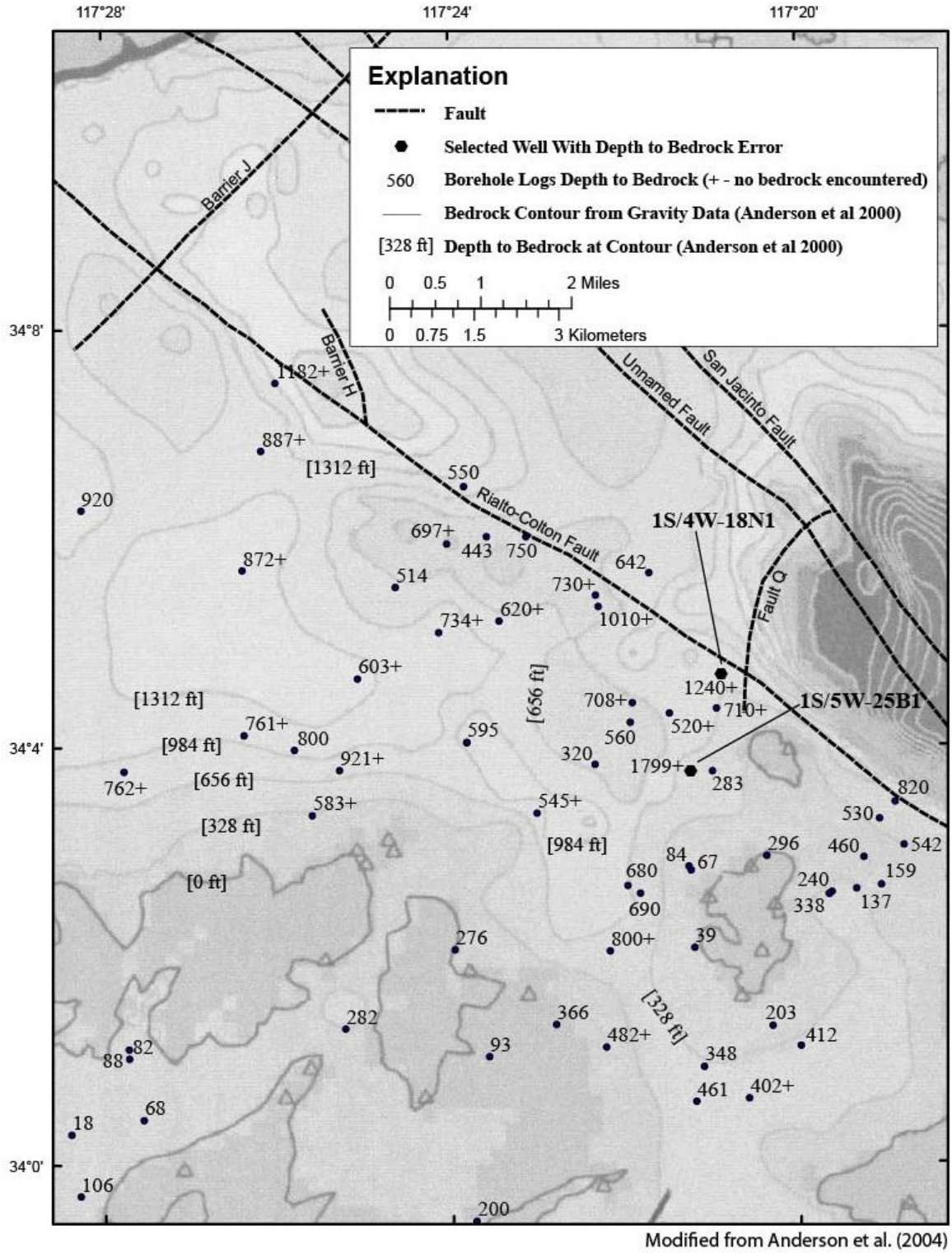

Figure 31: Depth to bedrock from gravity data and depth to bedrock from borehole logs.

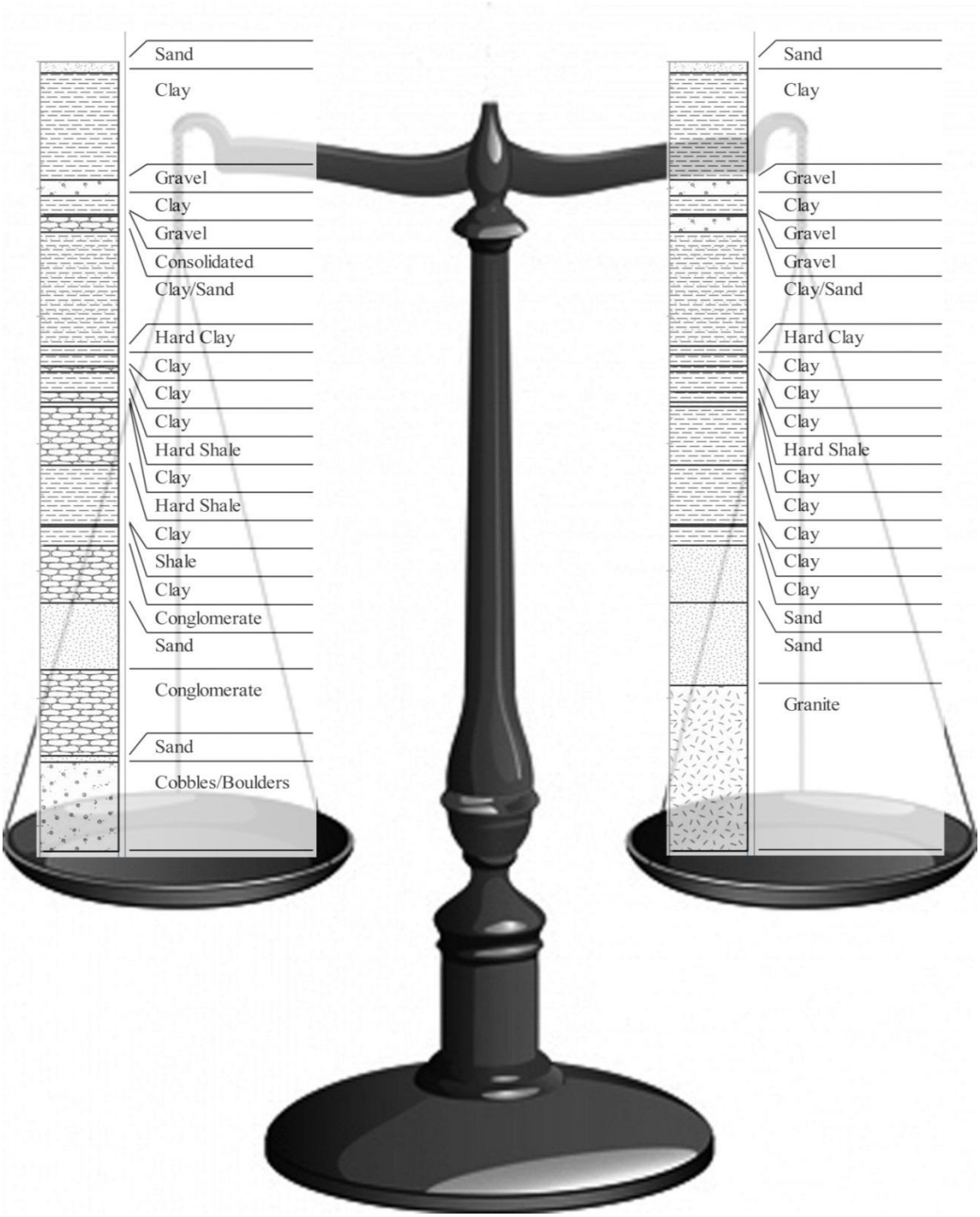

Figure 32: Actual (left) and modified (right) lithologic columns for 1S/4W-18N1

Since shale, limestone and conglomerate sedimentary deposits are denser than the basin fill assumed in Anderson et al (2004), areas where there are significant amounts of these sedimentary deposits will have higher densities than those assumed in Anderson et al (2004). The discrepancies between bedrock elevation from Anderson et al (2004) and the drillers' logs can be partially explained by these discrepancies in density.

To estimate the percent of the basin depth discrepancy that can be explained by the discrepancies in density, it was assumed that the alluvium in North Riverside Basin has the density of basin fill given by Anderson et al (2004). The mass of the column of sediment and sedimentary rocks was then calculated for 1S/5W-25B1 and 1S/4W-18N1, from top to bottom of the borehole, based on the densities previously given.

Table 22: Summary of possible error due to sedimentary deposits in selected wells from the North Riverside Basin

Well	**1S/5W-25B1**	**1S/4W-18N1**
Borehole Bedrock Depth (ft)	Greater than 1799	Greater than 1240
Gravity Bedrock Depth (ft)	Less than 656	Less than 984
Discrepancy in Bedrock Depth (ft)	Greater than 1143	Greater than 256
Thickness of Conglomerate (ft)	135	90
Thickness of Shale (ft)	502	167
Thickness of Limestone (ft)	192	
Estimated Change in Gravity Reading Due to Sedimentary Deposits (ft)	574	165
Percent of Discrepancy That Can Be Explained By Sedimentary Deposits	Up to 50 Percent	Up to 64 Percent

The combined amounts of basin fill and basement rock necessary to produce and equivalent mass of rock in each borehole were then calculated. Figure 32 shows the original lithologic column of 1S/5W-18N1 on the left and a lithologic column with sedimentary rocks replaced by basin fill and the bottom of the lithologic column replaced by basement rock. The amount of the column

replaced by basement rock is determined by balancing the weight of the original lithologic column on the left with the new lithologic column on the right.

The length of the basement rock column from this calculation was then used as the estimated change in gravity reading (ft) due to sedimentary deposits (table 22). This change was compared to the discrepancy in bedrock depths to get a percentage of the discrepancy that can be explained by the sedimentary deposits (table 22).

Given these discrepancies in bedrock elevation, the depths of grabens filled with sedimentary deposits may by underestimated in a gravity analysis. One such graben may be in the vicinity of 1S/5W-25B1 (figure 31), where boreholes 1S/5W-25B1 and 1S/5W-25A1 approximately a quarter mile apart have differences in bedrock elevation of at least 1492 ft.

6.3.2 Faults

The shale and (or) limestone grabens likely are much older than the overlying alluvium and any faults that formed the grabens are unlikely to cut the alluvium and act as a barrier to groundwater flow. However, a Wildermuth Chino Basin study (Wildermuth Environmental, Inc., 2003, figures 2-9, 2-10, and 2-12) indicates that the lower stratigraphic layers of Chino Basin (Chino Layer 1 and Chino Layer 2) terminate into the bedrock. Therefore, for the purposes of the stratigraphic model, vertical faults were used to bound areas where there was a significant change in aquifer depth and unit thickness (figure 10).

6.4 Hydrogeologic Framework Model of Chino and North Riverside Area

The three dimensional stratigraphic model of the Chino and North Riverside area constructed in EarthVision is represented in two dimension for Chino layers 1, 2 and 3 in figures 33, 34, and 35 respectively. The two dimensional figures show the elevation of the top of the layer and the layer

thickness. The stratigraphic layers generally followed the elevation contours of the land surface. Layer thickness varied from less than 100 feet in parts of the North Riverside area (figure 35) where bedrock is shallow, to over 600 feet in parts of the Chino area (figure 35).

Available borehole geophysical logs for this study in the Chino and North Riverside area were few, resulting in the interpolation of the stratigraphic units over much larger distances and increasing the likelihood that important stratigraphic features would be missed.

To aid in the stratigraphic model of this part of the study area cross sections from Wildermuth Environmental, Inc. (2003) were used to supplement the borehole logs. For each borehole shown in the Wildermuth Environmental, Inc. cross sections, stratigraphic boundary depths were used for the stratigraphic boundaries the borehole passed through. The interpolation and extrapolation of stratigraphic boundaries in the Chino and North Riverside area was done using both the stratigraphic boundary depths from cross section boreholes and the stratigraphic boundary depths obtained from borehole lithology logs.

Chino Layer 1 ranges from about 200 to 500 feet thick. It is thickest in the middle of this part of the study area, and thins to the northwest, south, and southeast (figure 33).

Chino Layer 2 ranges from 2 to 400 feet thick. Chino Layer 2 thins out in the northwest, southeast, and southwest regions of the model, and is thickest along the mid-section of the model (figure 34).

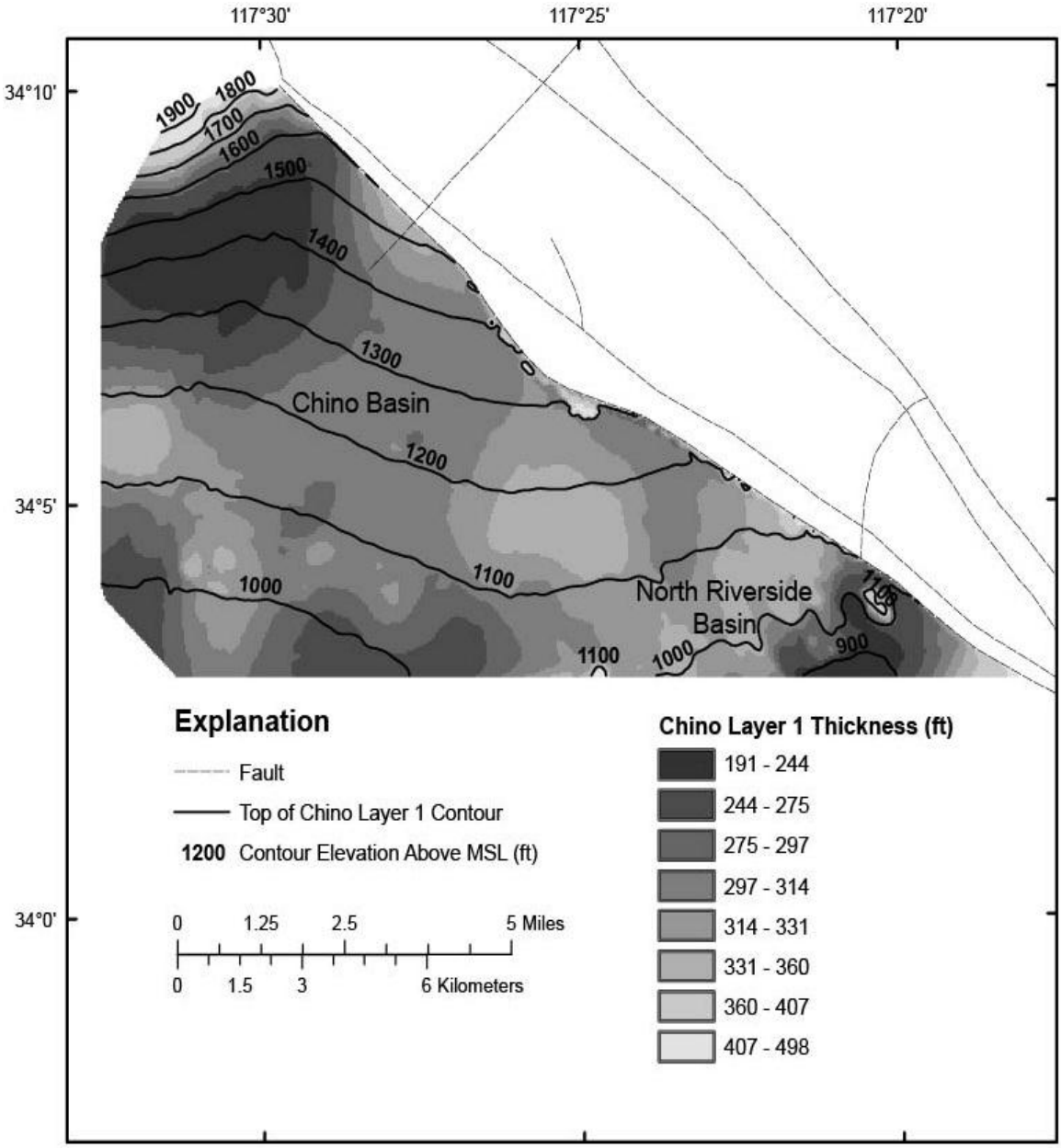

Figure 33: Chino Layer 1 top elevation and thickness.

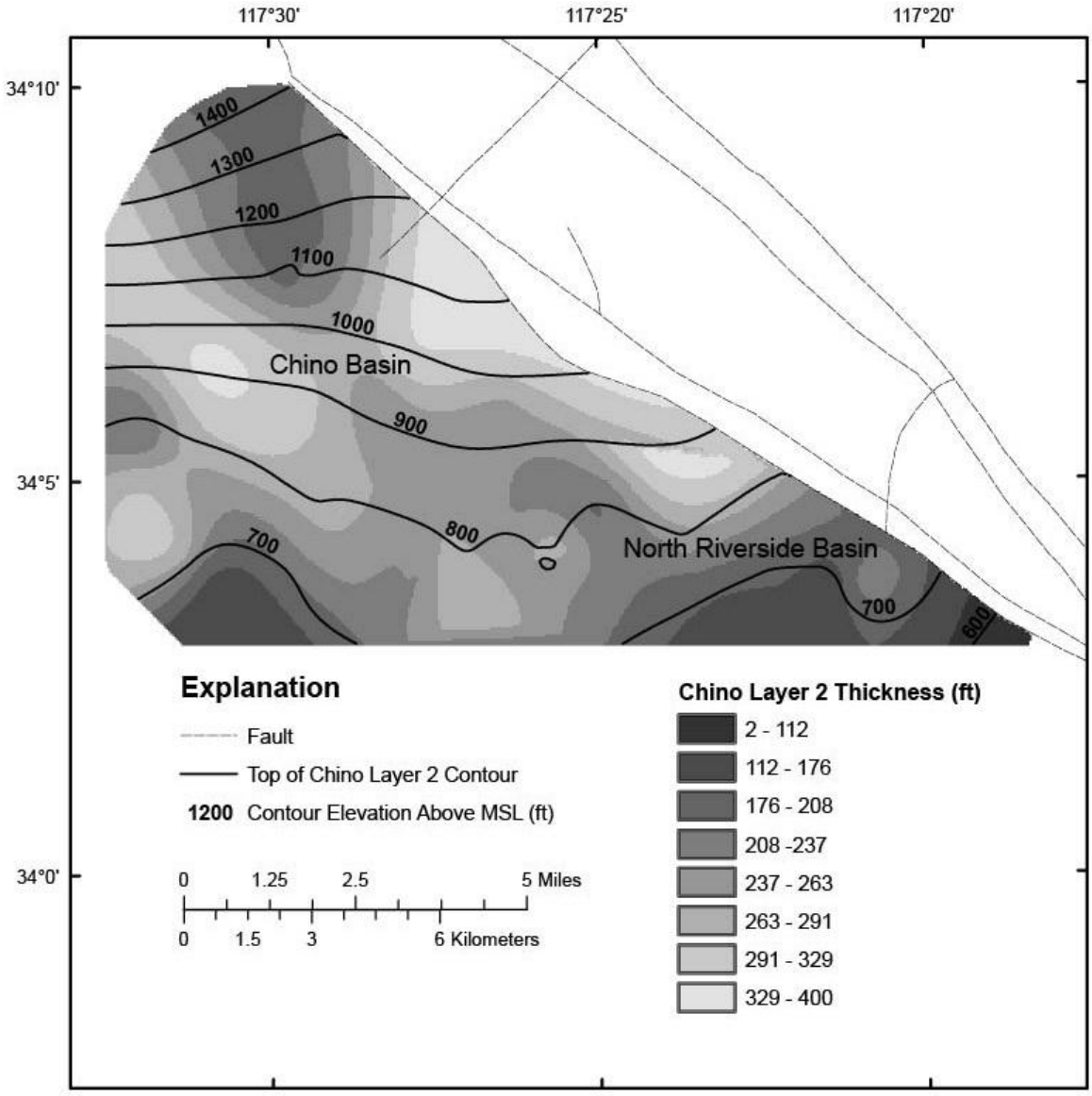

Figure 34: Chino Layer 2 top elevation and thickness.

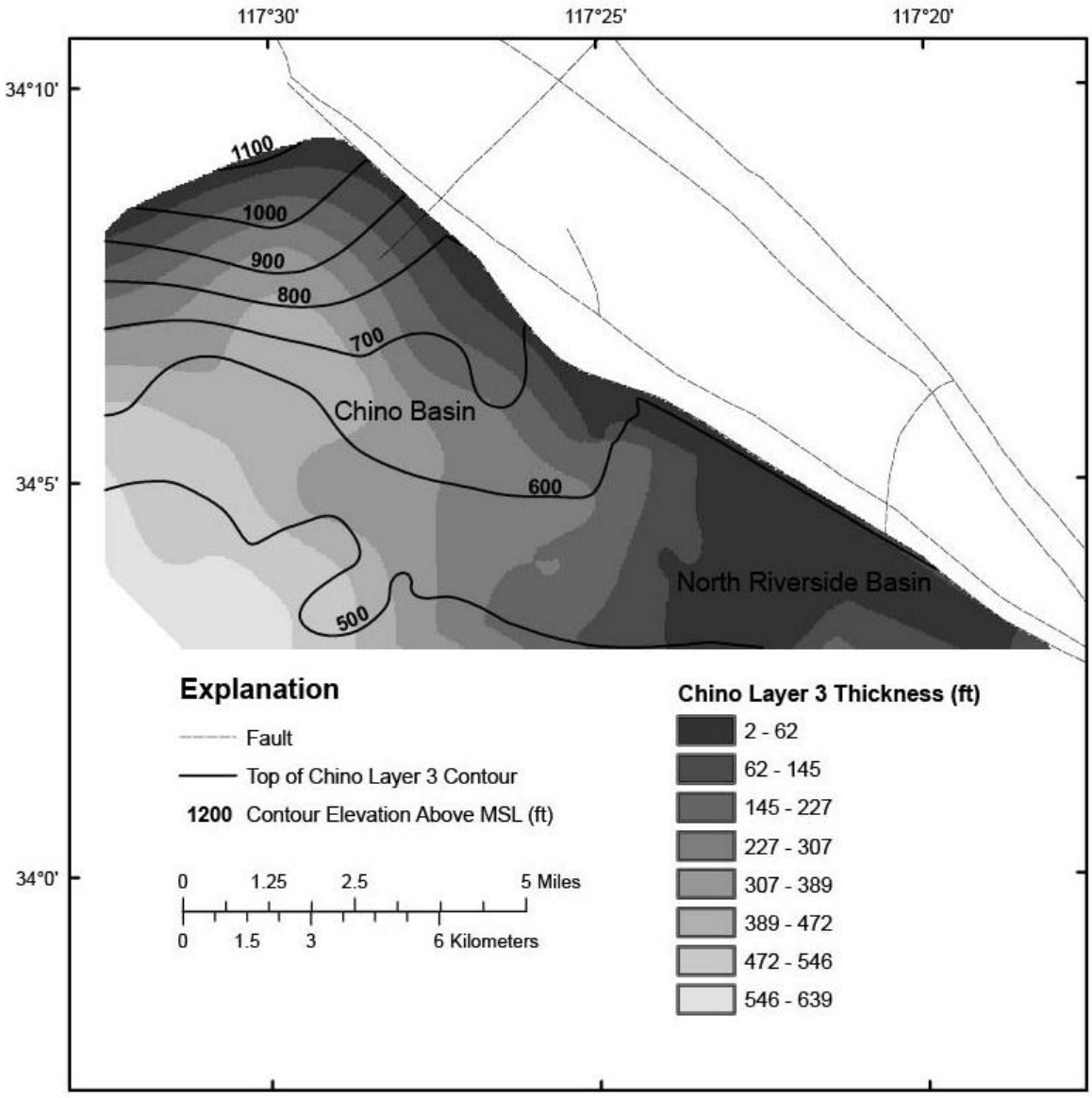

Figure 35: Chino Layer 3 top elevation and thickness.

Chino Layer 3 is less than 63 feet thick in areas of the North Riverside area where bedrock is near land surface (figure 35). It also thins along the western and northern border of the Chino area in the study area. Chino Layer 3 is thickest in the southwest part of the model area, ranging from 472 feet to 600 feet thick.

6.5 Textural Model of the Study Area

The interpolation of percent coarse values derived from borehole logs is shown in figures 36-45 below. Figures 36-37, 39, 41, and 43-45 show the distribution of percent coarse values for each stratigraphic unit averaged over the vertical thickness of the unit and the distribution of boreholes with data used in the interpolation.

Six zones defined based on fault blocks in the Rialto-Colton study area are described in table 23. The average (mean) percent coarse distribution for the zones described in table 23 is shown in figures 38, 40, and 42.

Table 23: Description of zones defined in the Rialto-Colton study area.

Zone	Description
Rialto-Colton Fault Zone	The Rialto-Colton Fault Zone is the area between the Rialto-Colton Fault West and Rialto-Colton Fault East.
Southeast Rialto-Colton Basin	Southeast Rialto-Colton Basin is the area to the southeast of Fault Q and to the northeast of the Rialto-Colton Fault East.
Northwest Rialto-Colton Basin	Northwest Rialto-Colton Basin is the area north of Barrier J in between the Rialto-Colton Fault East and the Unnamed Fault.
Middle Rialto-Colton Basin	Middle Rialto-Colton Basin is the area between the Rialto-Colton Fault East, the Unnamed Fault, Barrier J, and Fault Q.
Northeast Rialto-Colton Basin	Northeast Rialto-Colton Basin is the area to the northeast of the Unnamed Fault and to the northwest of Barrier J.
East of Unnamed Fault	East of Unnamed Fault is the area to the east of the Unnamed Fault between Barrier J and Fault Q.

6.5.1 River Deposits

The River Deposits contain fine sediments in the middle and coarse sediments near the edge of the stratigraphic unit (figure 36). Sediment coarseness varies from under 25 percent in the middle to about 100 percent at the edges. The boreholes with data used in this analysis were not uniformly distributed throughout the deposits. Most boreholes are located along a linear trend from northeast to southwest in the River Deposits (figure 36). The rest are widely scattered throughout this unit. There were a lack of borehole logs from the modeled northeast edge of the

river deposits to Fault Q (figure 37). Since there are no borehole logs to verify a lack of River Deposits in this region, the River Deposits may extend to the northeast as far as Fault Q.

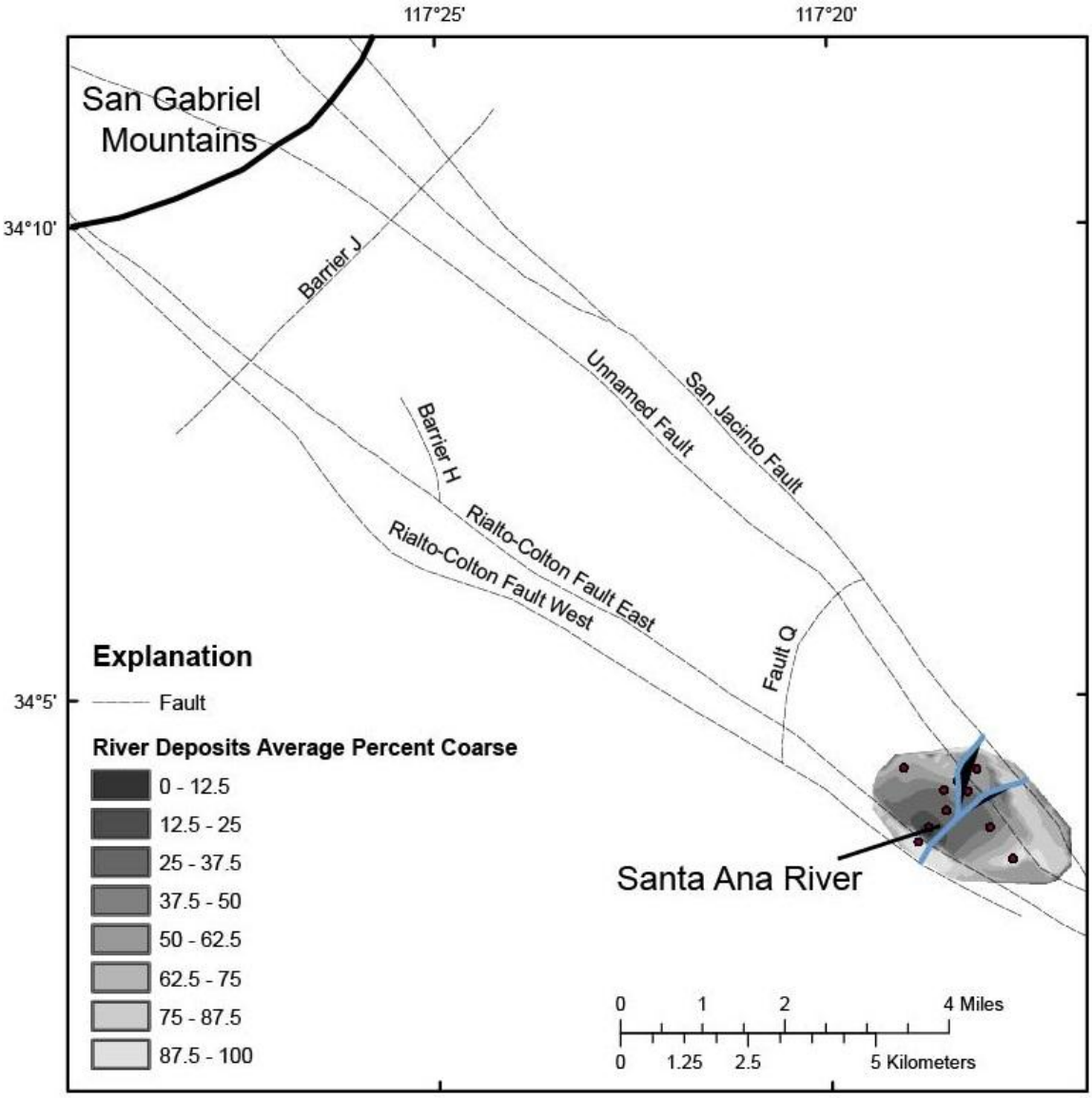

Figure 36: Average percent coarse values of the River Deposits.

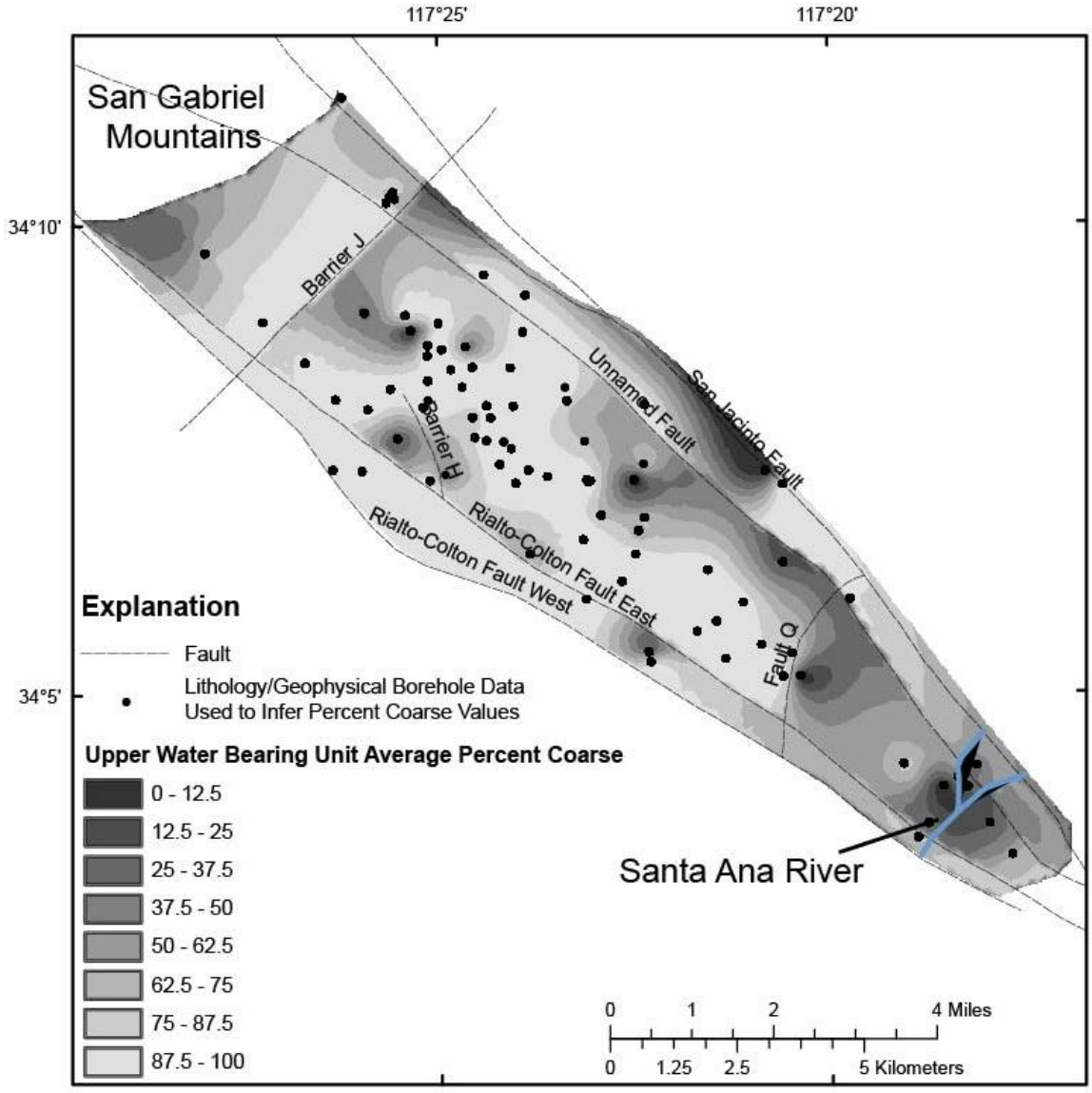

Figure 37: Average percent coarse values of the Upper Water-Bearing Unit.

6.5.2 Upper Water-Bearing Unit

The Upper Water-Bearing Unit consists primarily of coarse sediments (figure 37). Areas of fine sediments are located in the southeastern part of the Rialto-Colton Basin and in the vicinity of the Unnamed Fault. Much of the fine sediments in the southeastern part of the Rialto-Colton Basin are under the river deposits and southwest of the Unnamed Fault near Fault Q. In the vicinity of

the Unnamed Fault there are both areas of near 100 percent coarse sediments and areas of fine sediments.

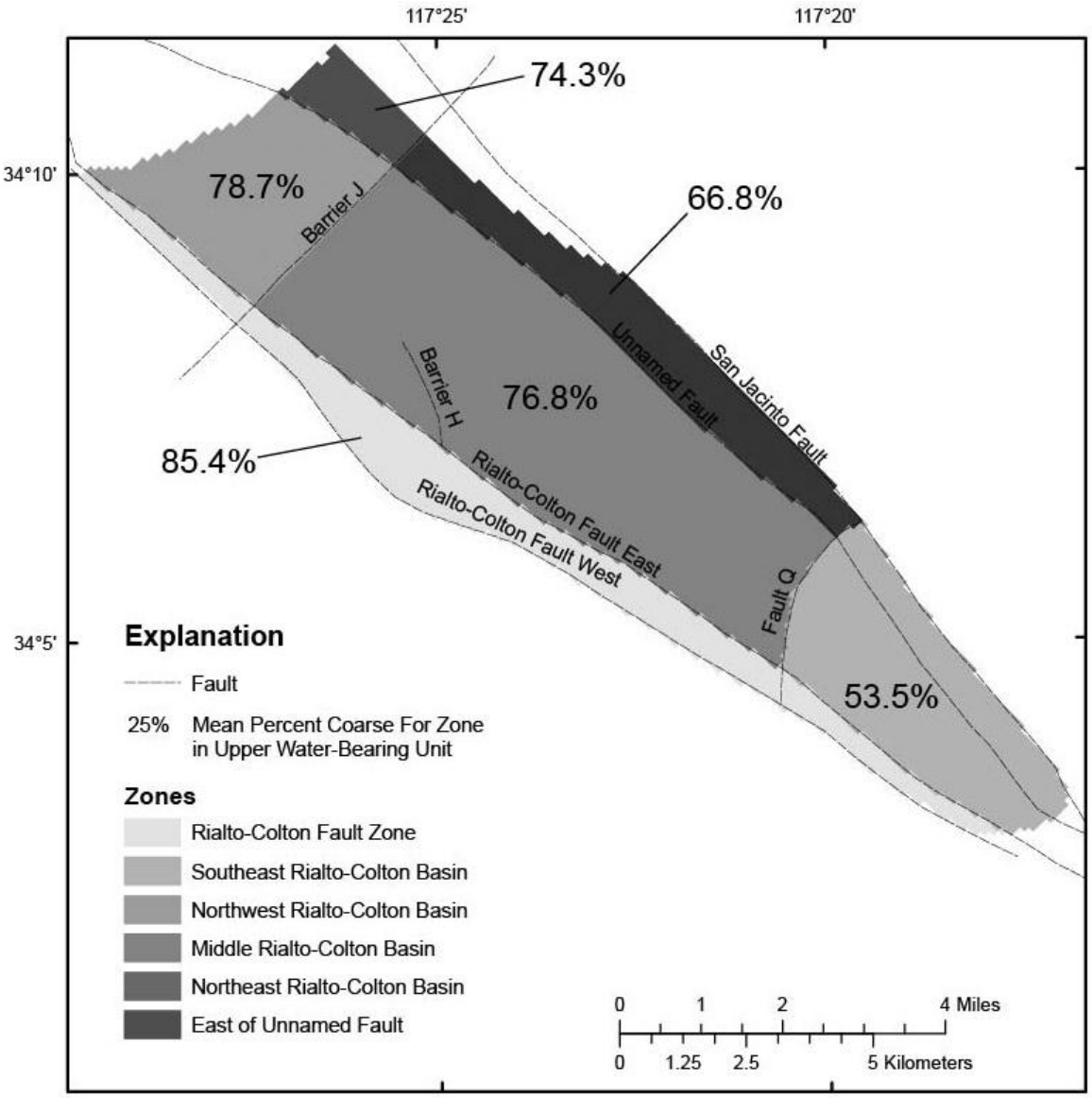

Figure 38: Average (mean) percent coarse by zone for the Upper Water-Bearing Unit.

Sediments are mostly coarse between Fault Q, Barrier J, the Rialto-Colton Fault West, and the Unnamed fault, with the majority of this area consisting of predominately coarse sediments. Sediments northwest of Barrier J between the Unnamed Fault and the Rialto-Colton Fault West

are over 87.5 percent coarse near Barrier J and trend toward finer sediments to the northwest with the northwest corner of the Rialto-Colton Basin under 37.5 percent coarse.

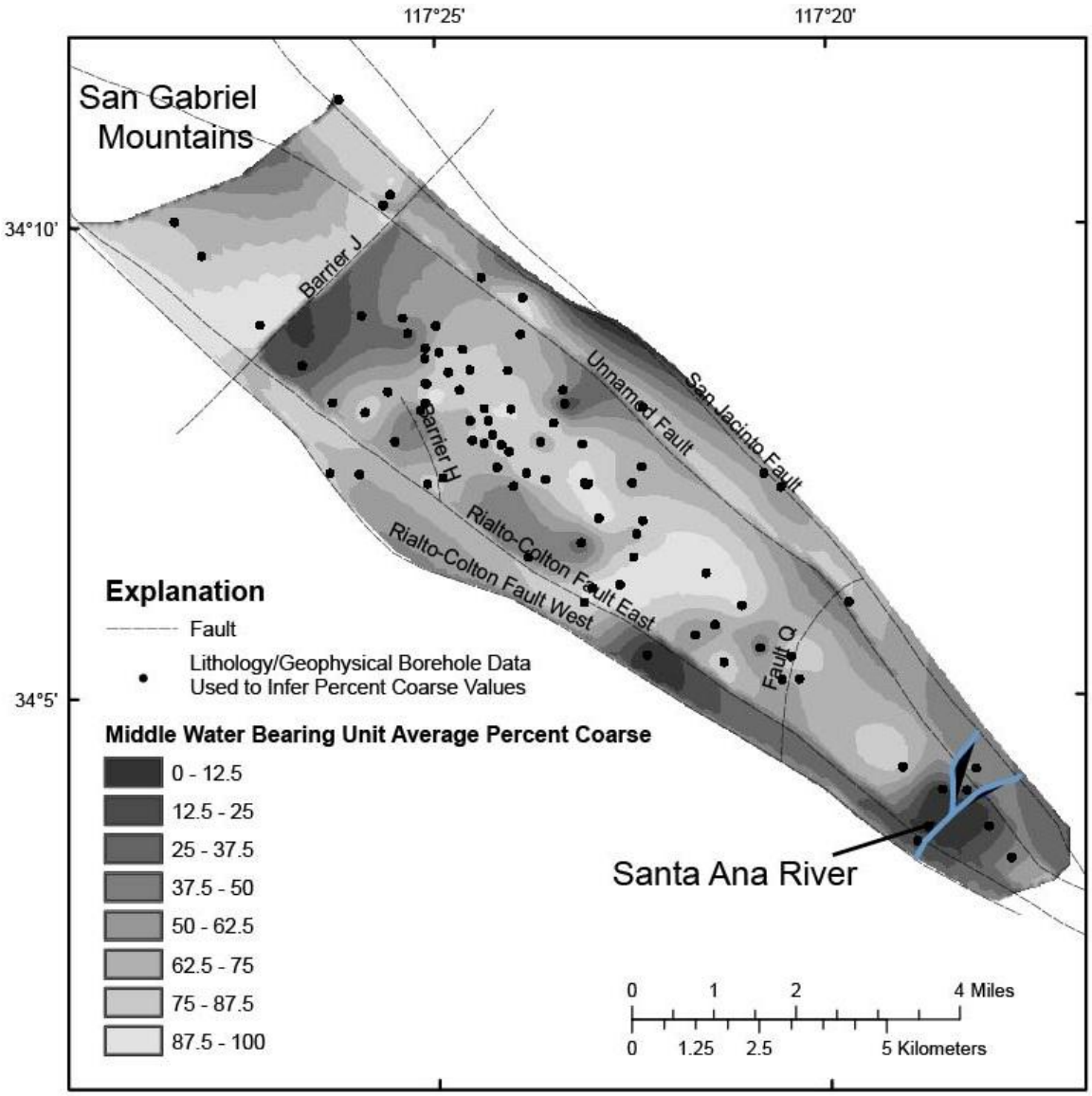

Figure 39: Average percent coarse values of the Middle Water-Bearing Unit.

The Upper Water-Bearing Unit has the highest average percent coarse in the Rialto-Colton Fault Zone (figure 38), with an average percent coarse value of 85.4 percent in this region. Northwest Rialto-Colton Basin has the next highest percent coarse, followed by Middle Rialto-Colton Basin,

Northeast Rialto-Colton Basin, and East of Unnamed Fault, which have 78.7, 76.8, 74.3, and 66.8 percent coarse respectively. The lowest average percent coarse is in Southeast Rialto-Colton Basin, which has only 53.5 percent coarse.

Boreholes with data used in this analysis are distributed throughout the basin, with the highest number in the middle of the basin. Fewer boreholes are located in the part of the basin north of Barrier J, just south of Fault Q, northeast of the Unnamed Fault, and southwest of the Rialto-Colton Fault East (figure 37).

6.5.3 Middle Water-Bearing Unit

The sediments in the Middle Water-Bearing Unit are on average not as coarse as in the Upper Water-Bearing Unit. In the Middle Water-Bearing Unit percent coarse values vary from 50 to 100 in the middle of the basin, with areas of percent coarse values between 0 and 50 in the vicinity of the southeastern and southwestern boundaries of the basin (figure 39). Southeastern Rialto-Colton Basin, between the Rialto-Colton Fault East and Rialto-Colton Fault West one to three miles northwest of Fault Q, and southeast of Barrier J between the Rialto-Colton Fault East and the Unnamed Fault are large areas of predominately fine sediments. There are predominately coarse sediments between the Rialto-Colton Fault East, the Unnamed Fault, Fault Q, and the northeastern end of Barrier H.

Northeast Rialto-Colton Basin and Northwest Rialto-Colton Basin have the highest average percent coarse values for the Middle Water-Bearing Unit, with 73.8 and 70.6 percent coarse respectively (figure 40). Average percent coarse values trend lower to the southeast. Rialto-Colton Fault Zone, Middle Rialto-Colton Basin, and East of Unnamed Fault have roughly the same percent coarse values at 56.5, 59.1, and 54.7 percent coarse respectively. Southeast Rialto-

Colton Basin has the lowest average percent coarse value for the Middle Water-Bearing Unit at 48.1 percent coarse.

The distribution of boreholes with data used in this analysis is similar to that of the Upper Water-Bearing Unit. Most boreholes containing sediments in the Upper Water Bearing Unit were deep enough to contain sediments in the Middle Water-Bearing Unit.

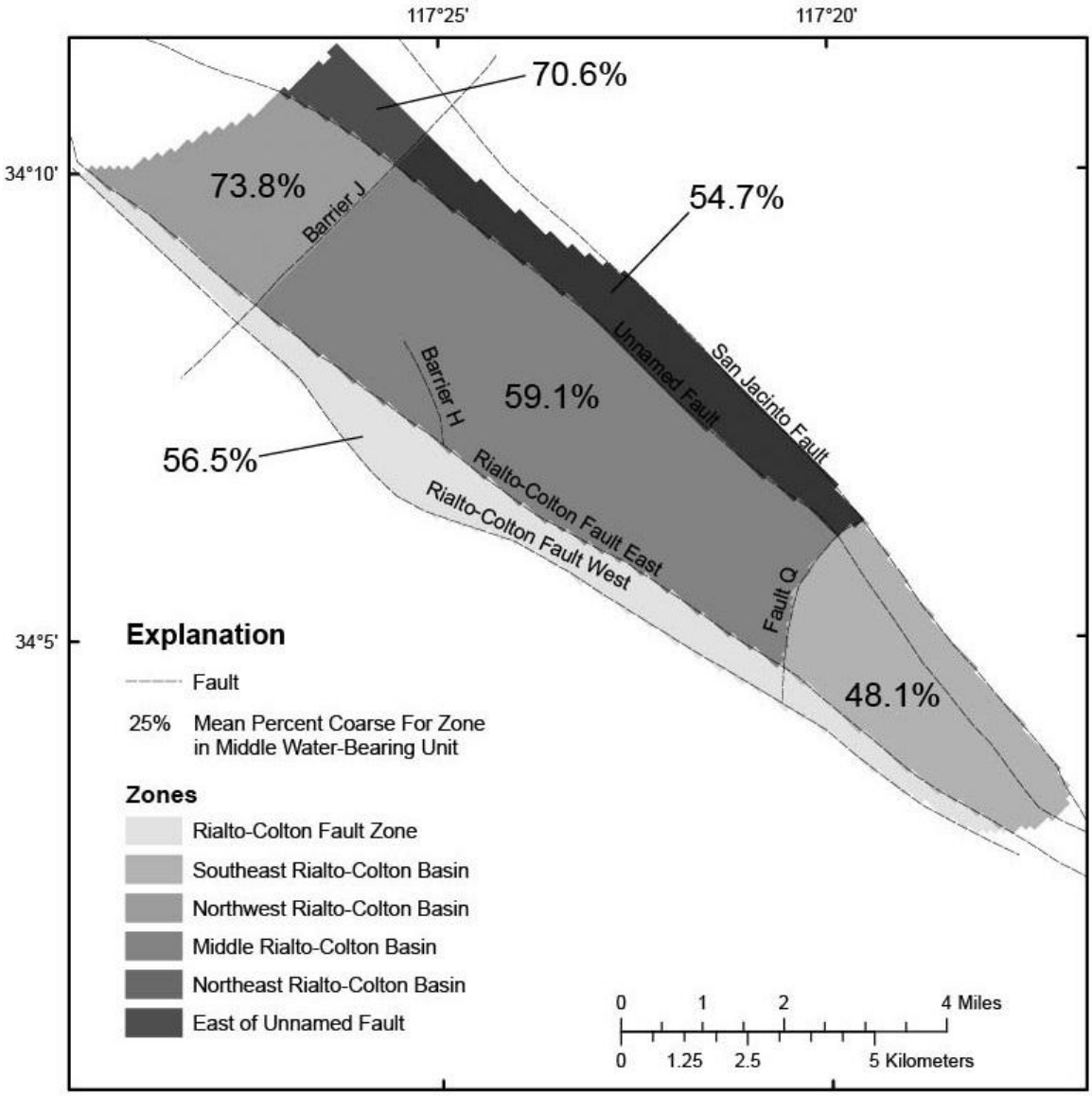

Figure 40: Average (mean) percent coarse by zone for the Middle Water-Bearing Unit.

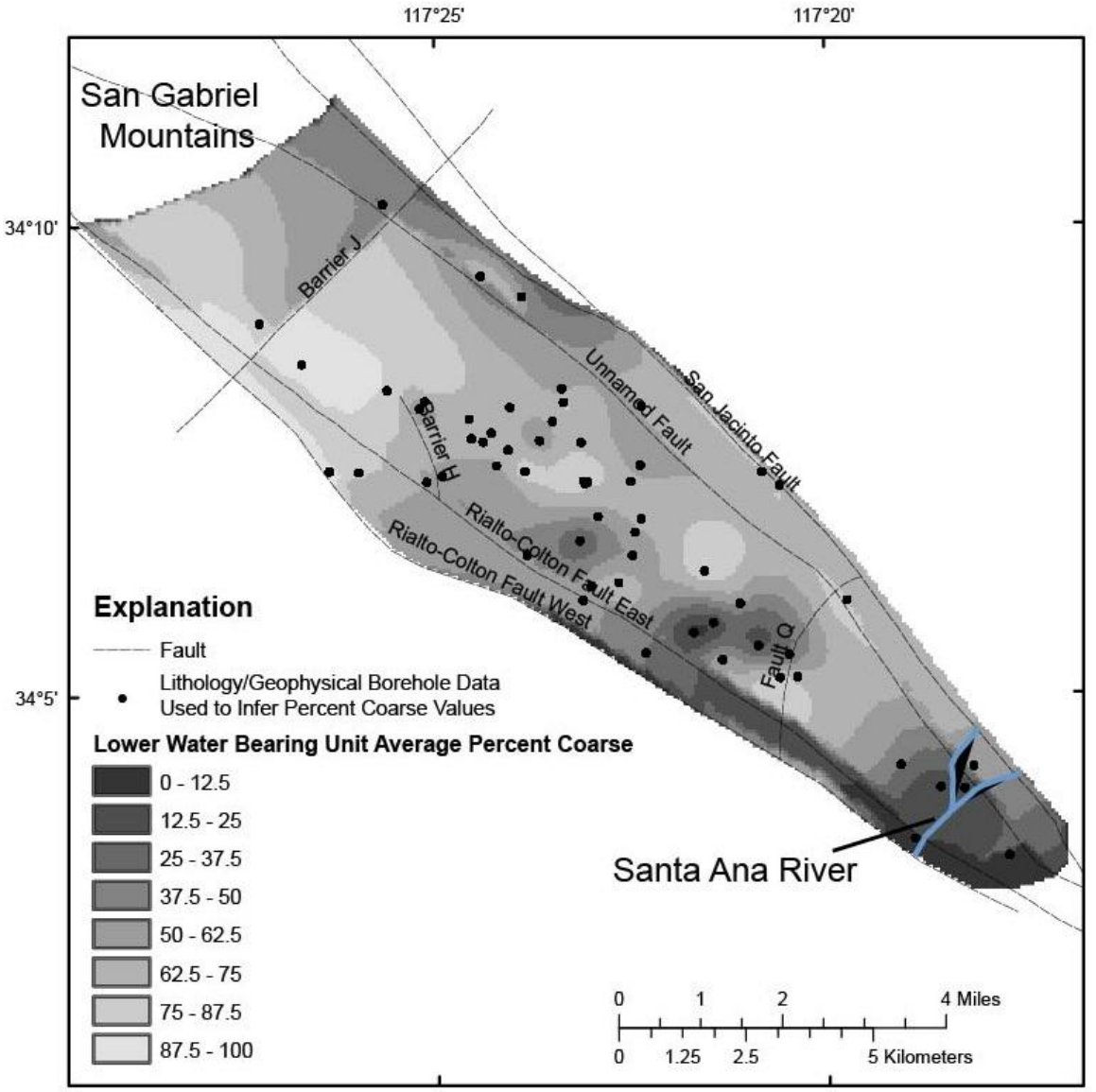

Figure 41: Average percent coarse values for the Lower Water-Bearing Unit.

6.5.4 Lower Water-Bearing Unit

The Lower Water-Bearing Unit contains a mixture of coarse and fine sediments with the finest sediments in the southeastern part of the basin (figure 41). Fine sediments ranging from 25 to 50 percent coarse are located in the northeastern part of the basin in the vicinity of the basin boundary; though due to the sparseness of data in this area, the percent coarse values in this area

are mostly an extrapolation. The coarsest sediment ranging from 75 to 100 percent coarse are located just south of Barrier J.

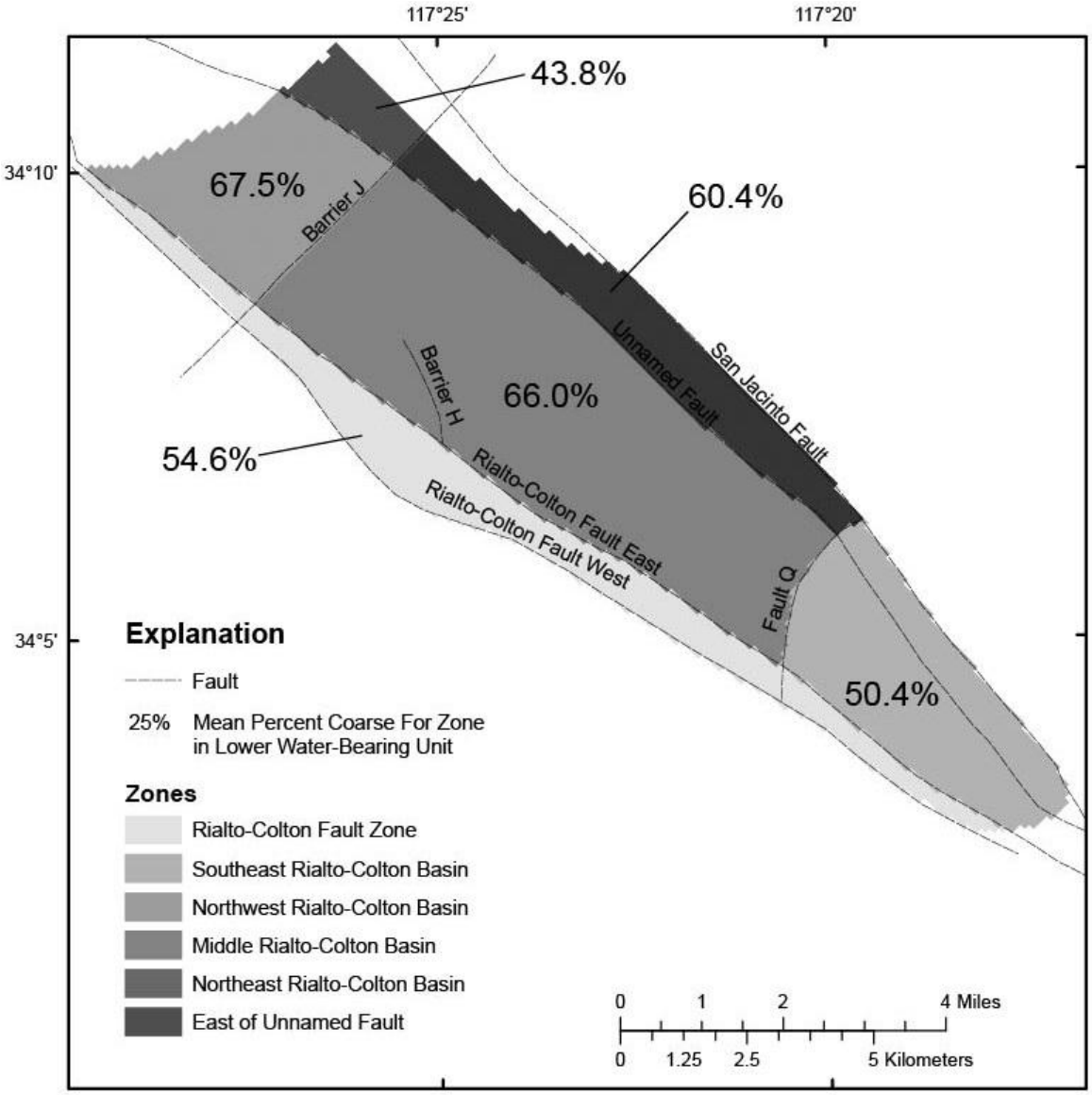

Figure 42: Average (mean) percent coarse by zone for the Lower Water-Bearing Unit.

Northwest Rialto-Colton Basin and Middle Rialto-Colton Basin has the highest average percent coarse in the Lower Water-Bearing Unit, with 67.5 and 66.0 percent coarse respectively (figure 42). East of Unnamed Fault, the Rialto-Colton Fault Zone, and Southeast Rialto-Colton Basin

have 60.4, 54.6, and 50.4 average percent coarse respectively. Northeast Rialto-Colton Basin has the lowest average percent coarse at 43.8 percent.

Less borehole data were available for the Lower Water-Bearing Unit due to the sparseness of wells drilled deep enough to tap this unit. The majority of data points were available in the area south of the northeastern terminus of Barrier H and northwest of Fault Q between the Rialto-Colton Fault East and the Unnamed Fault.

6.5.5 Chino Layer 1

The sediments in Chino Layer 1 vary from predominantly coarse in the vicinity of the Rialto-Colton Fault to predominantly fine in the vicinity of the western and southern boundaries of the study area (figure 43). The highest concentration of coarse sediment is in northeast Chino Basin around Barrier J. This area extends 2-3 miles to the northwest and southwest and extends 3-4 miles to the southeast of the intersection of Barrier J and the Rialto-Colton Fault West. This area has greater than 75 percent coarse sediment, with much of the area close to 100 percent coarse sediment. The lowest concentration of coarse sediment is on the western edge of the study area between latitude 34˚5’ and 34˚7.5’. This area is less than 25 percent coarse sediment.

The boreholes used in this analysis are distributed throughout this part of the study area, with a greater concentration of boreholes in the North Riverside area and a lesser concentration in the northern part of the study area. Boreholes outside the southern and western boundary of the study area were used in the interpolation.

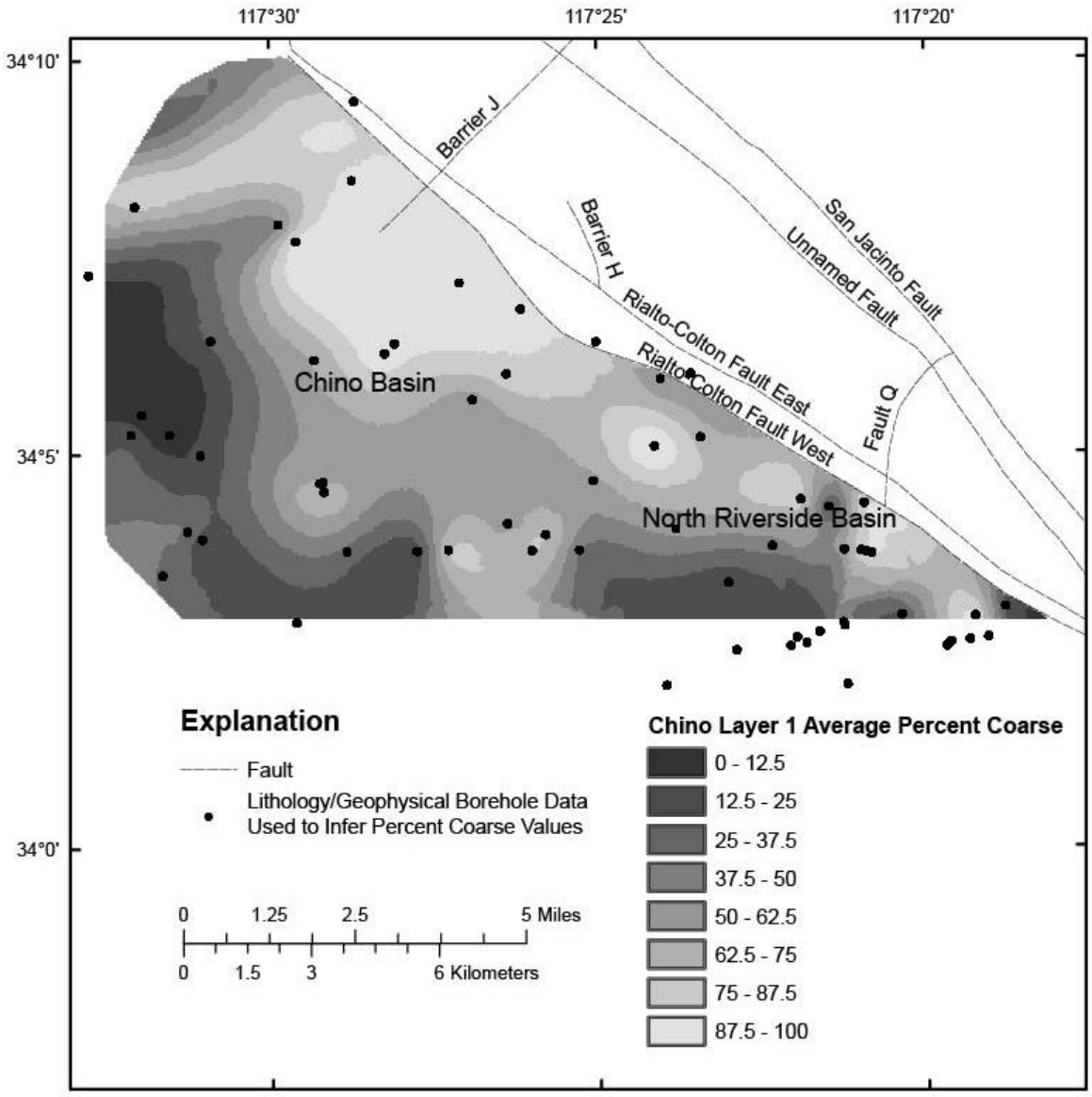

Figure 43: Average percent coarse values for Chino Layer 1.

6.5.6 Chino Layer 2

Sediments in Chino Layer 2 are comparatively fine in the southeastern and the western part of the study area, and comparatively coarse sediments in the middle part of the study area (figure 44). Chino Layer 2 like Chino Layer 1 has an area of high percent coarse near Barrier J and an area of lower percent coarse on the western edge of the study area. These areas are less concentrated in

Chino Layer 2, with the area near Barrier J having lower percent coarse than Chino Layer 1, and the western edge of the study area having higher percent coarse than Chino Layer 1. There are also more fines in North Riverside Basin on the southern boundary of the study area in Chino Layer 2 than Chino Layer 1, with predominantly fine sediments throughout the southeast corner of the study area.

The distribution of boreholes with data for this layer is similar to that of Chino Layer 1, except there are fewer boreholes in the southeastern part of the study area (figure 44). Chino Layer 2 has more boreholes in the southern part of the study area than the northern part, though boreholes are more evenly distributed than in Chino Layer 1.

6.5.7 Chino Layer 3

The sediments in Chino Layer 3 range from 0 to 37.5 percent coarse in the southeastern part of the study area, from 0 to 62.5 percent coarse to in the northern part, and between 37.5 and 100 percent coarse in between (figure 45). The southeastern part of the study area has far more fine sediments in Chino Layer 3 than in Chino Layers 1 and 2. The area of coarse sediments near Barrier J in Chino Layers 1 and 2 is about 2 miles to the southeast in Chino Layer 3. The area of coarse sediments on the western edge of the study area in Chino Layers 1 and 2 is not present in Chino Layer 3.

There is less available borehole data for Chino Layer 3 than Chino Layers 1 and 2. There is a lack of data for Chino Layer 3 in both the northwest and southeast corners of the study area. Data is distributed throughout the rest of the study area, with more data available in the southern half of the study area.

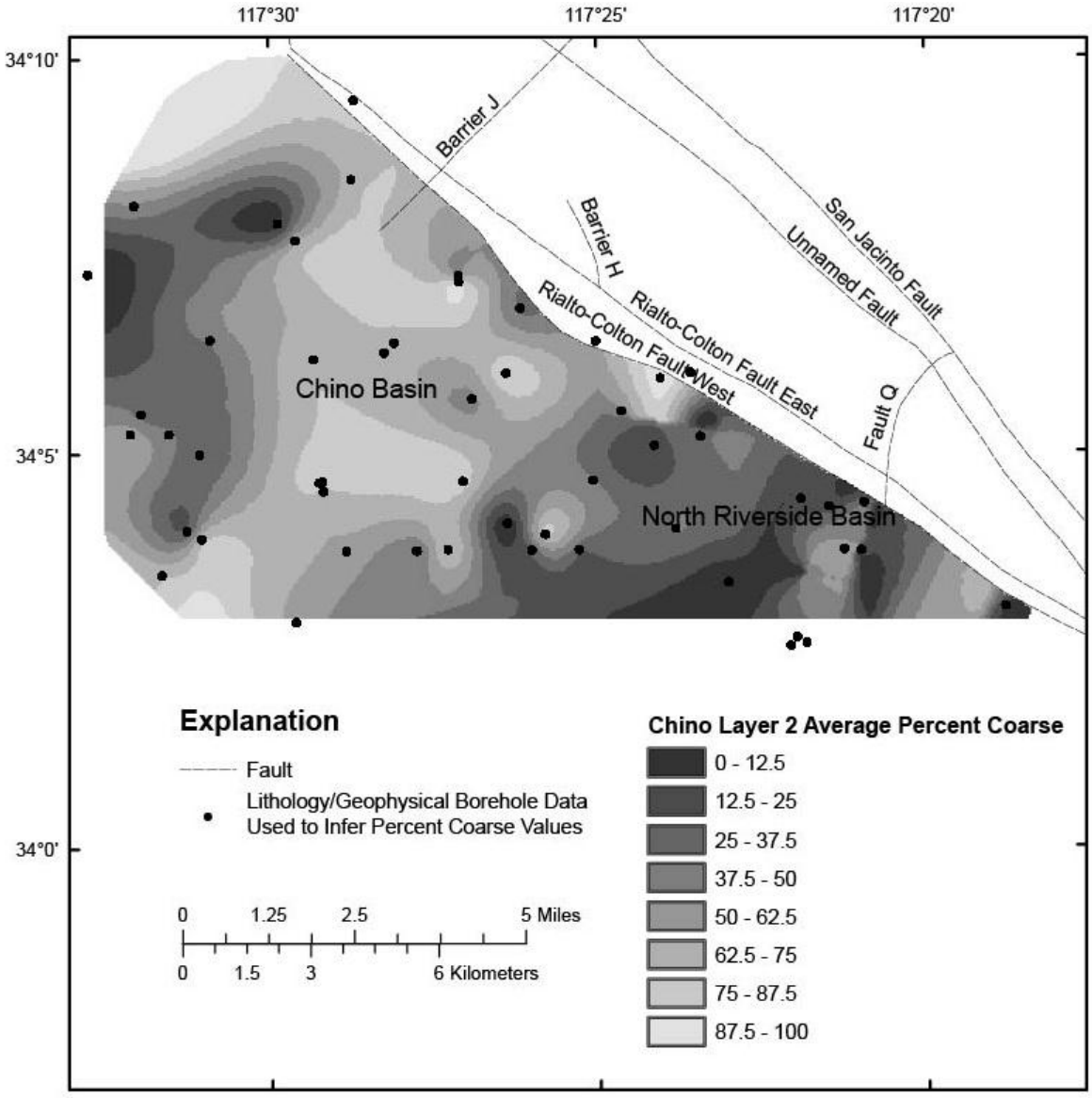

Figure 44: Average percent coarse values for Chino Layer 2.

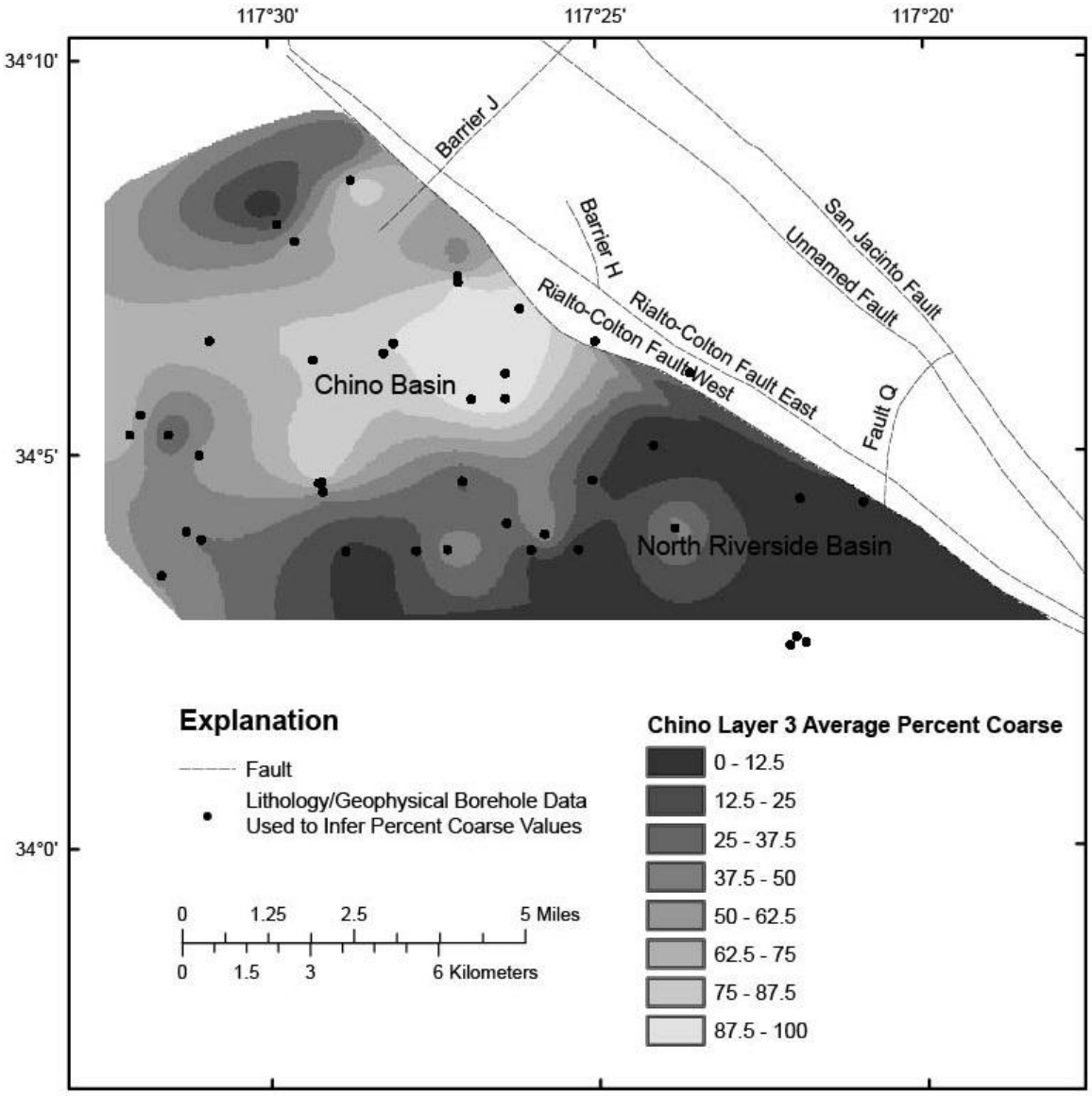

Figure 45: Average percent coarse values for Chino Layer 3.

7 Conclusions

The location of the many faults in the Rialto-Colton Basin is not precisely known. Some of these faults may act as barriers to groundwater flow and may offset alluvial deposits. There was a need to more precisely define the location and extent of these faults for both the conceptual and hydraulic models of the basin. To address this need, previous studies and available seismic, gravity, aeromagnetic, and borehole data were examined in order to construct a structural model of the Rialto-Colton Basin that can be used to gain a better understanding of the fault geometry in the basin.

Previous studies conclude that the Rialto-Colton Fault is part of a larger Rialto-Colton Fault Zone (figure 10). A Rialto-Colton Fault Zone with an eastern and western Rialto-Colton Fault was extended throughout the length of the basin based on previous seismic, gravity, aeromagnetic, and water level studies.

Gravity and InSAR data suggest that a fault (Fault Q) may bound a large sediment-filled graben in the southeastern part of the Rialto-Colton Basin (figure 16). InSAR data suggests this fault may act as a barrier to groundwater flow (figure 18). InSAR and seismic data suggests that the Unnamed Fault may splay from the San Jacinto Fault further to the southeast than previously mapped (figure 18). Seismic data indicates the existence of additional faults in the southeastern part of the Rialto-Colton Basin (figure 16). However, data were not available to determine the extent of these faults to the northwest.

There are several signs of past tectonic stresses in the Rialto-Colton Basin. Gravity data show a graben between the Rialto-Colton Fault and Barrier H (figure 12). The deep graben in the northwestern part of the Rialto-Colton Basin may be due to oblique strike-slip faulting of the Rialto-Colton Fault and Barrier H. The available evidence for the existence of Barrier H

indicates a fault about one mile in length splaying from the eastern trace of the Rialto-Colton Fault Zone at a 35 to 45 degree angle.

Alluvial fans typically approximate the shape of a cone segment with a convex-up cross-sectional profile (Boggs, 2006). The water bearing units in the Rialto-Colton Basin are thicker to the northwest near the San Gabriel Mountains (figure 11). This trend is consistent with the San Gabriel Mountains being the main sediment source of these alluvial fan deposits, with the deposits having a convex-up cross sectional profile that is thickest in the center and thins away from the source. The Rialto-Colton Basin water bearing units are also thicker to the northeast near the San Jacinto Fault (figure 11). This trend is consistent with subsidence occurring during deposition along the subsidence contours from Wisely and Schmidt (2010).

Around the Rialto-Colton Fault Zone and the San Gabriel Mountains there are similar trends in thickness between the water bearing units in the Chino and North Riverside area and corresponding water bearing units in the Rialto-Colton area. The thicknesses of the Upper Water-Bearing Unit and Chino Layer 1 are greatest near the base of the San Gabriel Mountains to the northeast, with the Upper Water-Bearing Unit between 314 and 546 feet thick and Chino Layer 1 between 407 and 498 feet thick in this area. The thicknesses of the Middle Water-Bearing Unit and Chino Layer 2 are greatest near the Rialto-Colton Fault Zone between the San Gabriel Mountains and Barrier H. The Middle Water-Bearing Unit ranges from 496 to 676 feet thick and Chino Layer 2 ranges from 176 to 400 feet thick in this area. The thicknesses of the Lower Water-Bearing Unit and Chino Layer 3 are least near the Rialto-Colton Fault Zone between the San Gabriel Mountains and the Santa Ana River. The Lower Water Bearing Unit ranges from 18 to 400 feet and Chino Layer 3 ranges from 2 to 62 feet in this area.

The interpolation of percent coarse data indicated that higher concentrations of fine sediments occur in the southeastern part of the Rialto-Colton Basin while much of the middle part of the basin contains higher concentrations of coarse sediment (figures 37-42). In the Chino and North Riverside areas, fine sediments generally occur in the southern and western parts of the study area and coarse sediments generally occur in the northern half of the study area near the Rialto-Colton Fault Zone (figures 43-45).

Appendix A: Borehole Geophysical and Lithological Logs with Stratigraphic Interpretations for Selected Boreholes

Borehole lithology, 16 inch normal resistivity, gamma, and spontaneous potential logs were analyzed to determine the boundaries of water bearing units in the Rialto-Colton Basin. The locations of analyzed boreholes are shown in figure 46. The analyzed lithological and geophysical logs for each borehole are shown in figures 47-76.

A shift in the resistivity, gamma, and/or spontaneous potential logs often occurs at the boundaries of water bearing units (Woolfenden and Kadhim, 1997). This shift was most often seen at the boundary of the upper and middle water bearing units and at the boundary of the lower water bearing unit and the consolidated deposits.

A change in lithology, as described in the drillers' logs, was not consistently observed at the boundaries of the water bearing units. At the boundary of the upper and middle water bearing units the lithology often changed from coarse gravel and sand in the upper unit to finer sediment in the middle unit. At the boundary of the lower water bearing unit and consolidated deposits there was often an increase in lithologies described as "hard", "compacted", or "cemented" in the consolidated deposits.

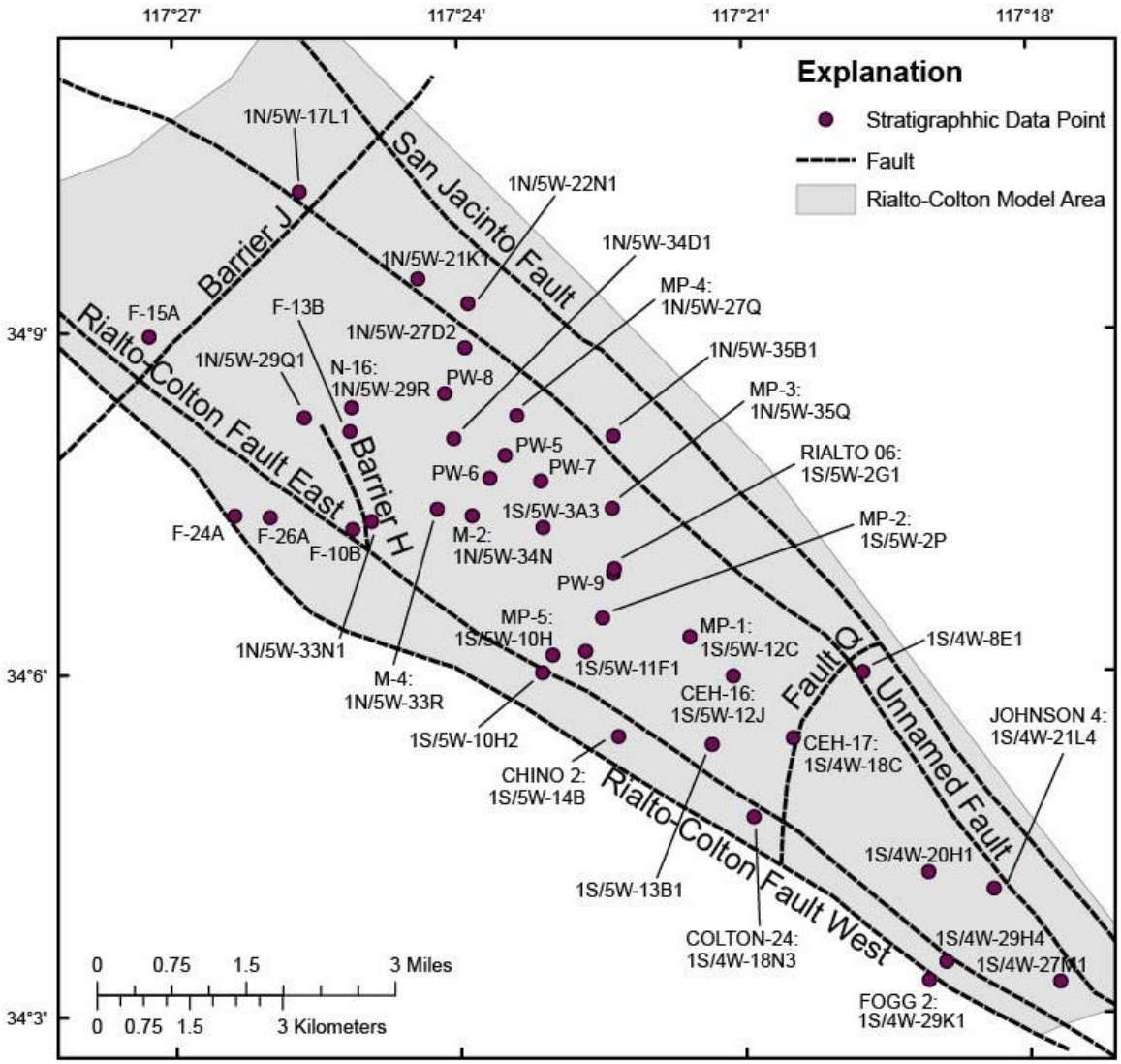

Figure 46: Selected boreholes with stratigraphic interpretations in the Rialto-Colton model area.

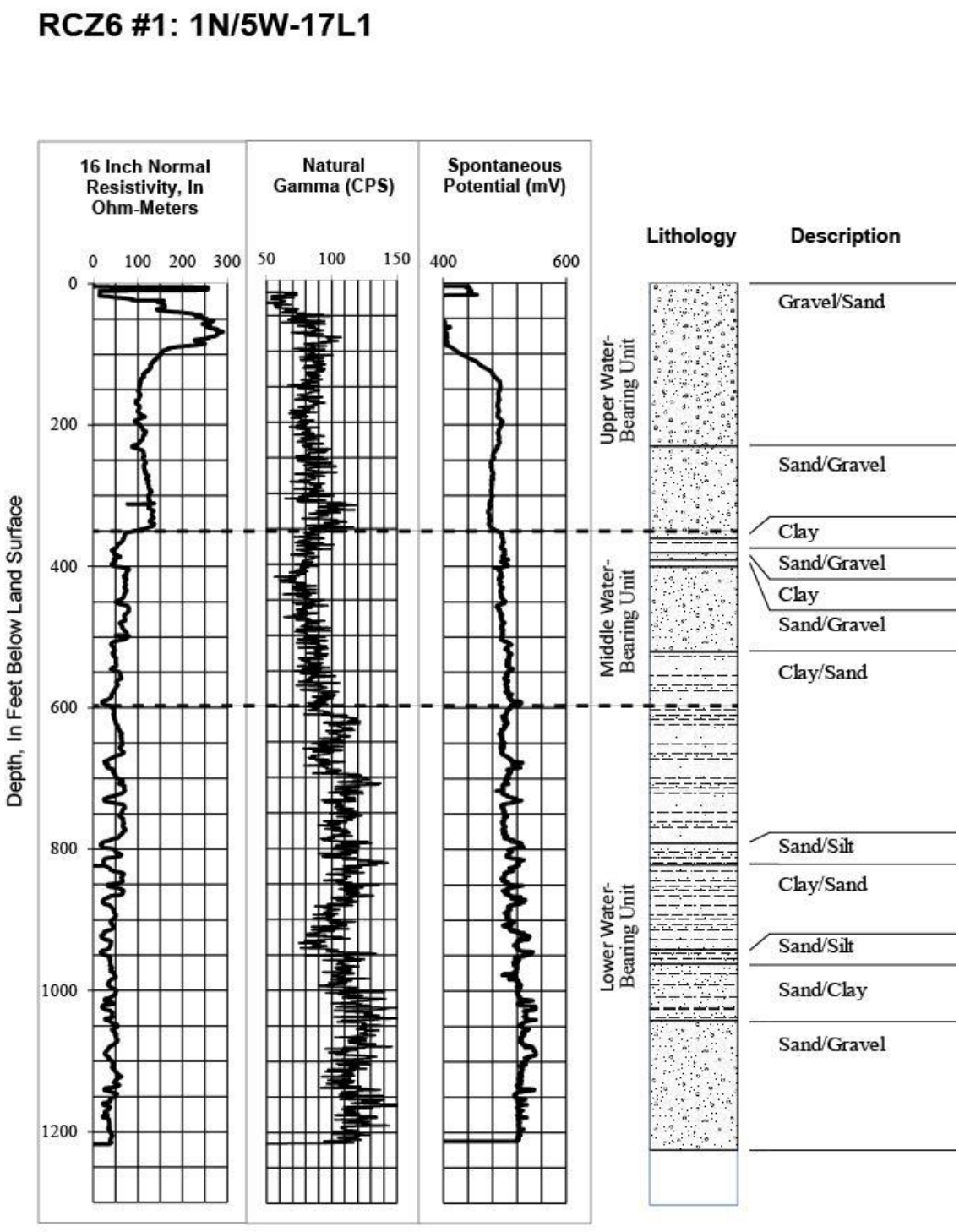

Figure 47: Borehole geophysical logs and lithology logs for RCZ6 #1.

Dashed lines represent interpreted boundaries of water-bearing units.

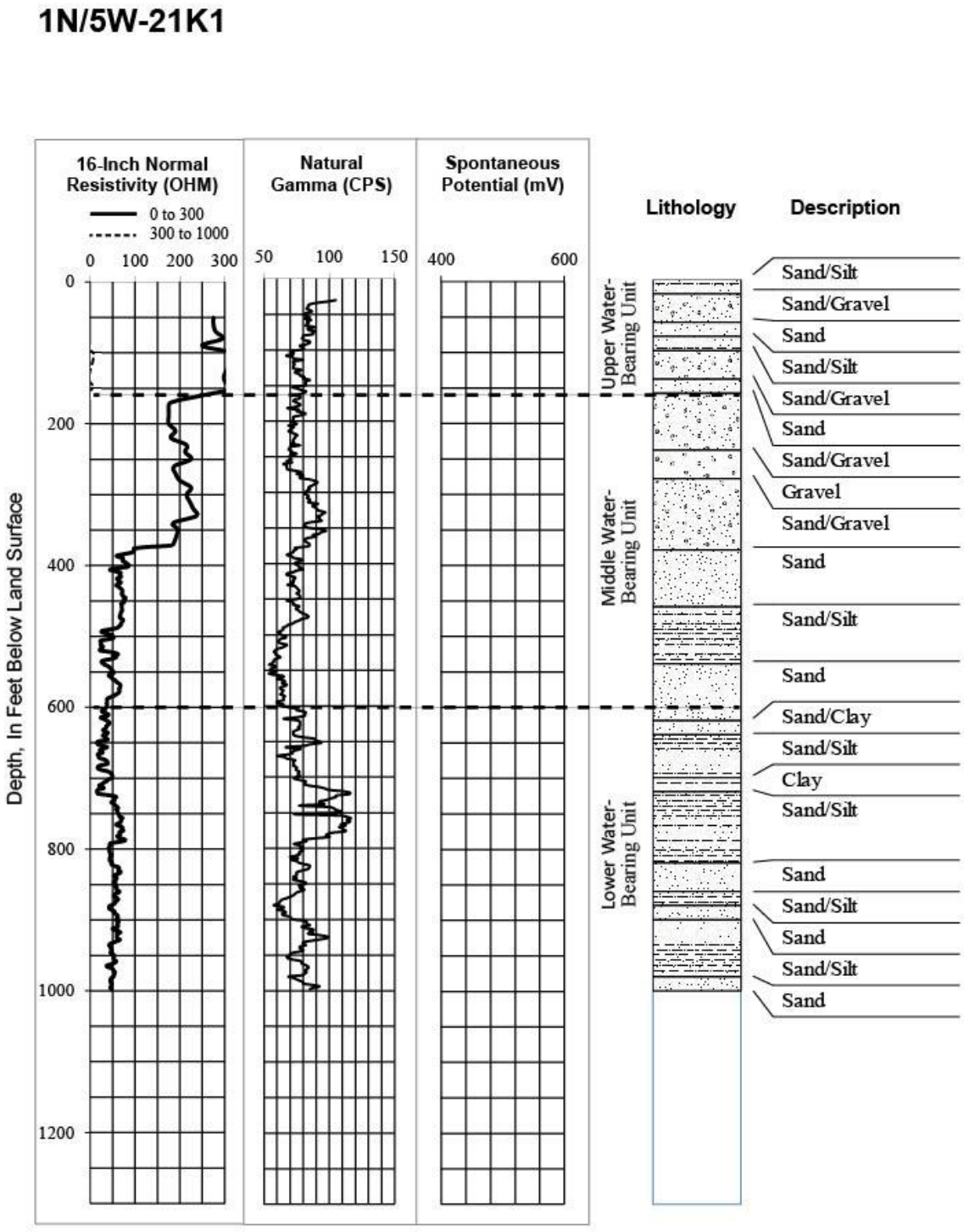

Figure 48: Borehole geophysical logs and lithology logs for 1N/5W-21K1.

Dashed lines represent interpreted boundaries of water-bearing units.

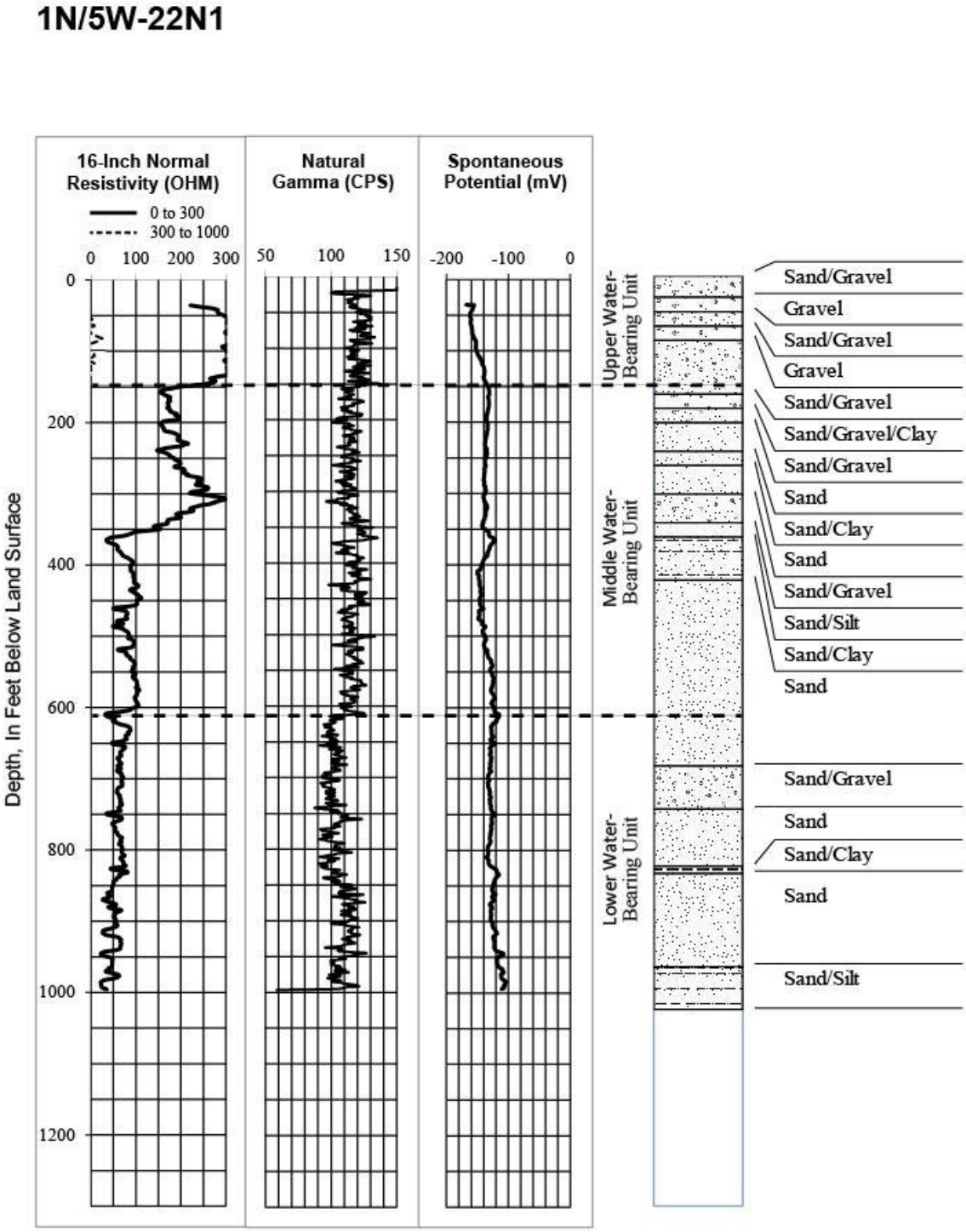

Figure 49: Borehole geophysical logs and lithology logs for 1N/5W-22N1.

Dashed lines represent interpreted boundaries of water-bearing units.

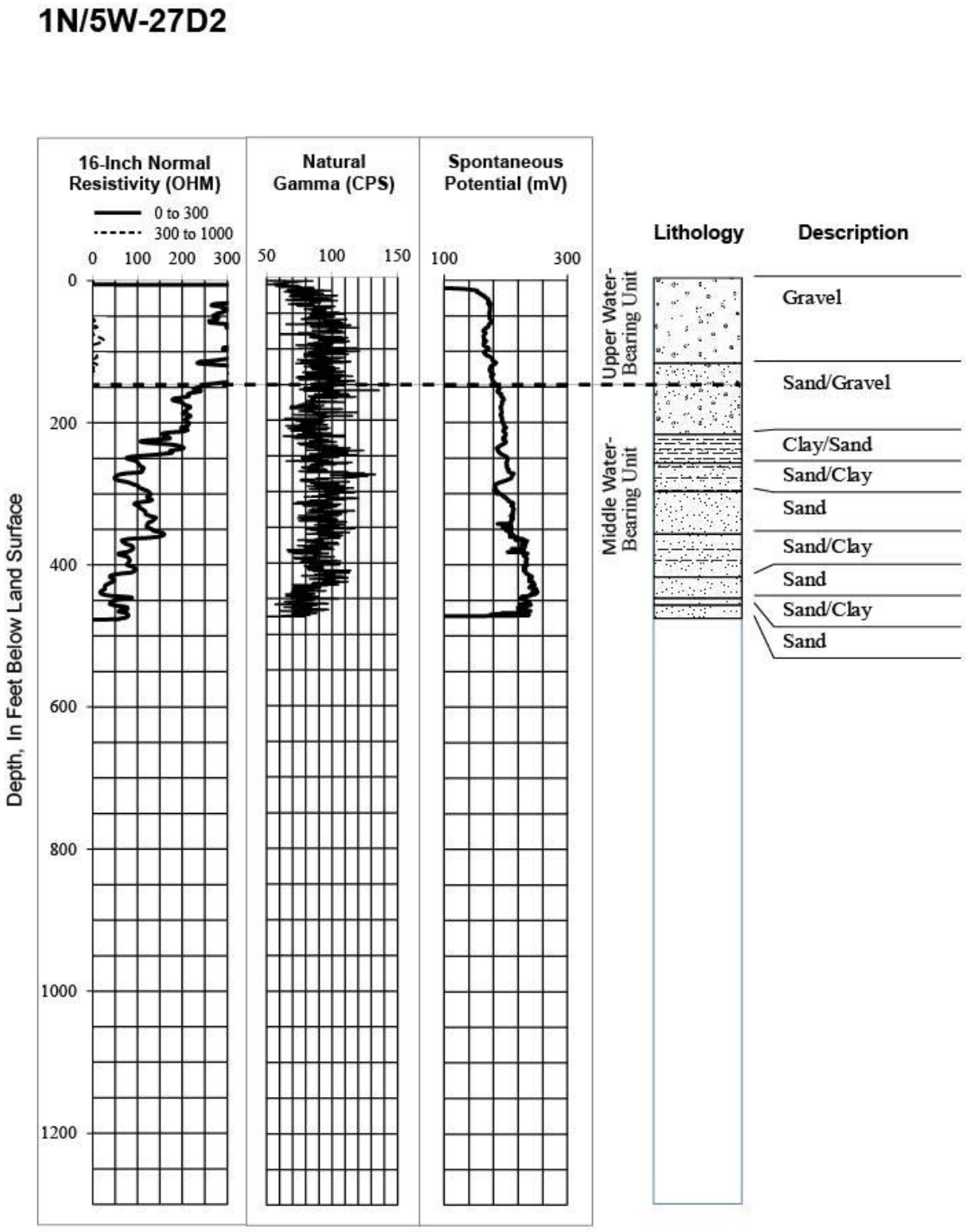

Figure 50: Borehole geophysical logs and lithology logs for 1N/5W-27D2.

Dashed lines represent interpreted boundaries of water-bearing units.

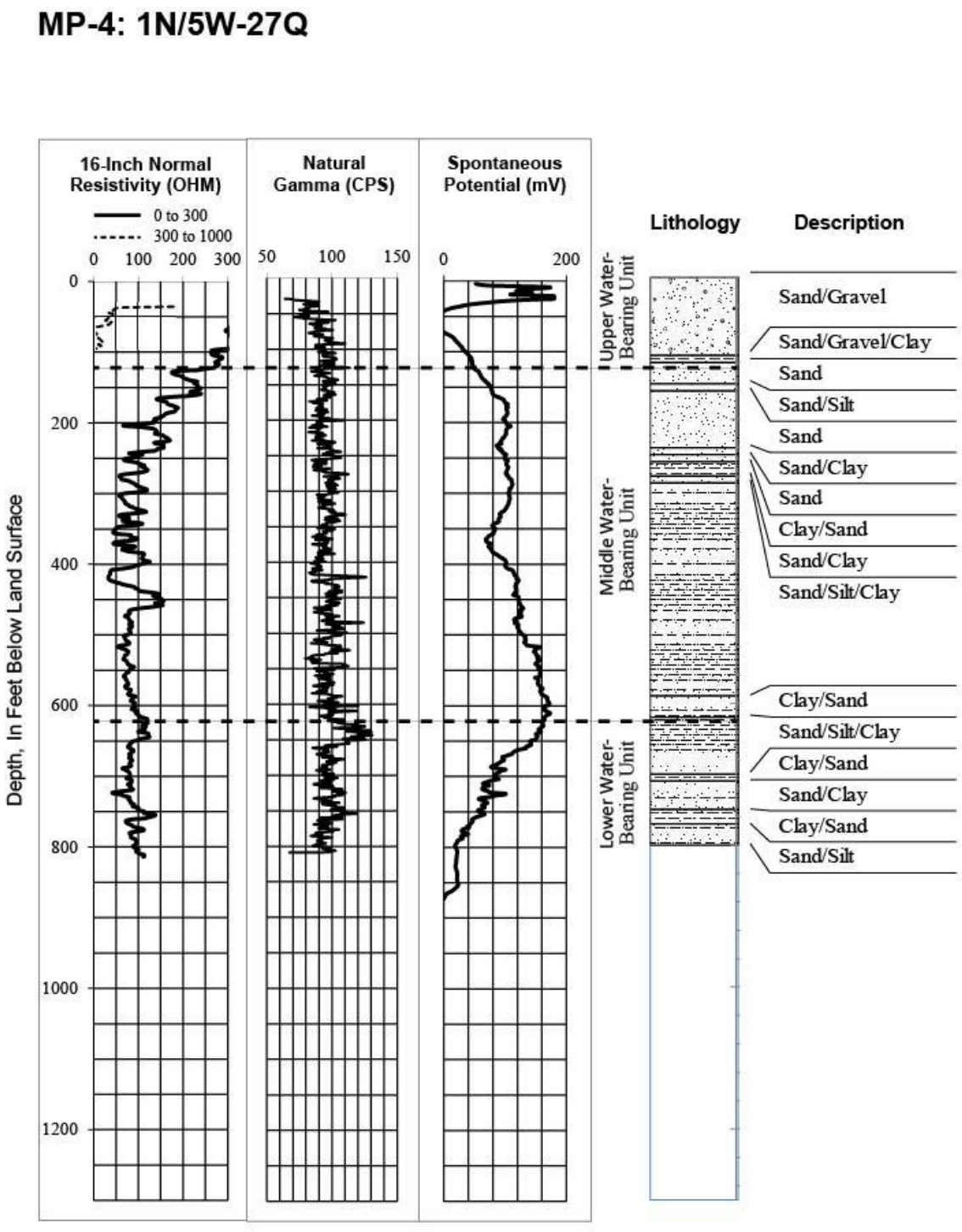

Figure 51: Borehole geophysical logs and lithology logs for MP-4.

Dashed lines represent interpreted boundaries of water-bearing units.

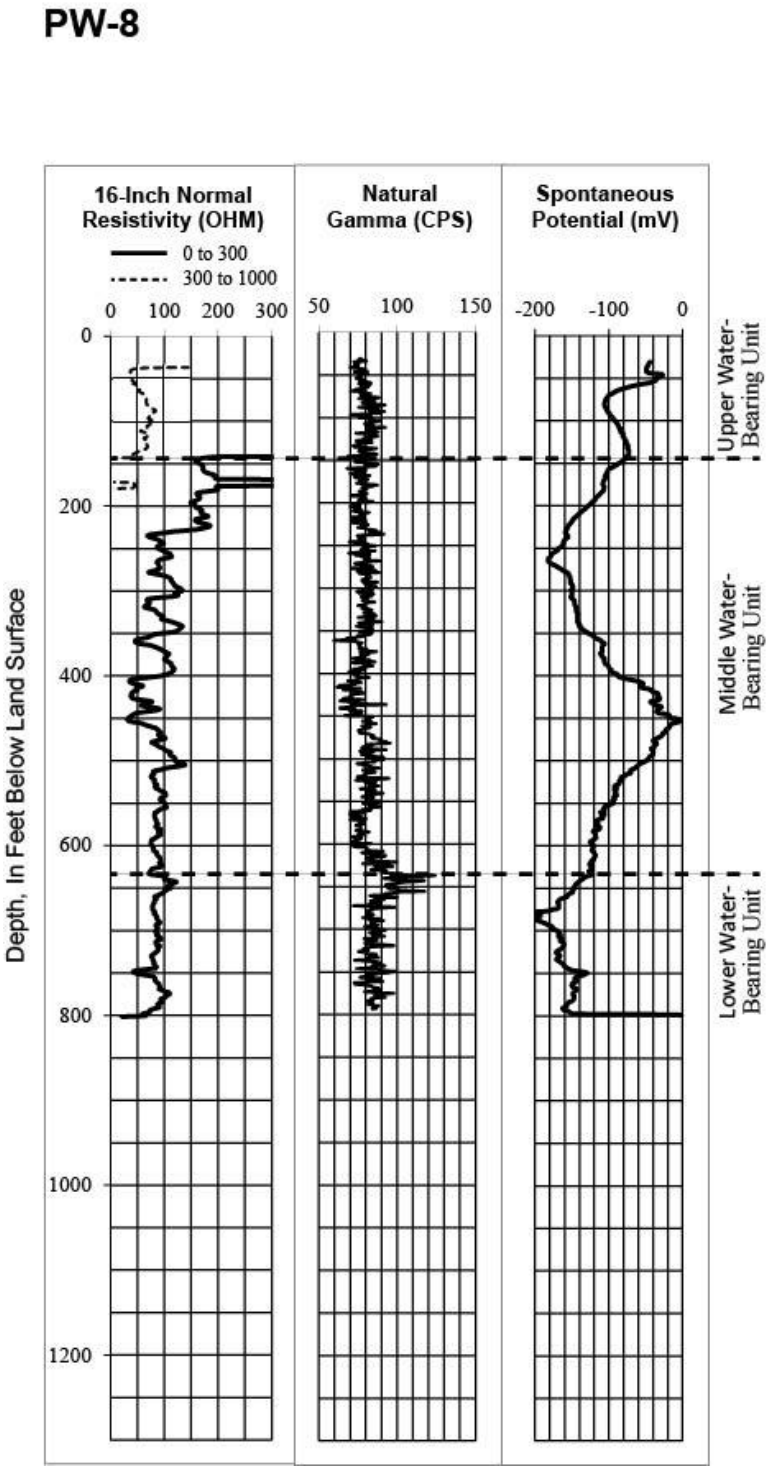

Figure 52: Borehole geophysical logs and lithology logs for PW-8.

Dashed lines represent interpreted boundaries of water-bearing units.

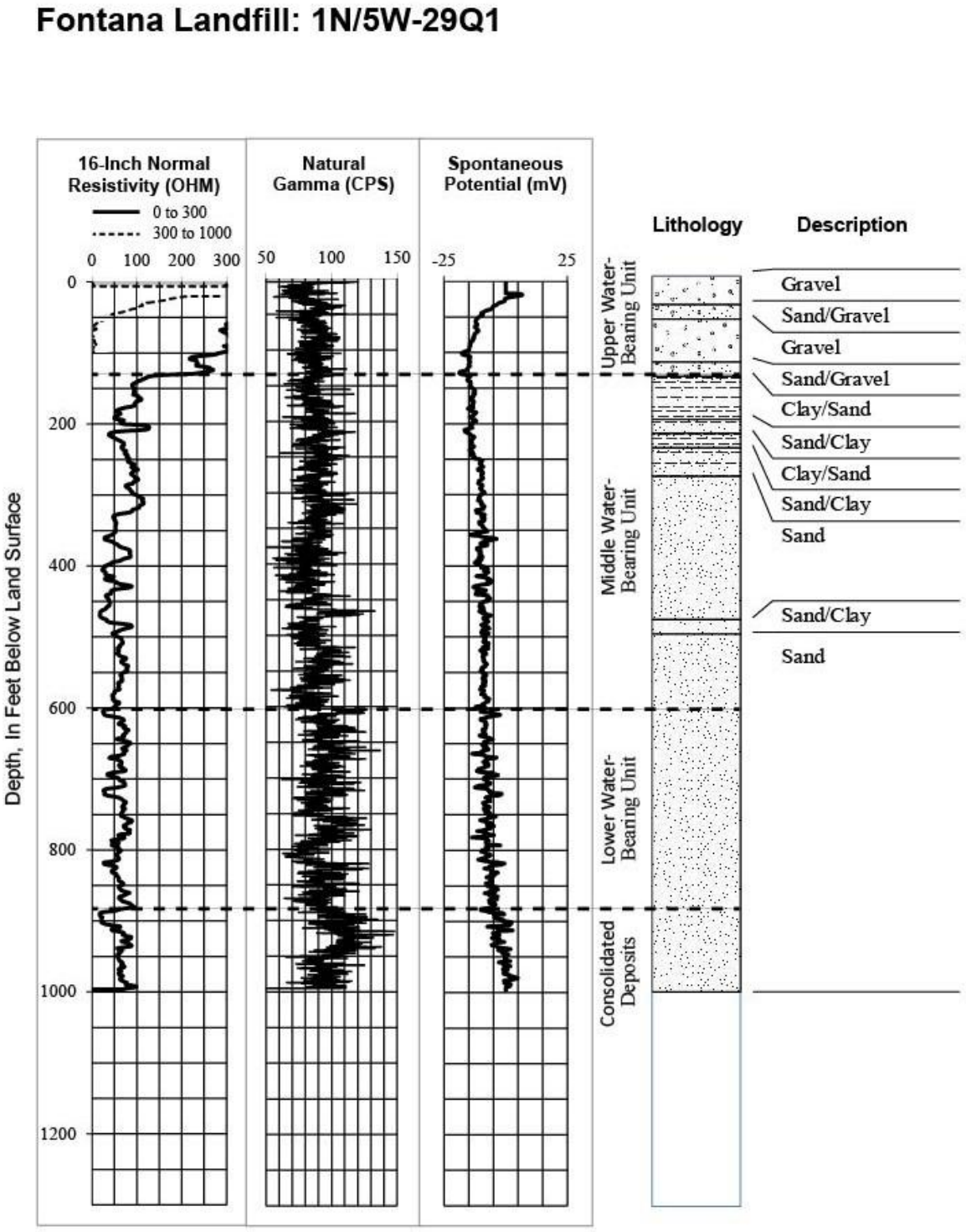

Figure 53: Borehole geophysical logs and lithology logs for 1N/5W-29Q1.

Dashed lines represent interpreted boundaries of water-bearing units.

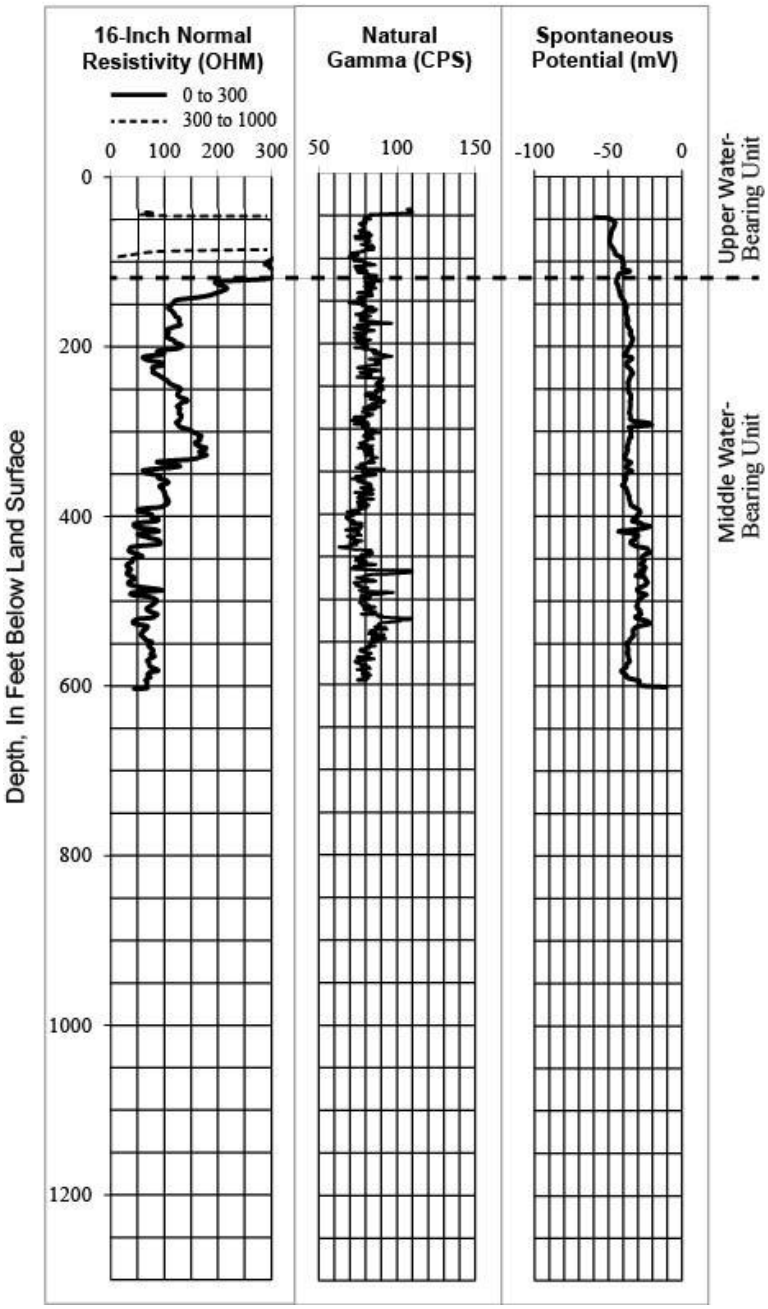

Figure 54: Borehole geophysical logs and lithology logs for 1N/5W-29R.

Dashed lines represent interpreted boundaries of water-bearing units.

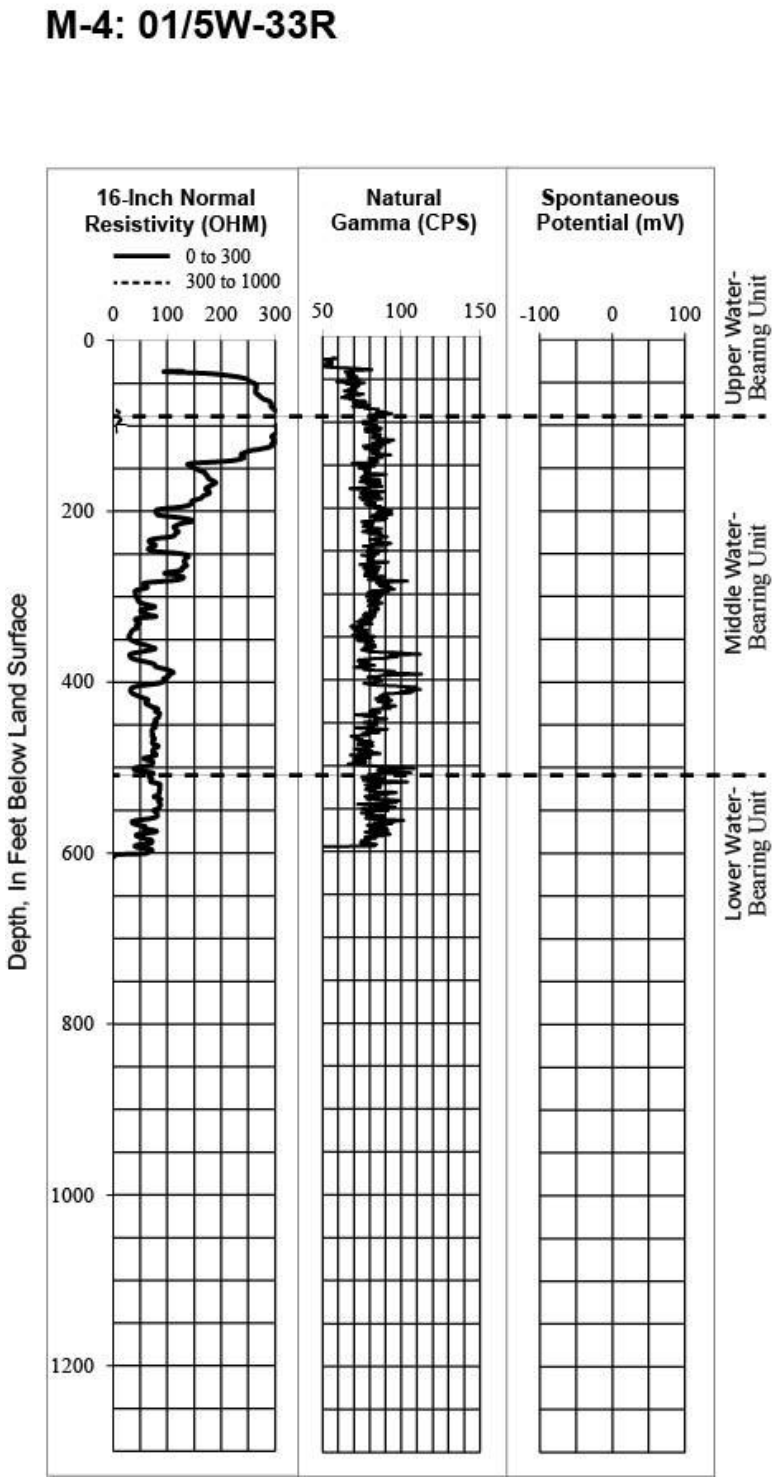

Figure 55: Borehole geophysical logs and lithology logs for M-4.

Dashed lines represent interpreted boundaries of water-bearing units.

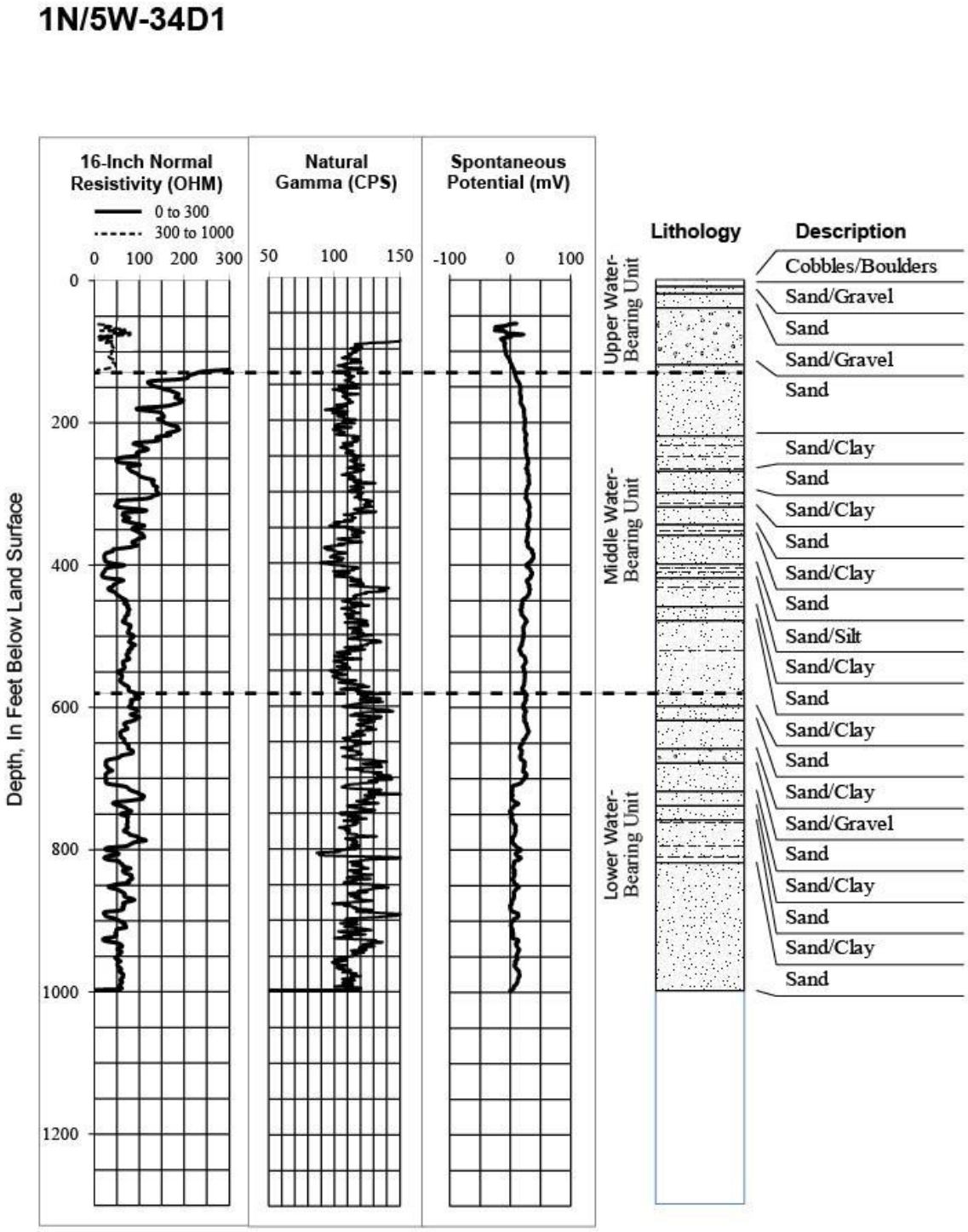

Figure 56: Borehole geophysical logs and lithology logs for 1N/5W-34D1.

Dashed lines represent interpreted boundaries of water-bearing units.

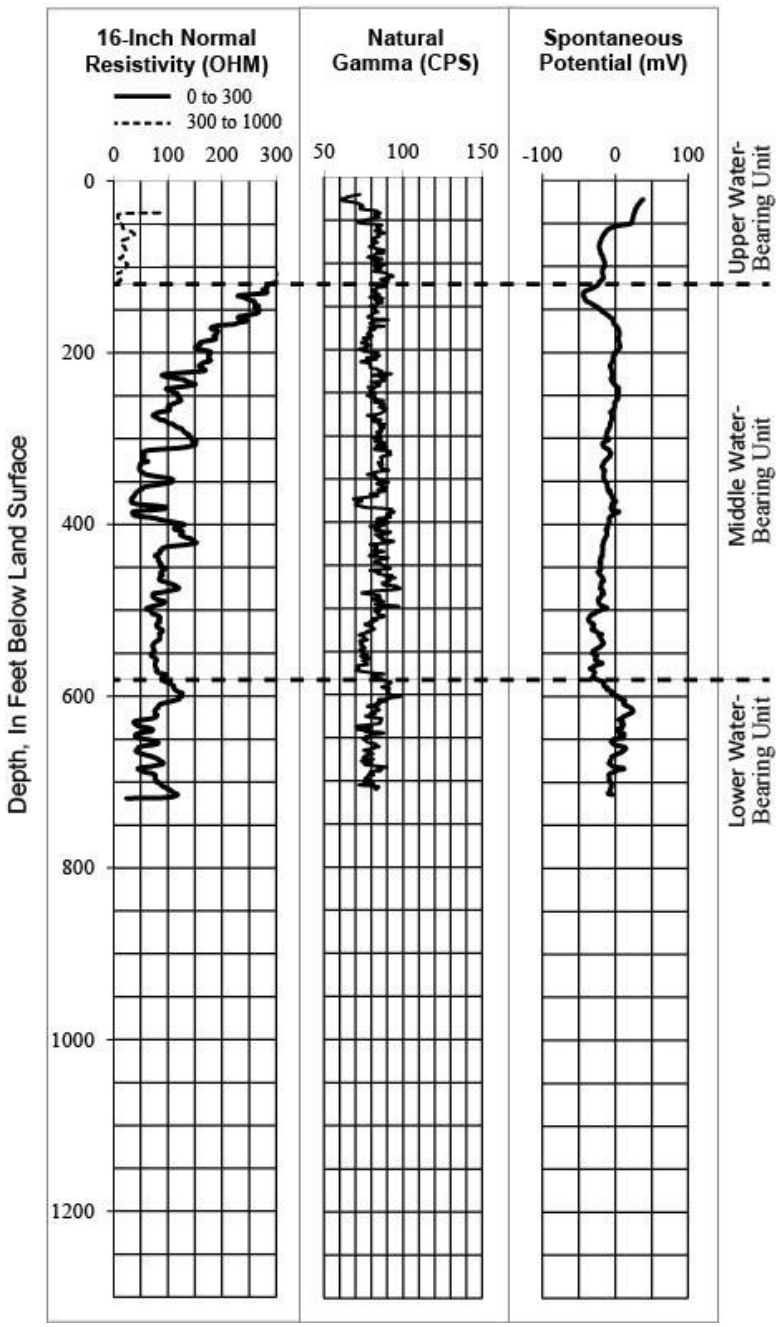

Figure 57: Borehole geophysical logs and lithology logs for PW-5.

Dashed lines represent interpreted boundaries of water-bearing units.

PW-7

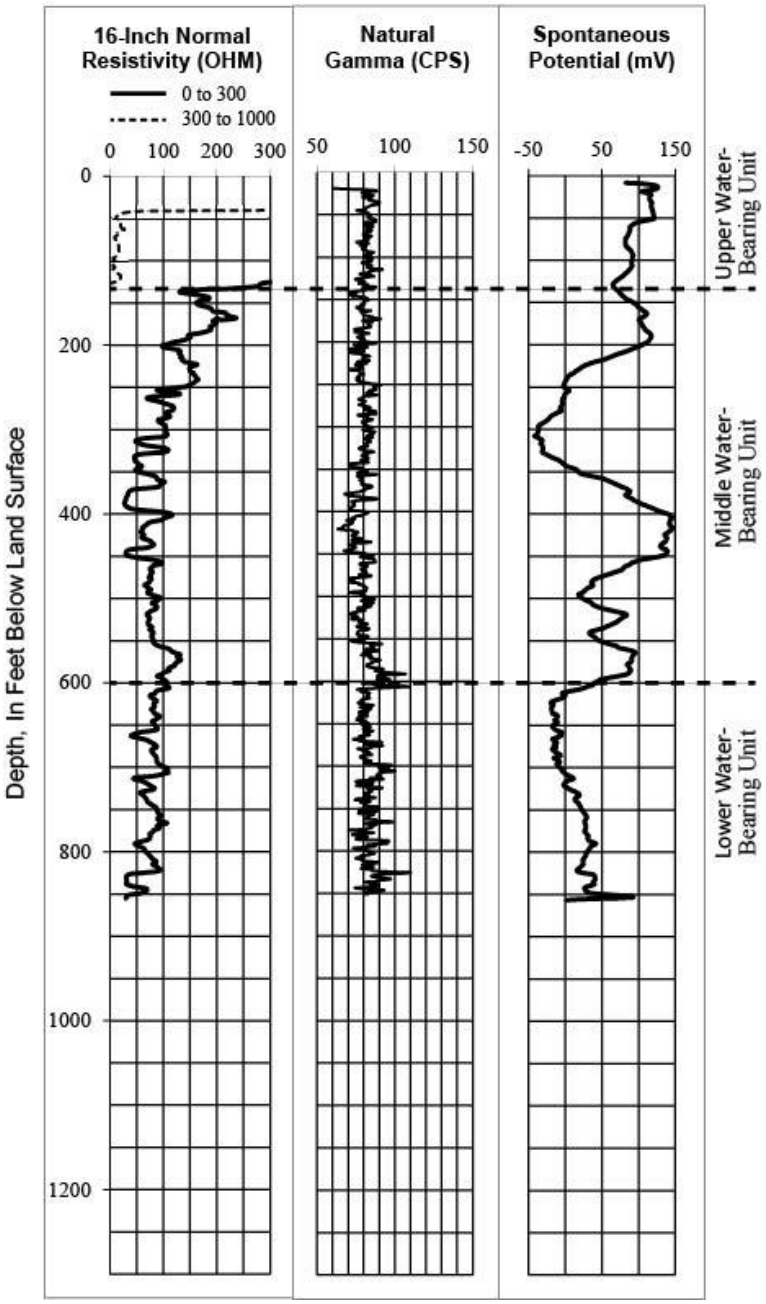

Figure 58: Borehole geophysical logs and lithology logs for PW-7.

Dashed lines represent interpreted boundaries of water-bearing units.

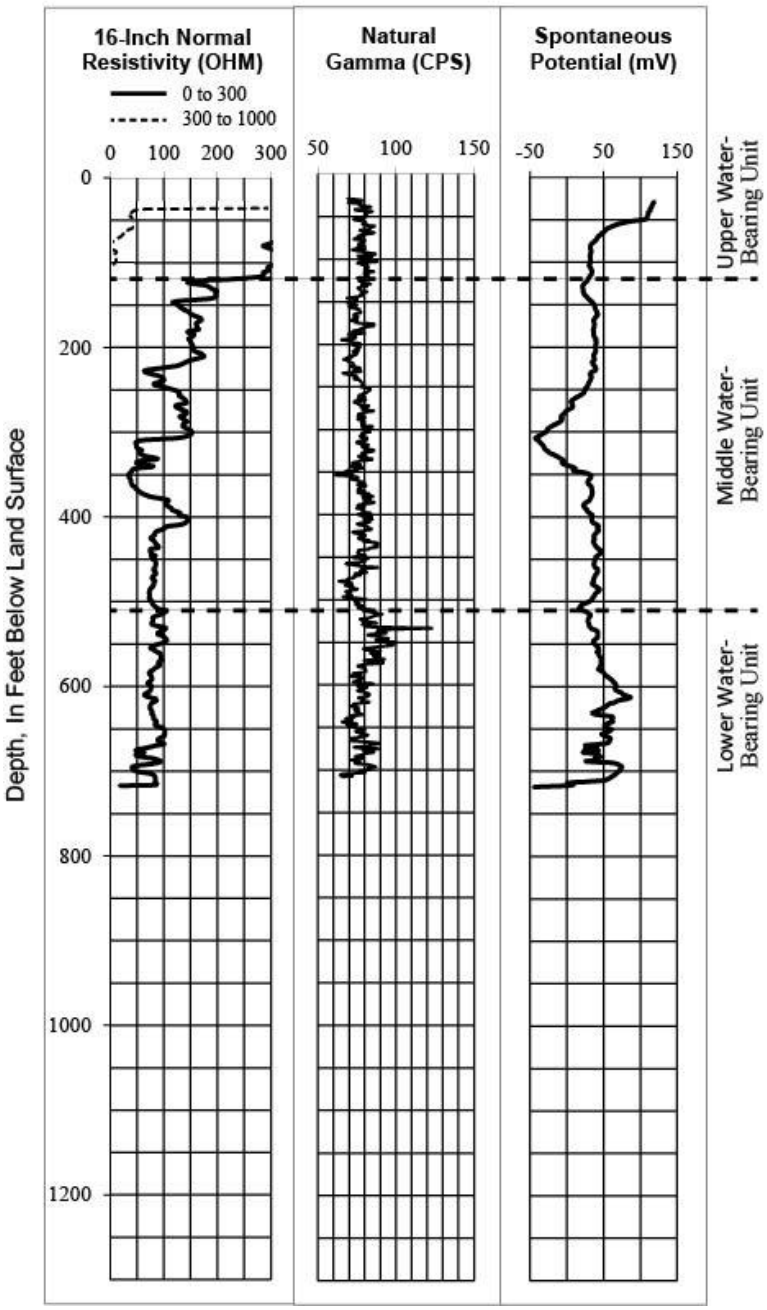

Figure 59: Borehole geophysical logs and lithology logs for PW-6.

Dashed lines represent interpreted boundaries of water-bearing units.

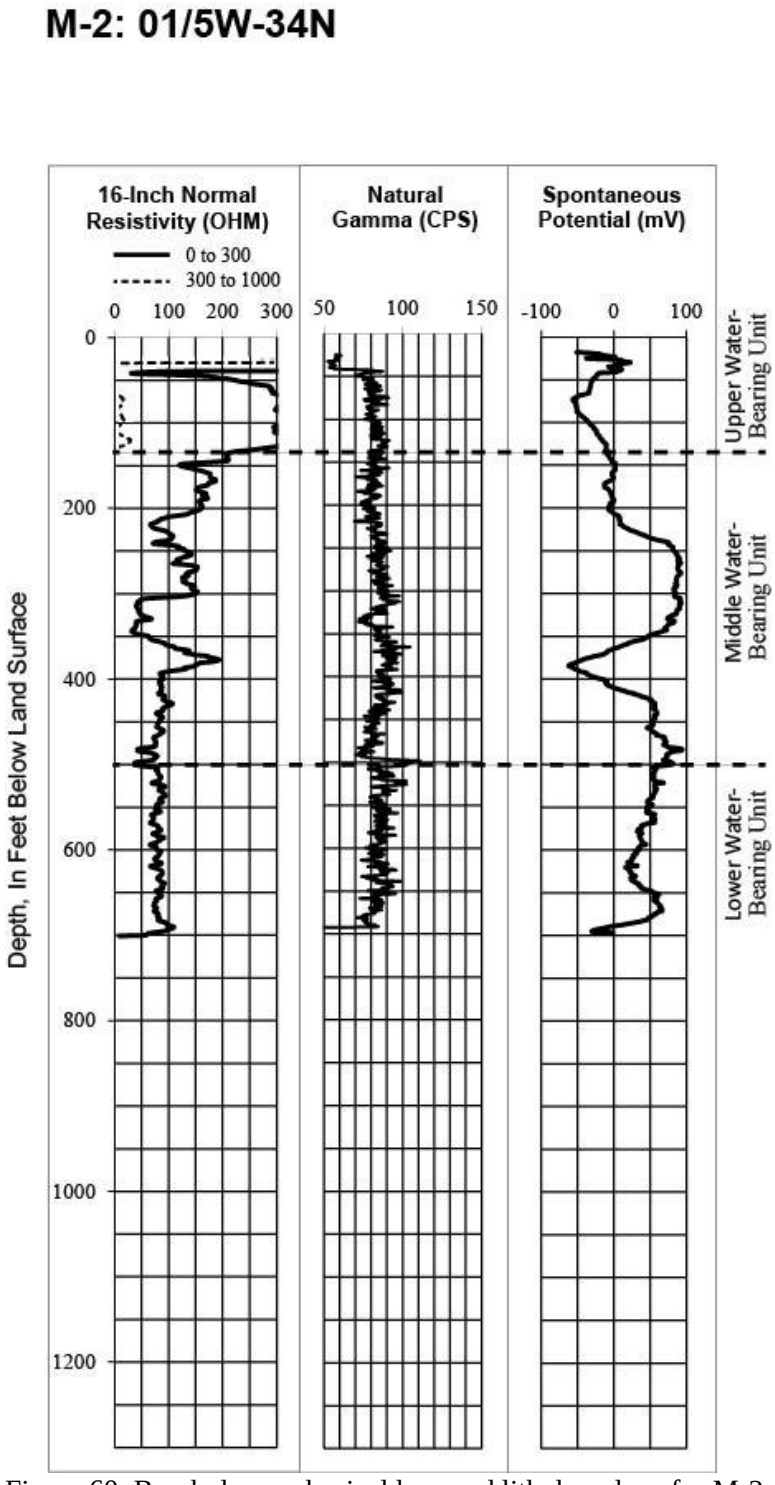

Figure 60: Borehole geophysical logs and lithology logs for M-2.

Dashed lines represent interpreted boundaries of water-bearing units.

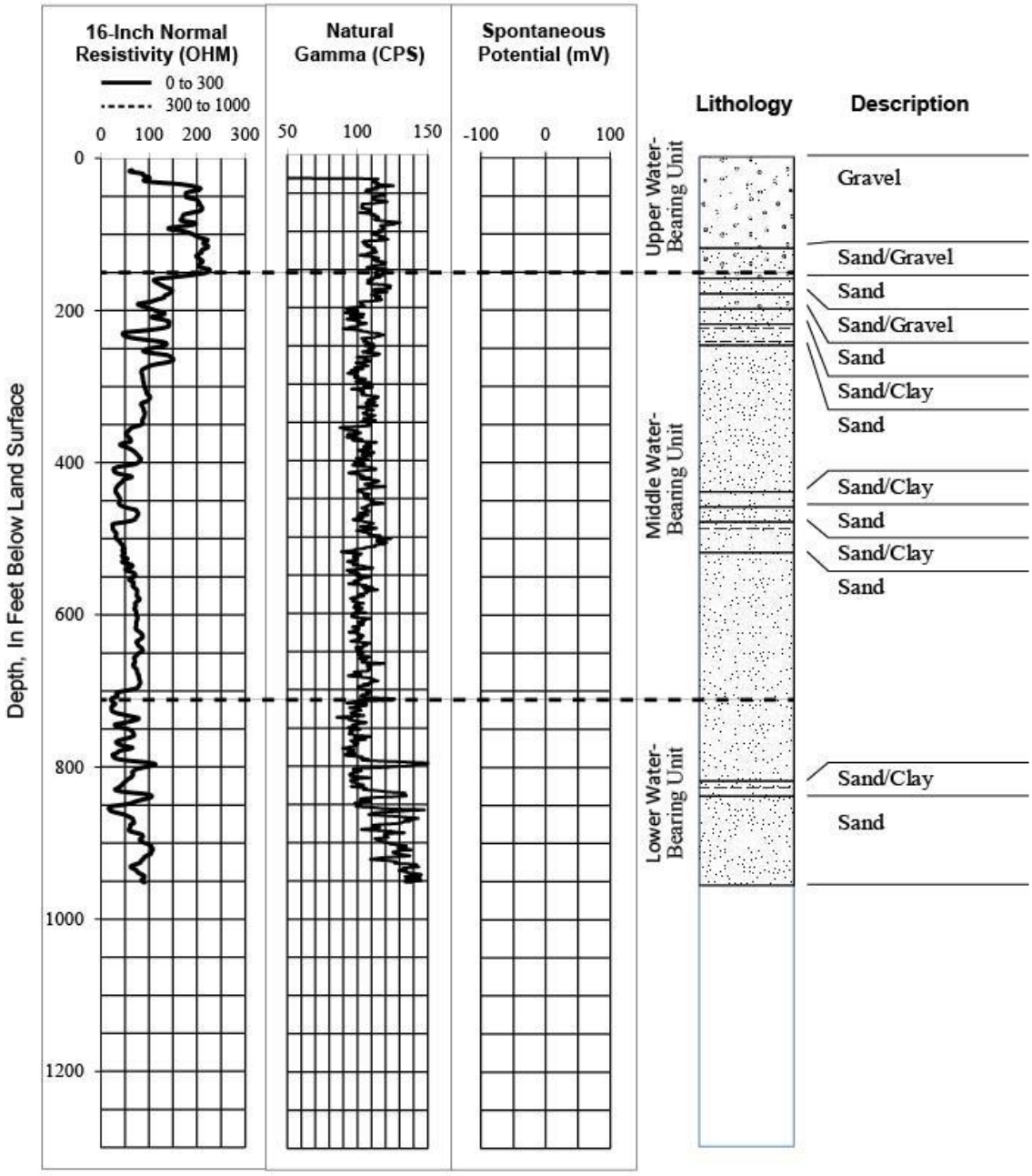

Figure 61: Borehole geophysical logs and lithology logs for 1N/5W-35B1.

Dashed lines represent interpreted boundaries of water-bearing units.

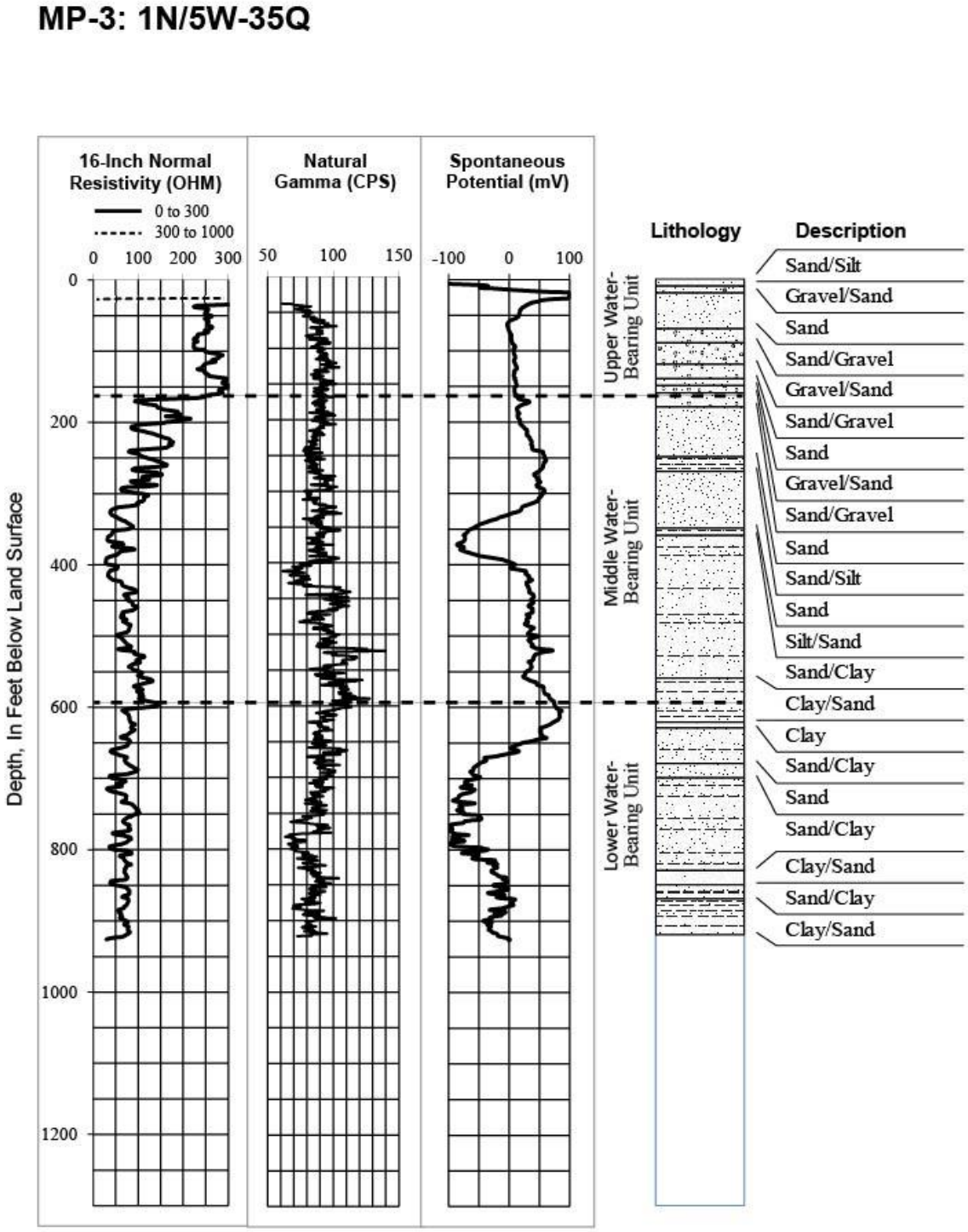

Figure 62: Borehole geophysical logs and lithology logs for MP-3.

Dashed lines represent interpreted boundaries of water-bearing units.

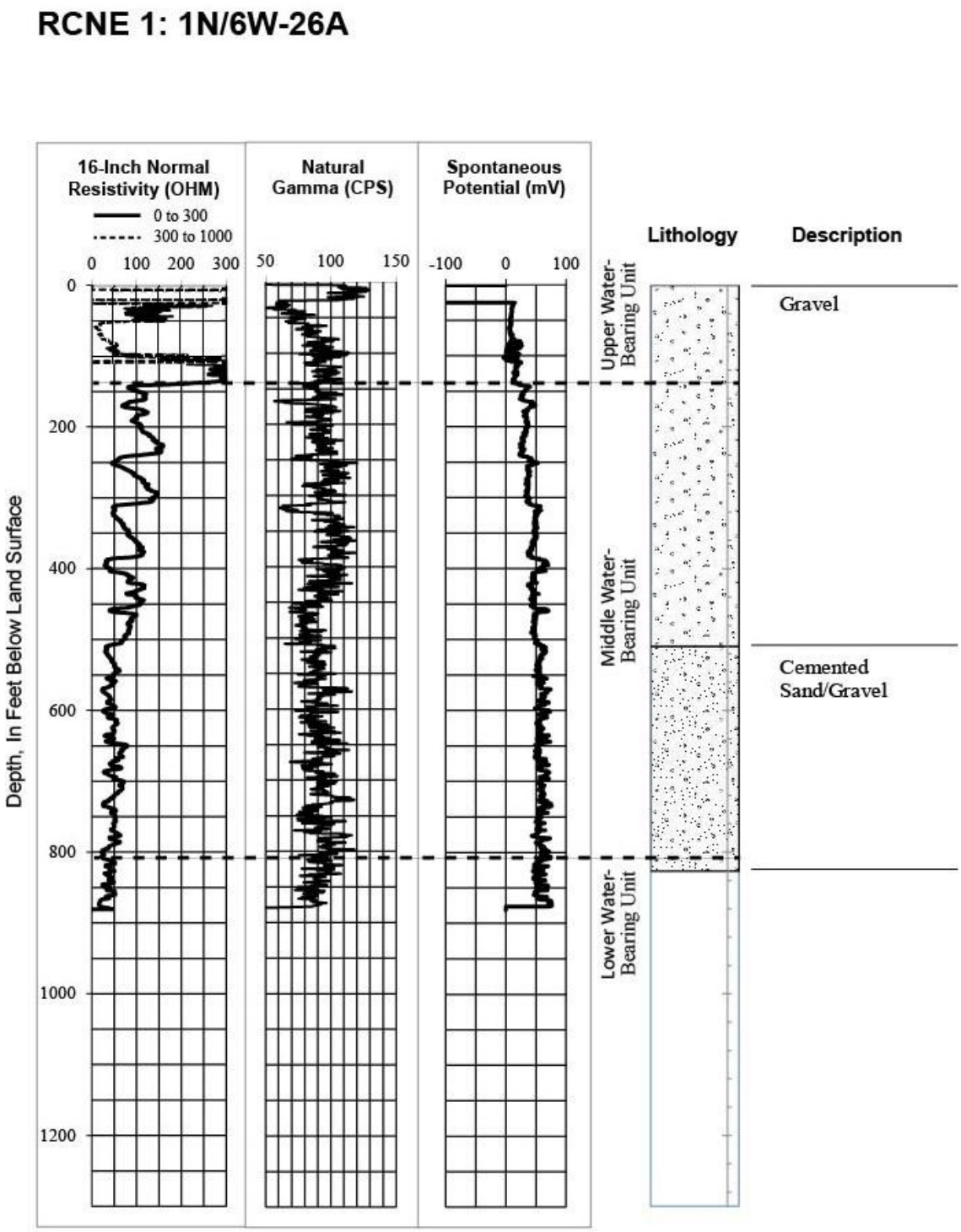

Figure 63: Borehole geophysical logs and lithology logs for RCNE 1.

Dashed lines represent interpreted boundaries of water-bearing units.

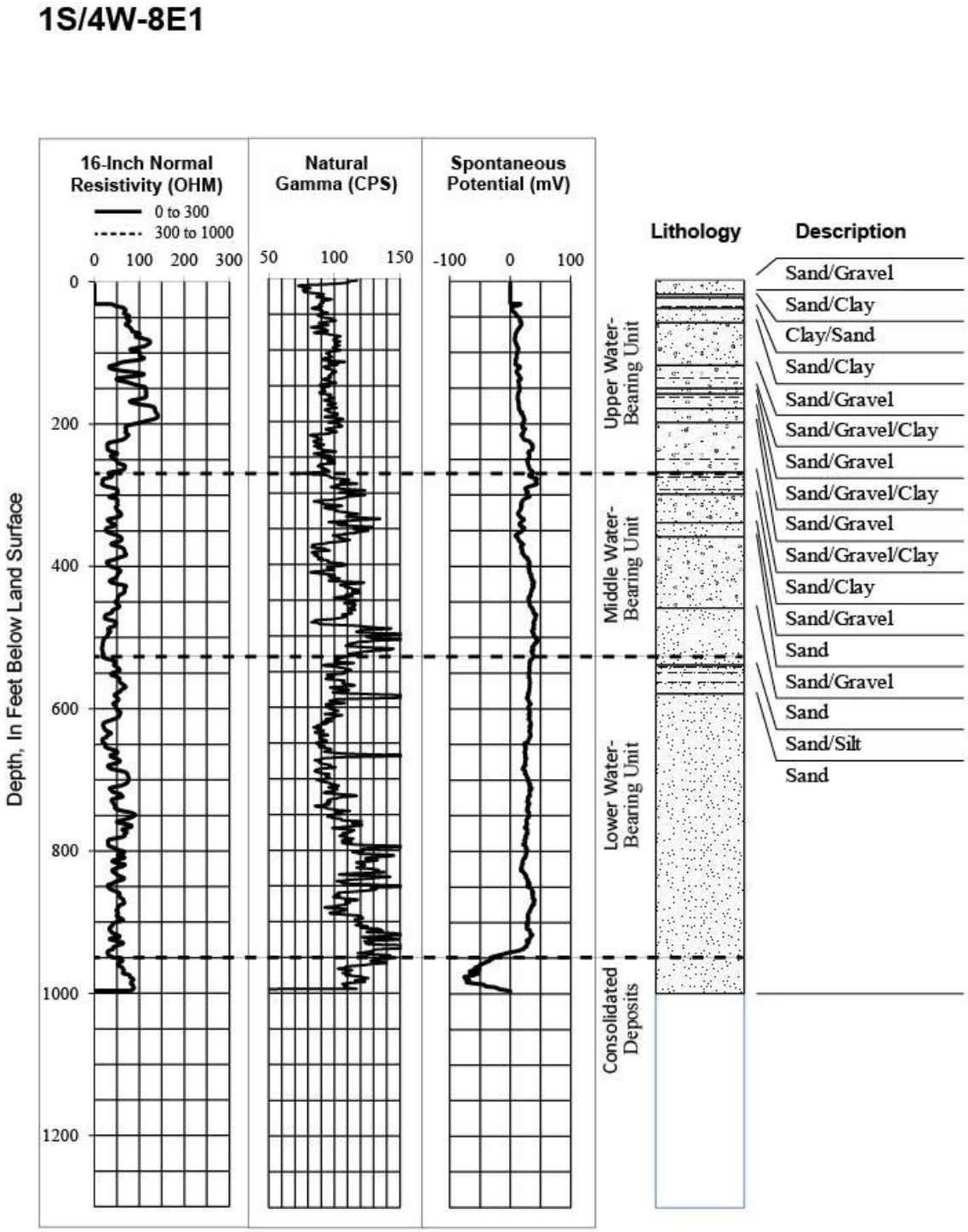

Figure 64: Borehole geophysical logs and lithology logs for 1S/4W-8E1.

Dashed lines represent interpreted boundaries of water-bearing units.

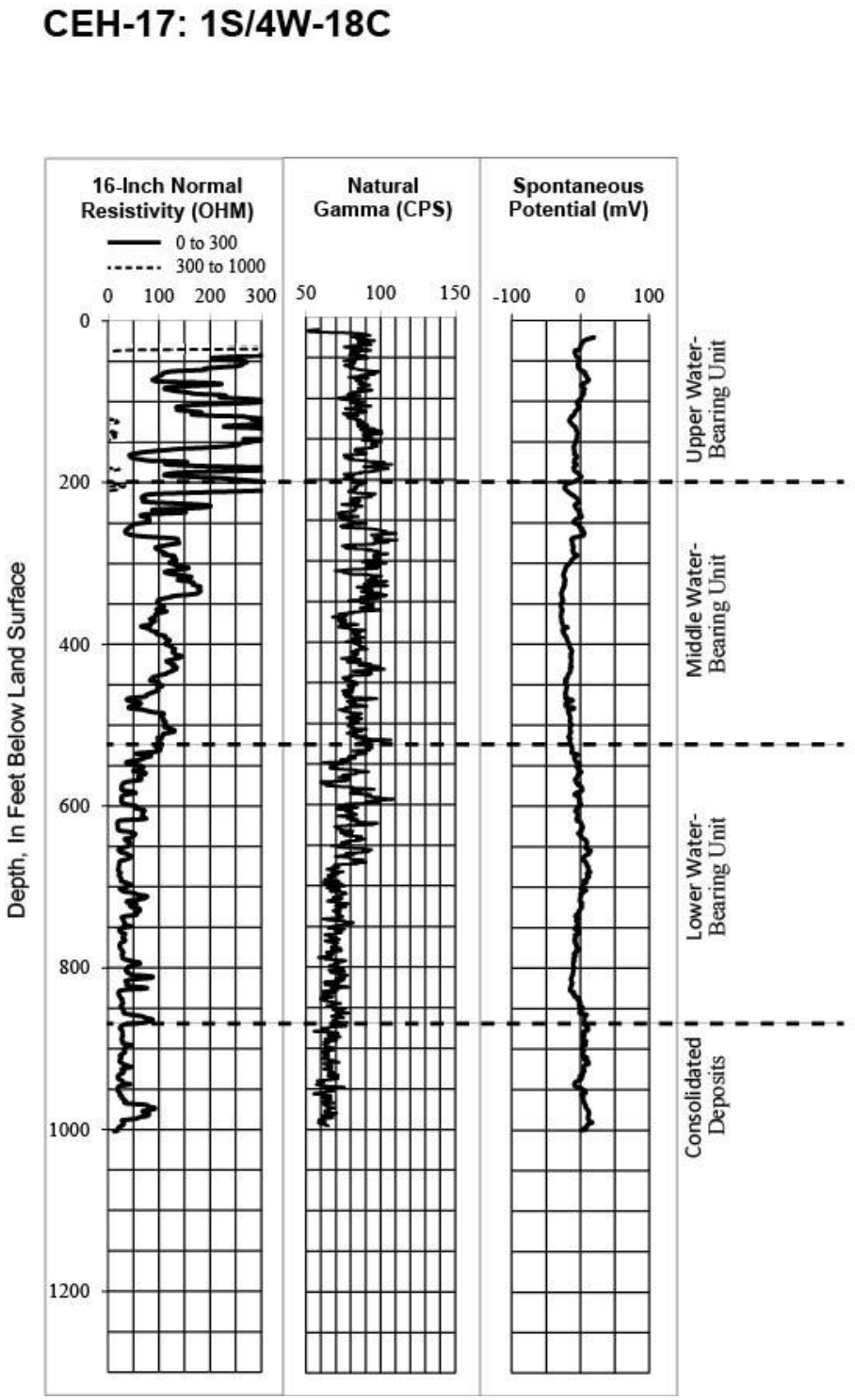

Figure 65: Borehole geophysical logs and lithology logs for CEH-17.

Dashed lines represent interpreted boundaries of water-bearing units.

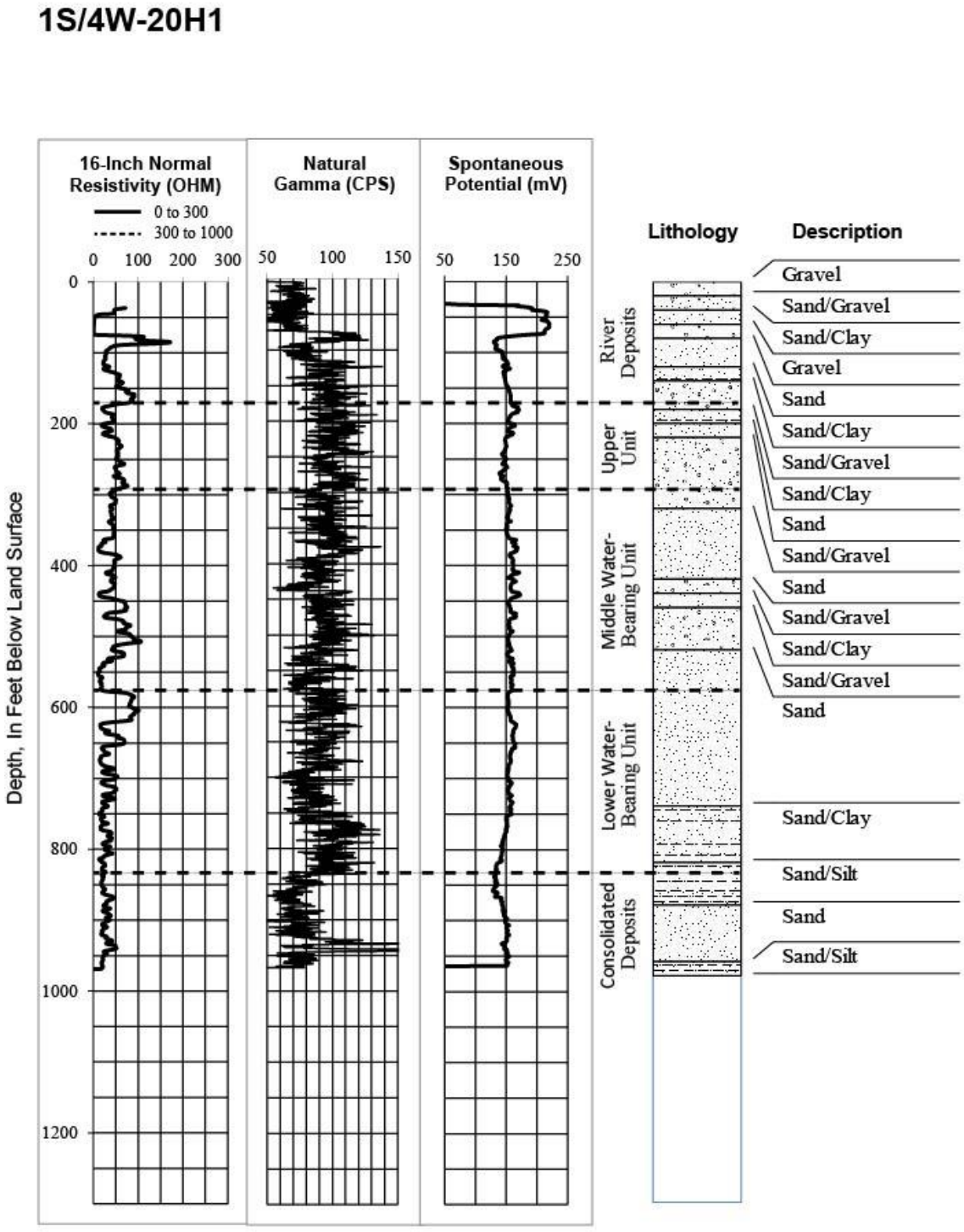

Figure 66: Borehole geophysical logs and lithology logs for 1S/4W-20H1.

Dashed lines represent interpreted boundaries of water-bearing units.

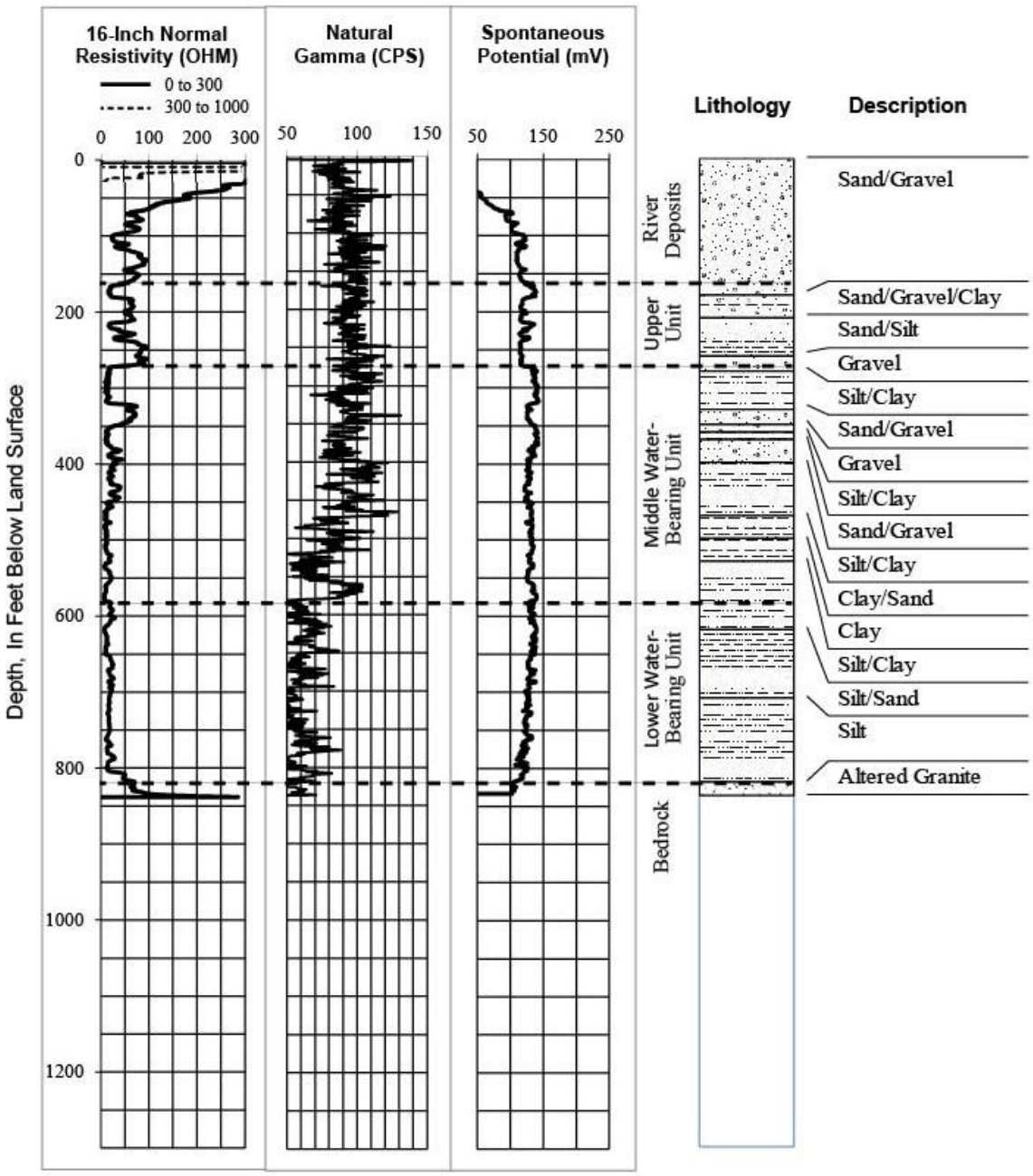

Figure 67: Borehole geophysical logs and lithology logs for 1S/4W-29H4.

Dashed lines represent interpreted boundaries of water-bearing units.

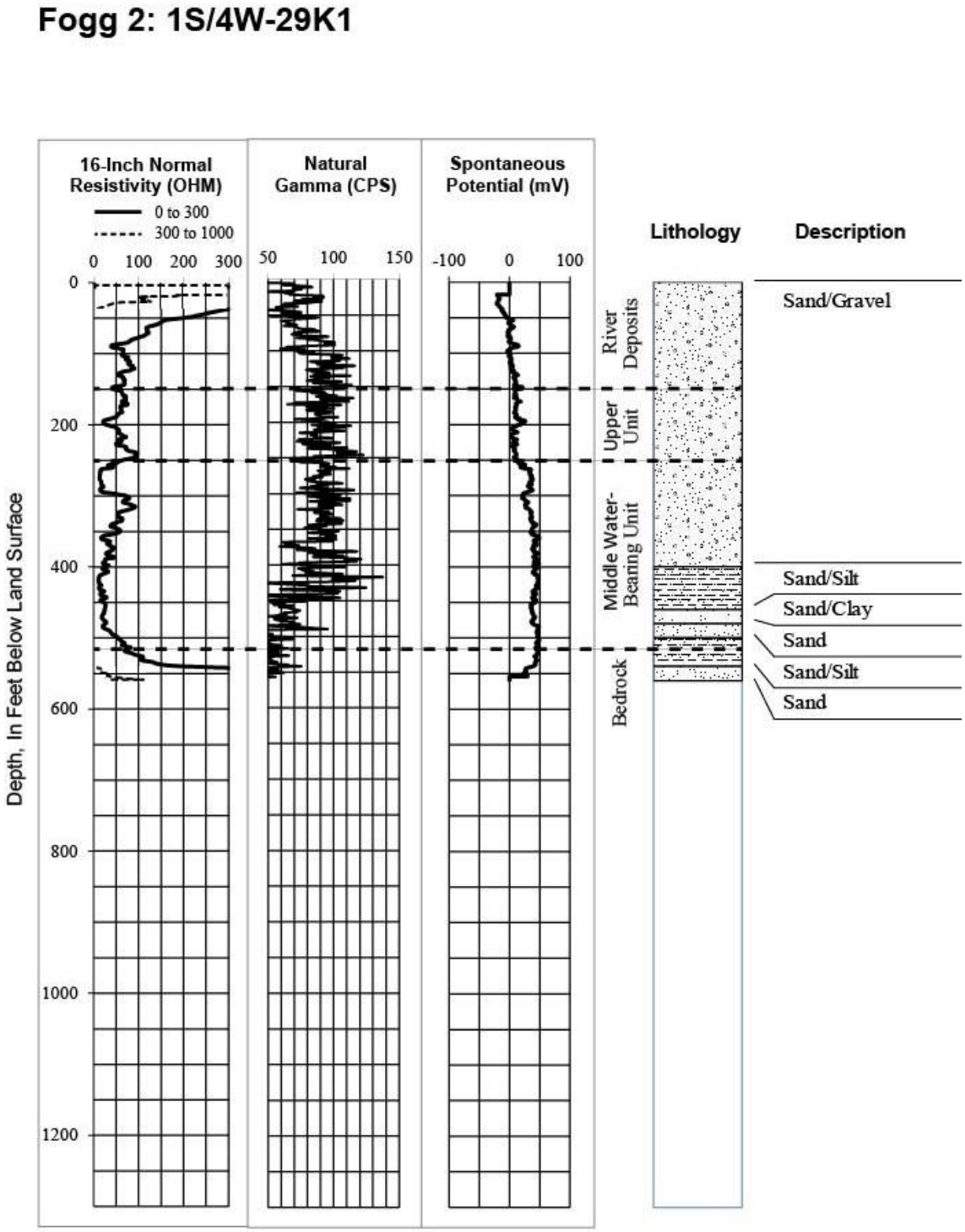

Figure 68: Borehole geophysical logs and lithology logs for Fogg 2.

Dashed lines represent interpreted boundaries of water-bearing units.

PW-9

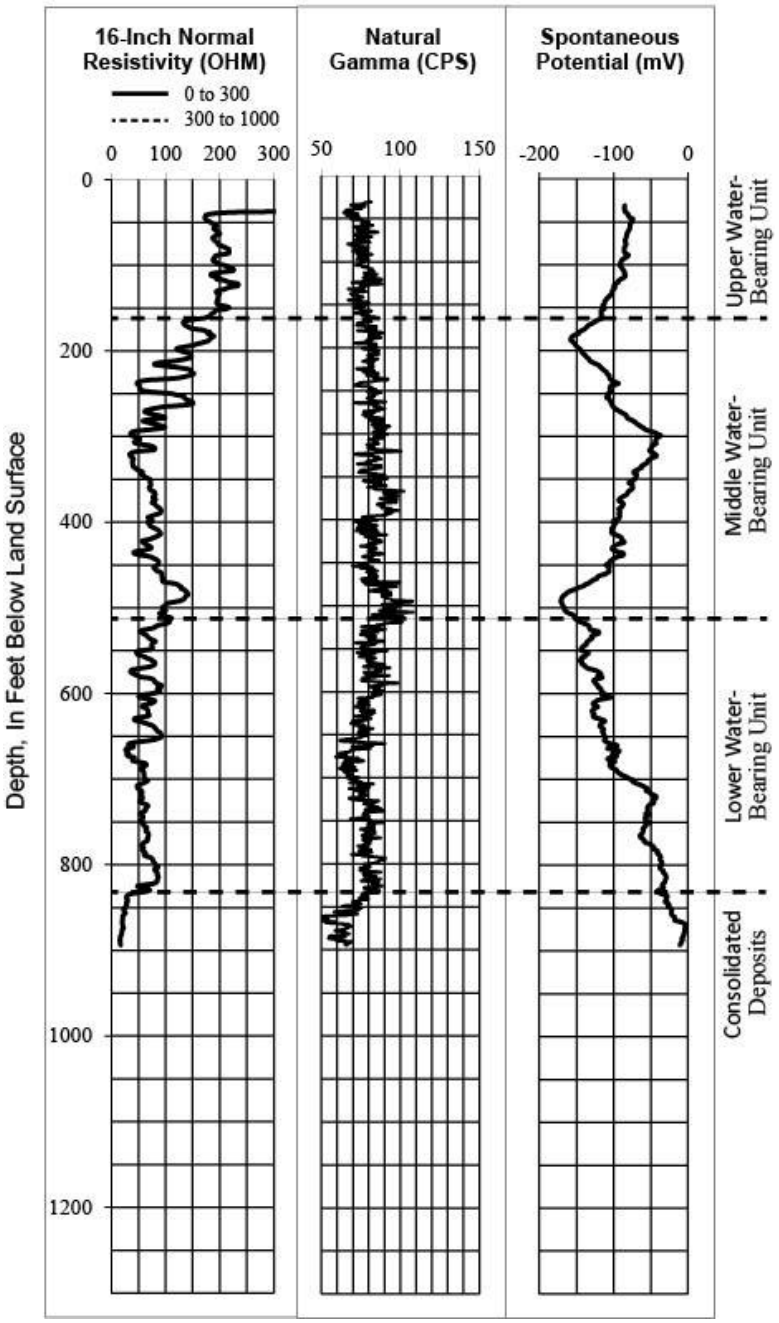

Figure 69: Borehole geophysical logs and lithology logs for PW-9.

Dashed lines represent interpreted boundaries of water-bearing units.

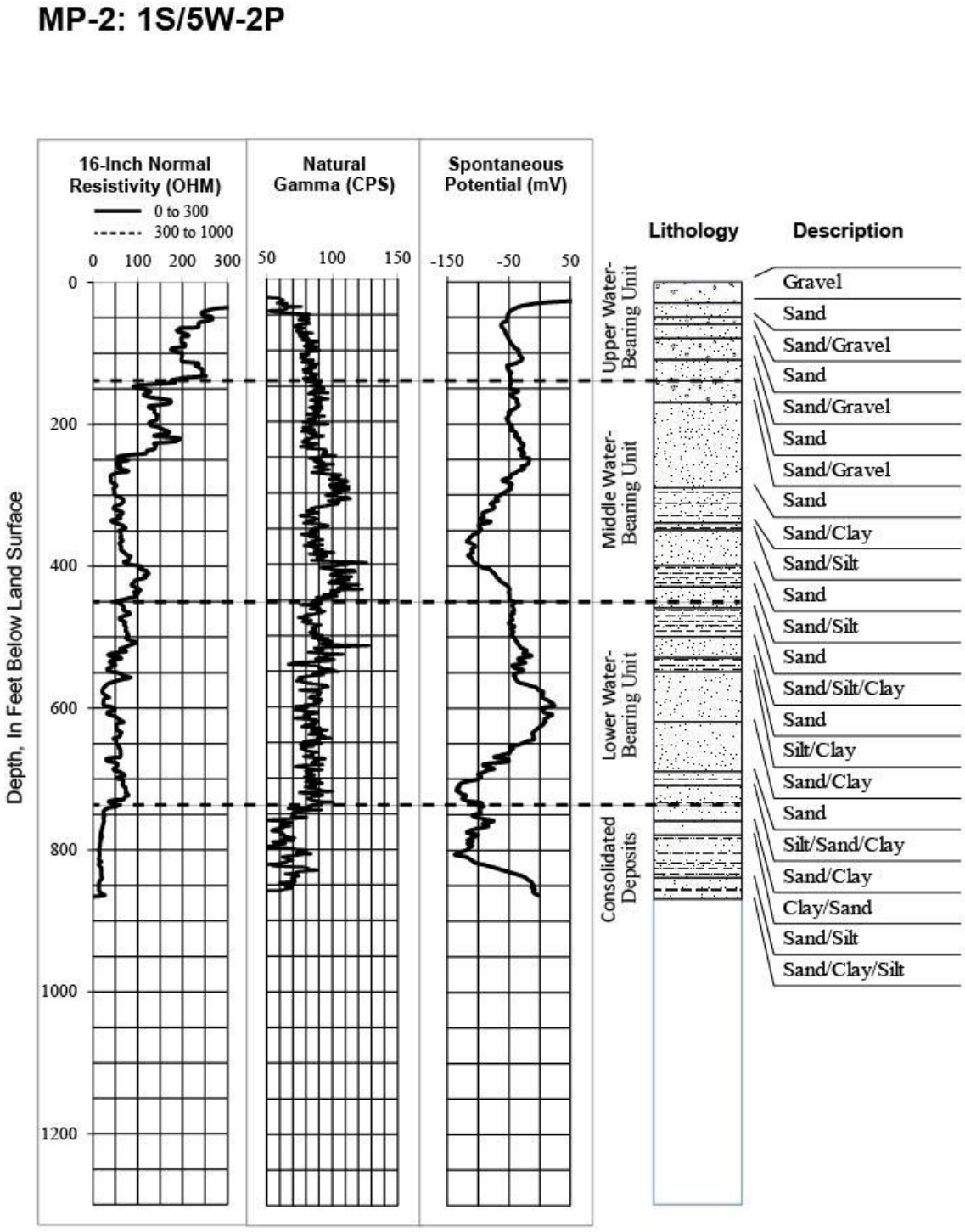

Figure 70: Borehole geophysical logs and lithology logs for MP-2.

Dashed lines represent interpreted boundaries of water-bearing units.

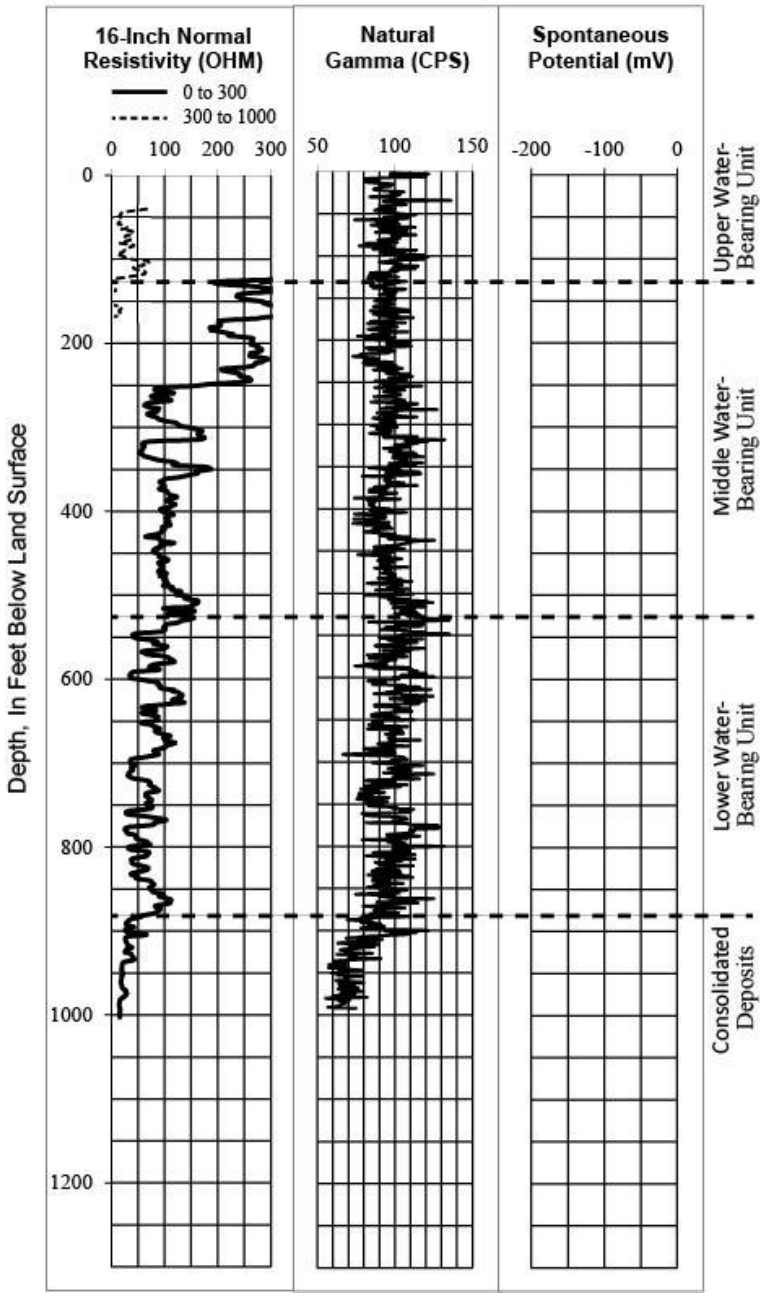

Figure 71: Borehole geophysical logs and lithology logs for 1S/5W-3A3.

Dashed lines represent interpreted boundaries of water-bearing units.

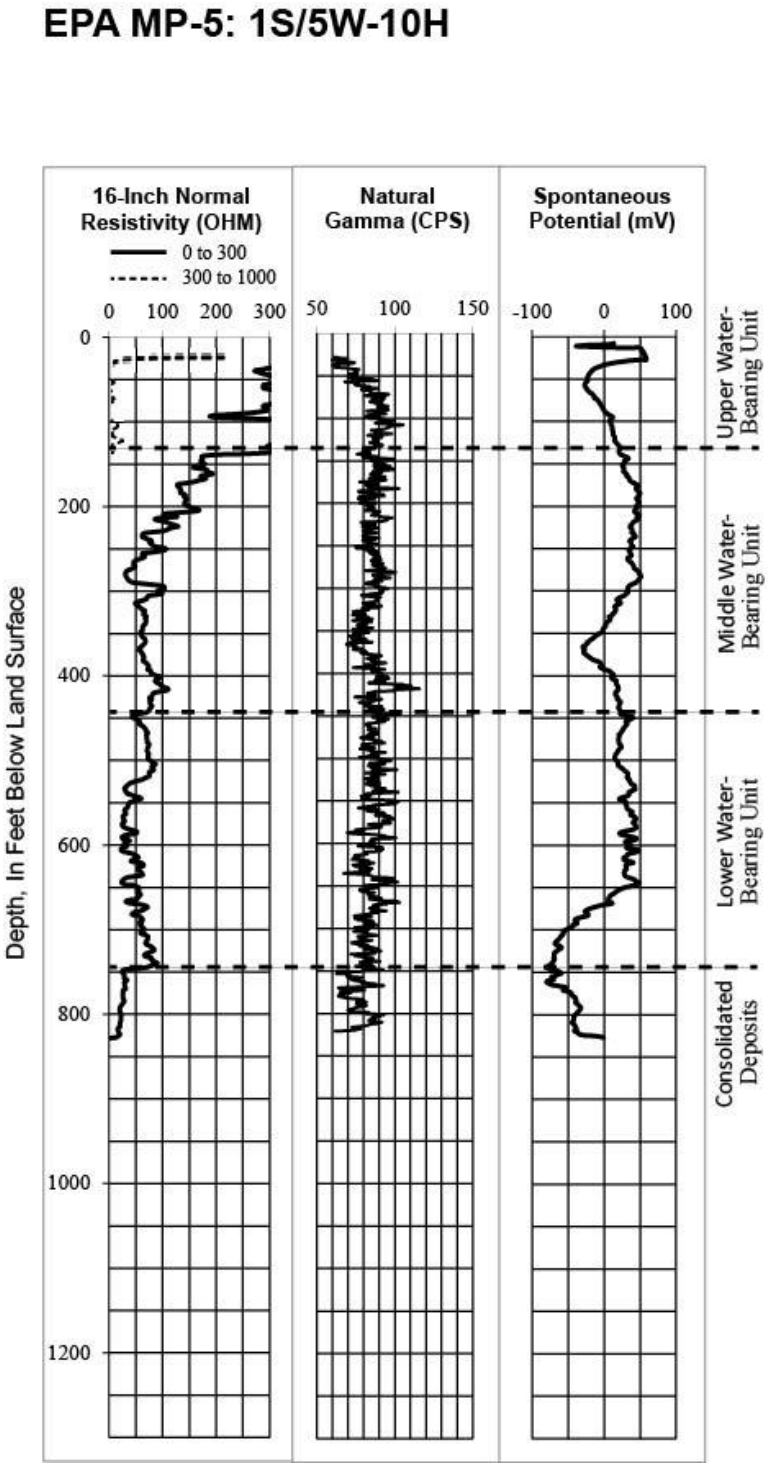

Figure 72: Borehole geophysical logs and lithology logs for EPA MP-5.

Dashed lines represent interpreted boundaries of water-bearing units.

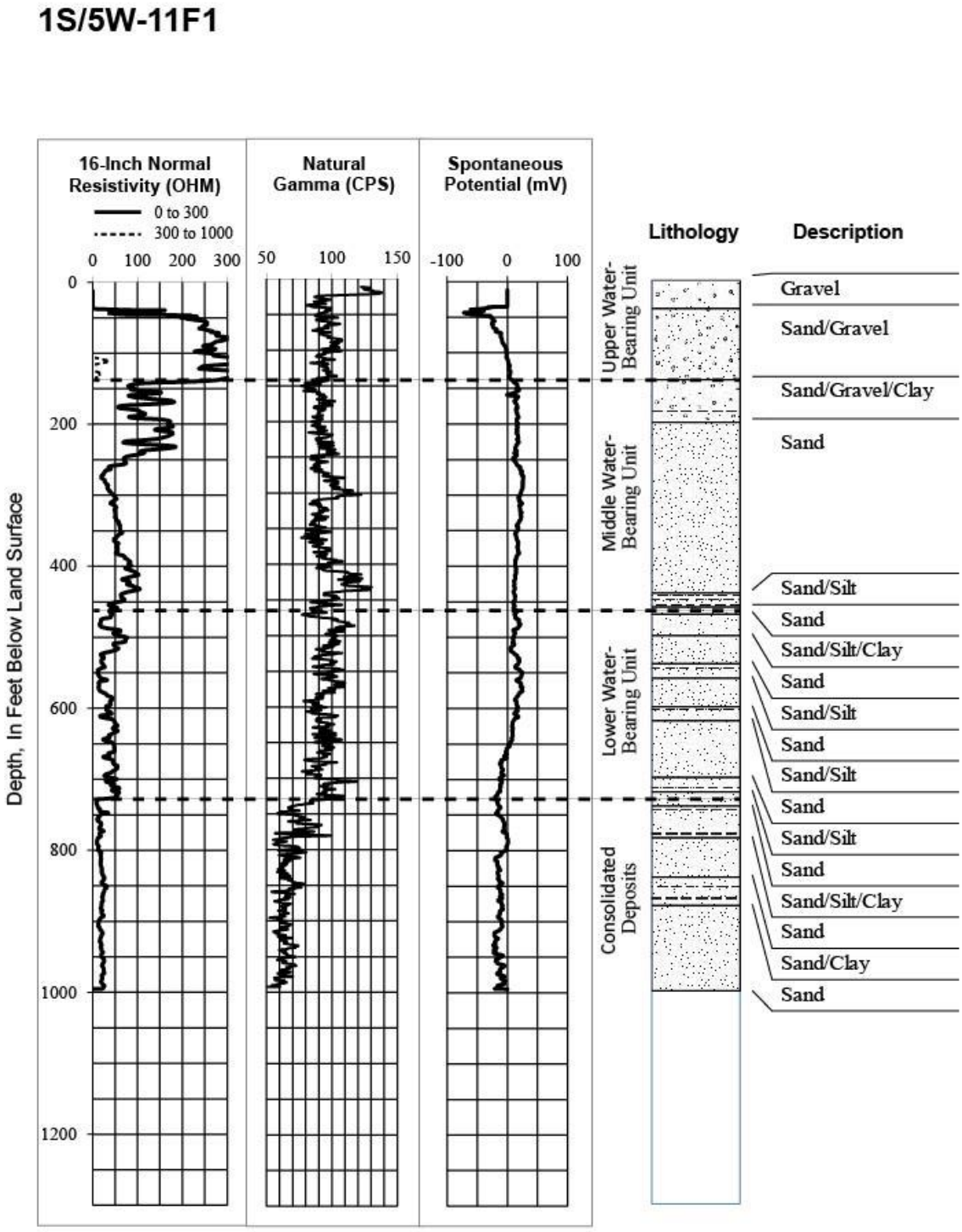

Figure 73: Borehole geophysical logs and lithology logs for 1S/5W-11F1.

Dashed lines represent interpreted boundaries of water-bearing units.

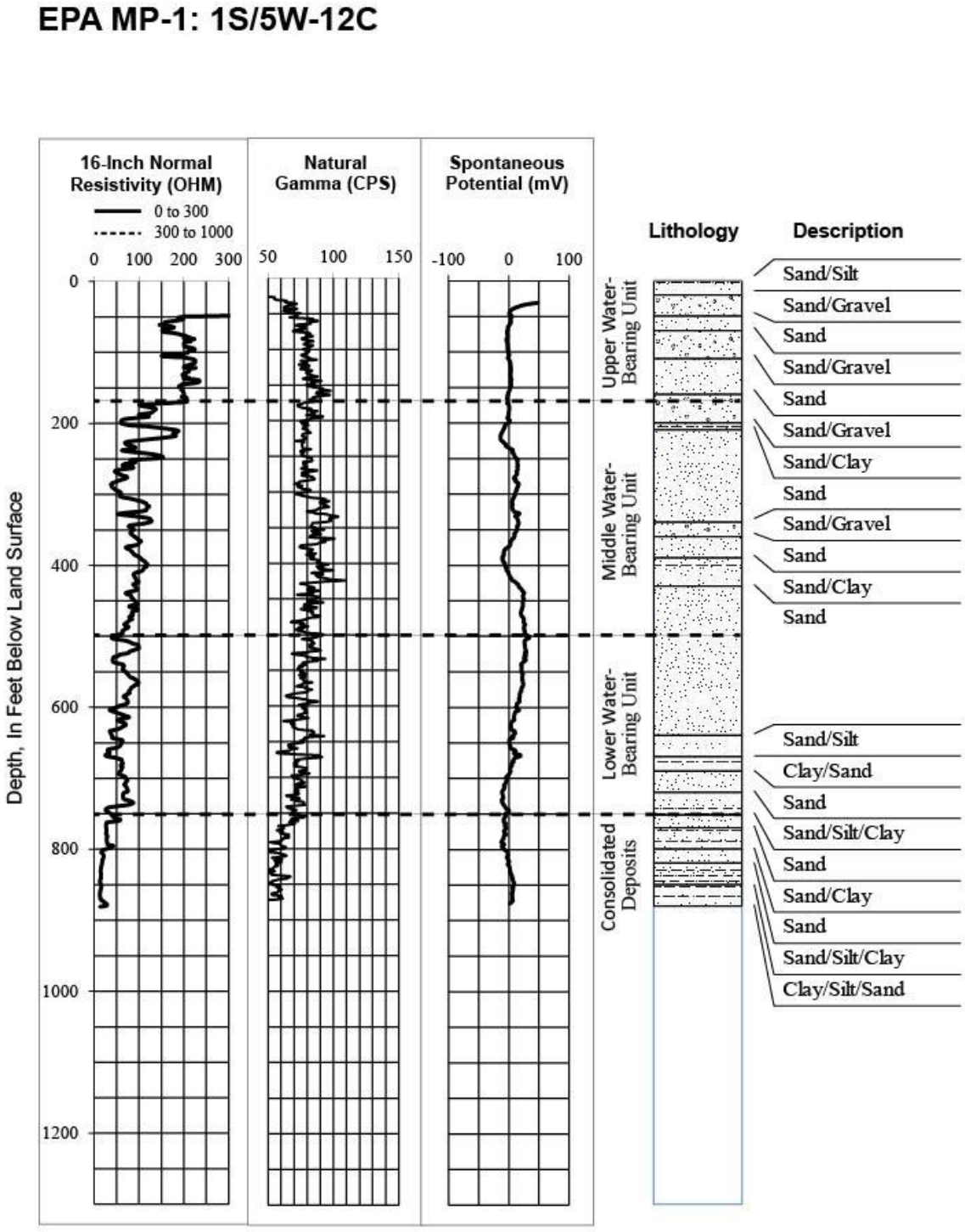

Figure 74: Borehole geophysical logs and lithology logs for EPA MP-1.

Dashed lines represent interpreted boundaries of water-bearing units.

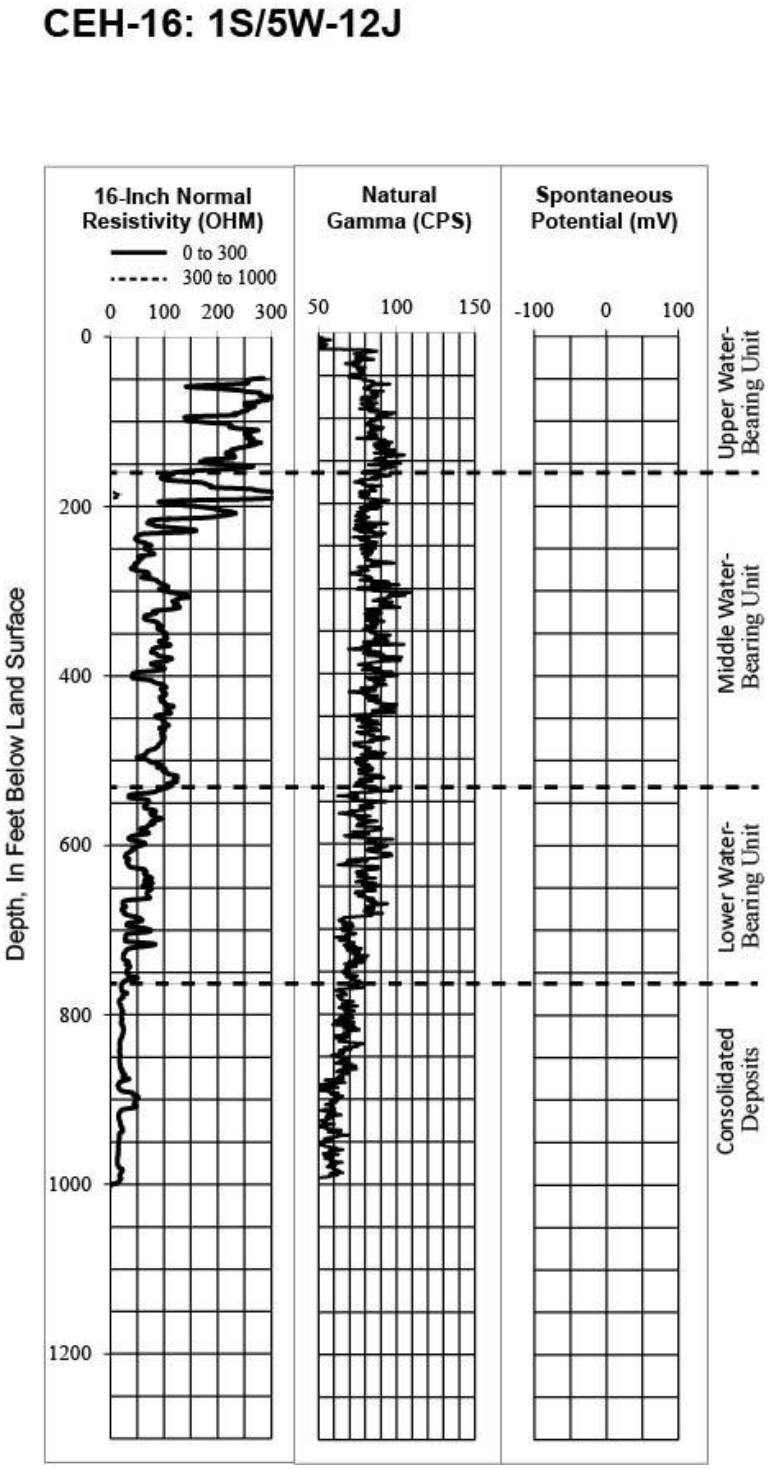

Figure 75: Borehole geophysical logs and lithology logs for CEH-16.

Dashed lines represent interpreted boundaries of water-bearing units.

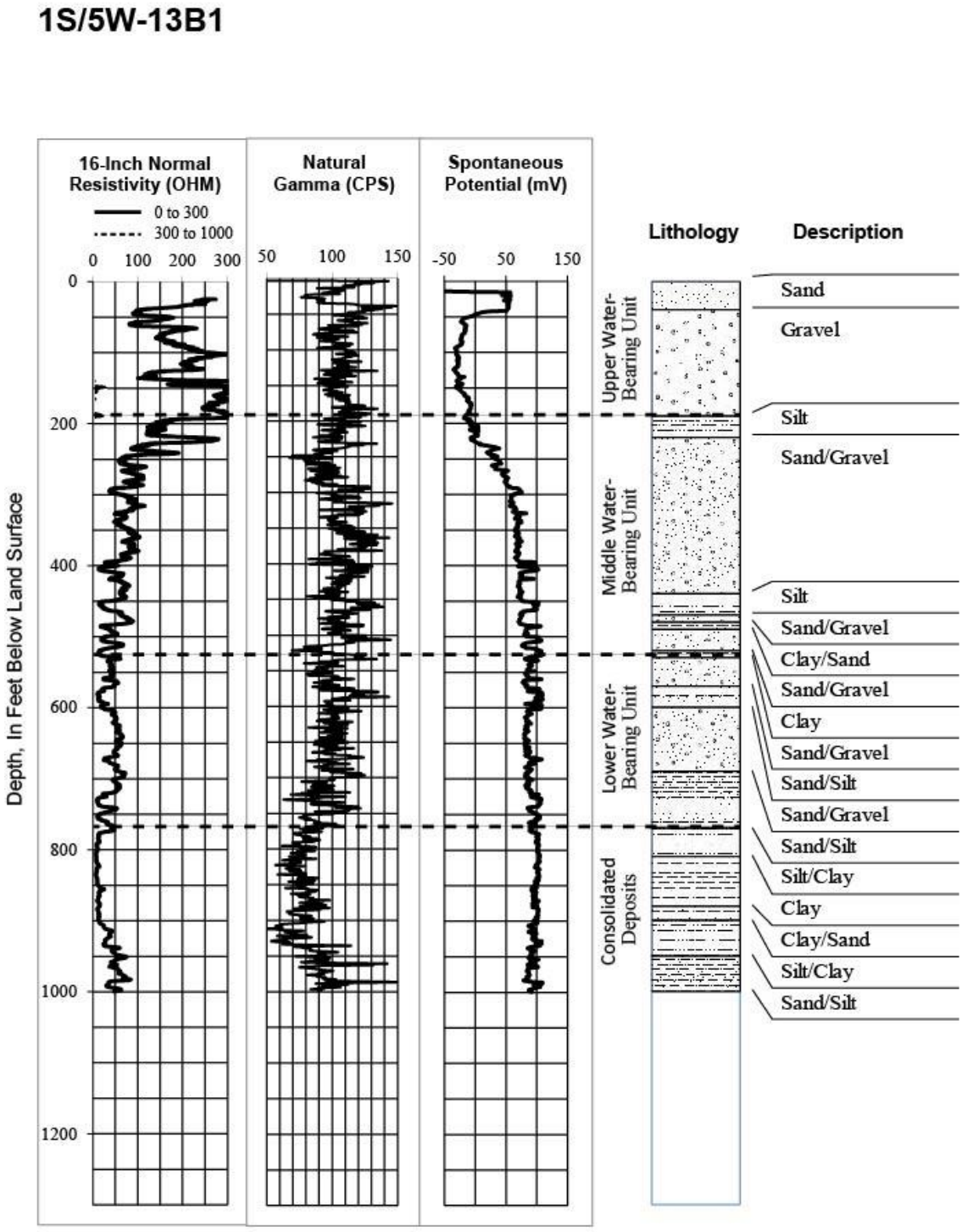

Figure 76: Borehole geophysical logs and lithology logs for 1S/5W-13B1.

Dashed lines represent interpreted boundaries of water-bearing units.

Appendix B: Cross Sections of the Rialto-Colton Basin

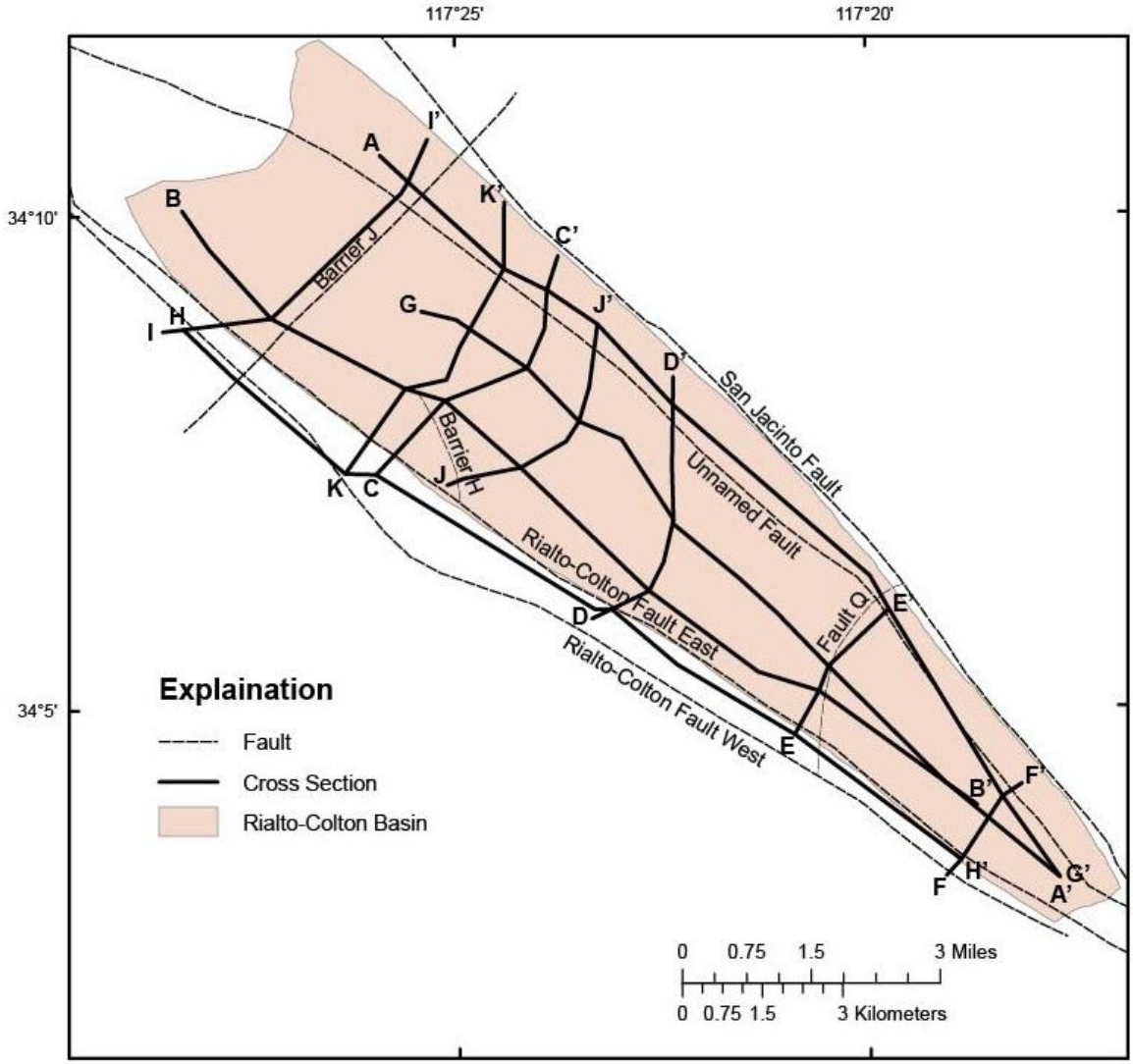

Figure 77: Rialto-Colton Basin cross sections.

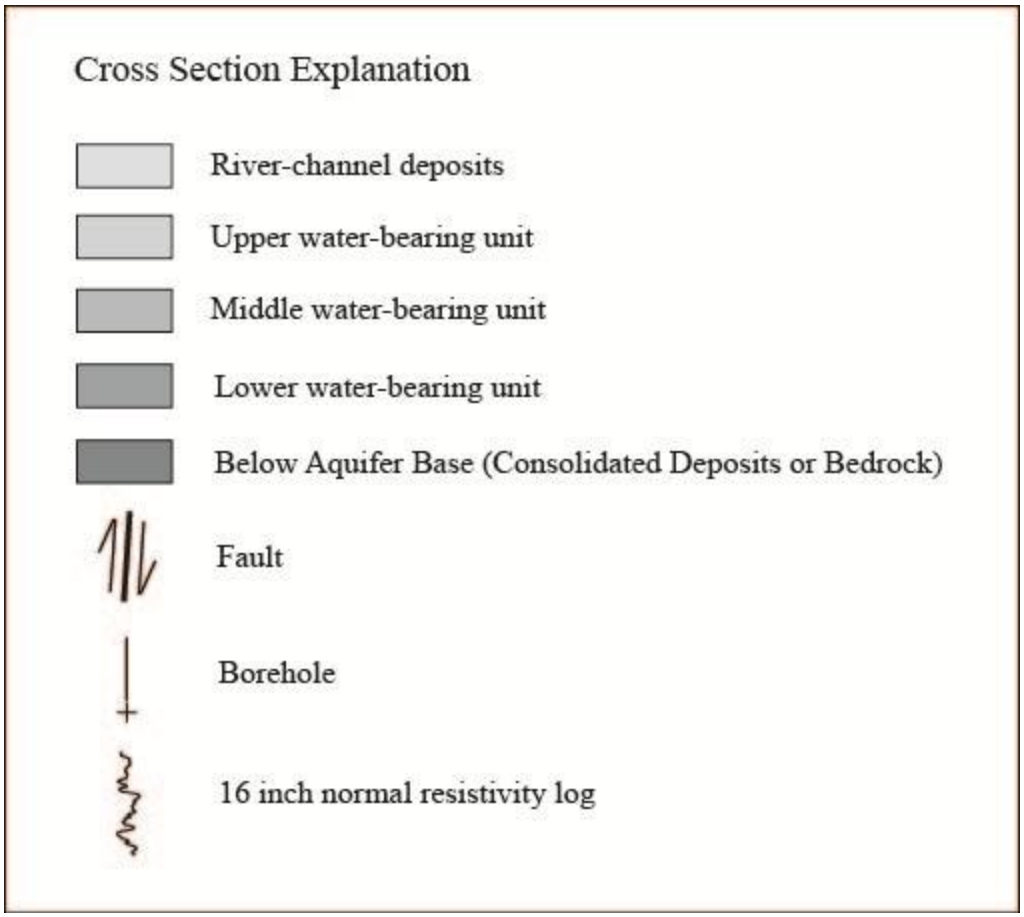

Figure 78: Explanation of cross sections

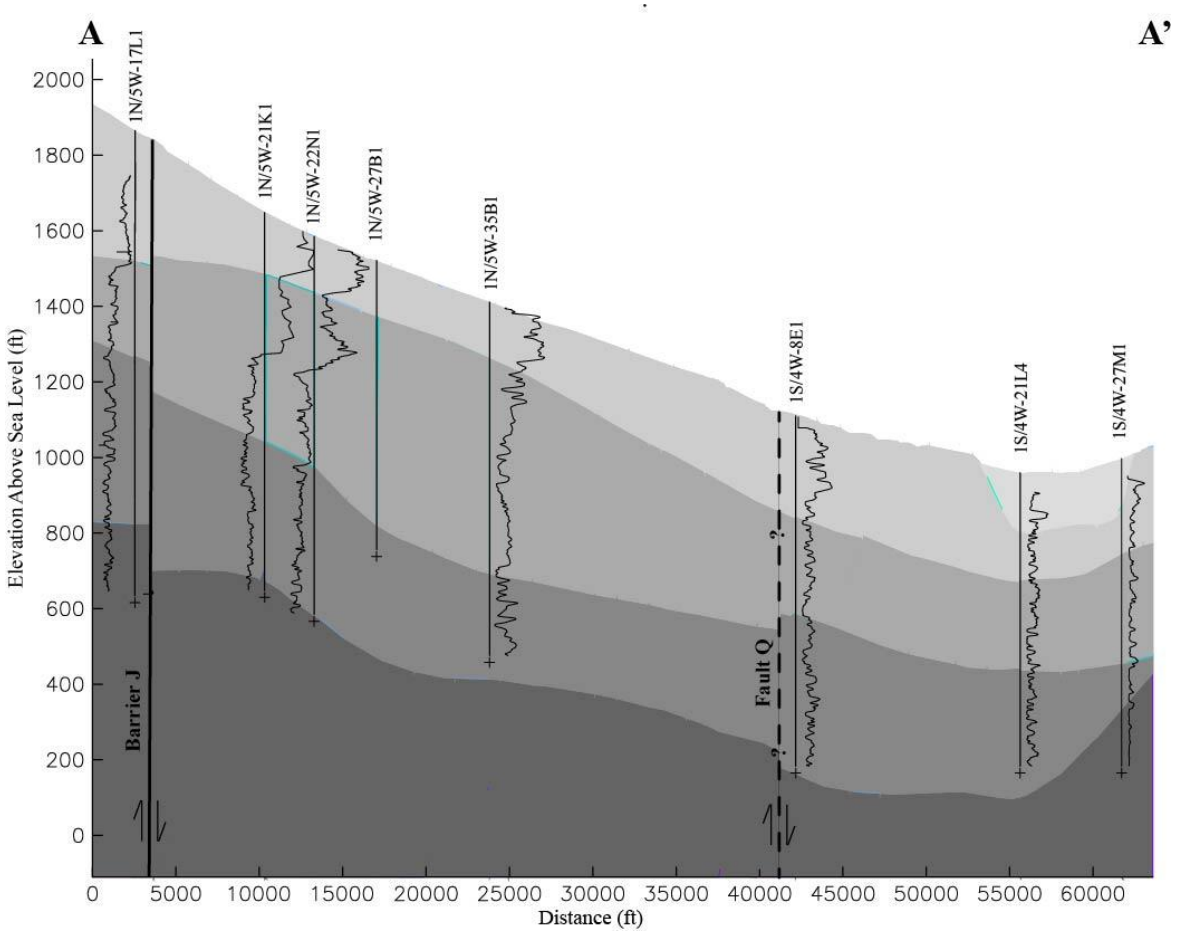

Figure 79: Cross Section A-A'.

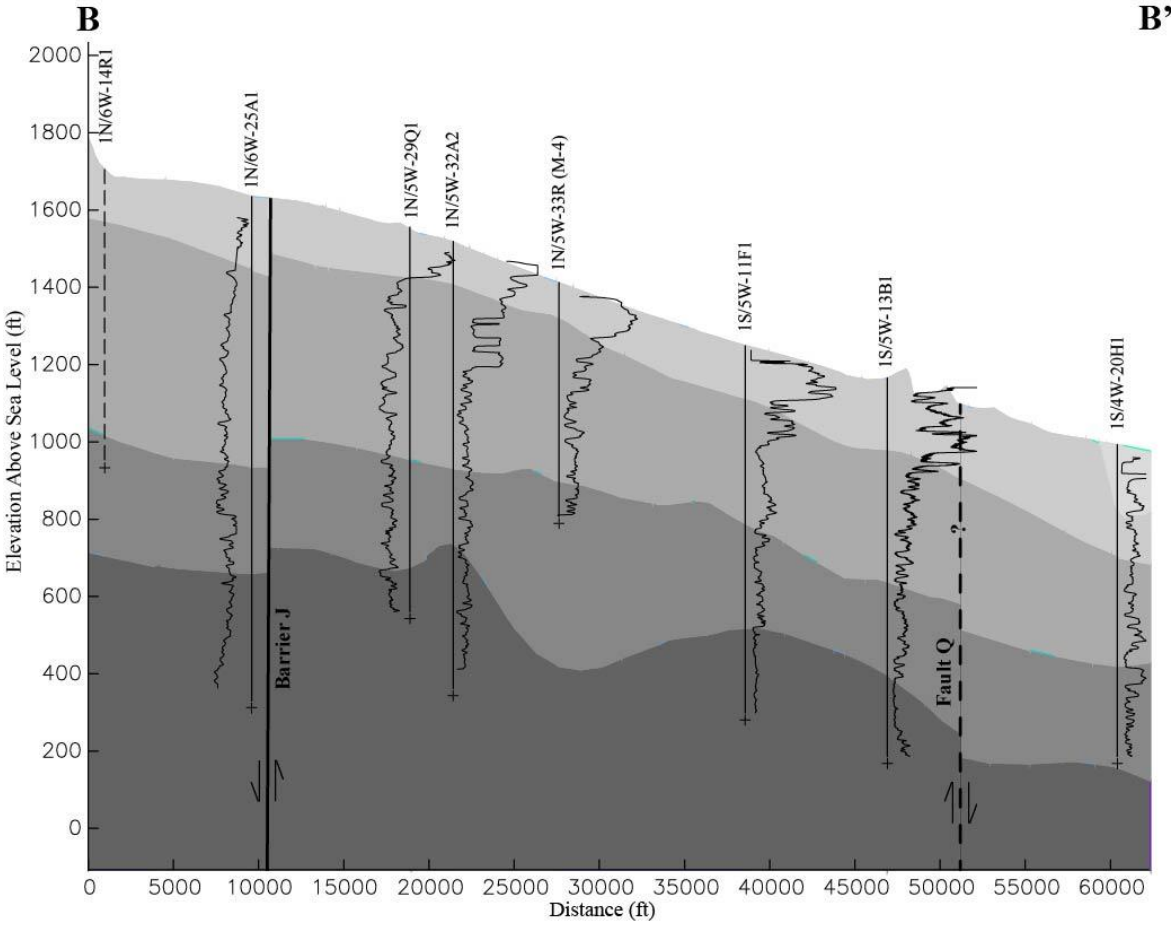

Figure 80: Cross Section B-B'.

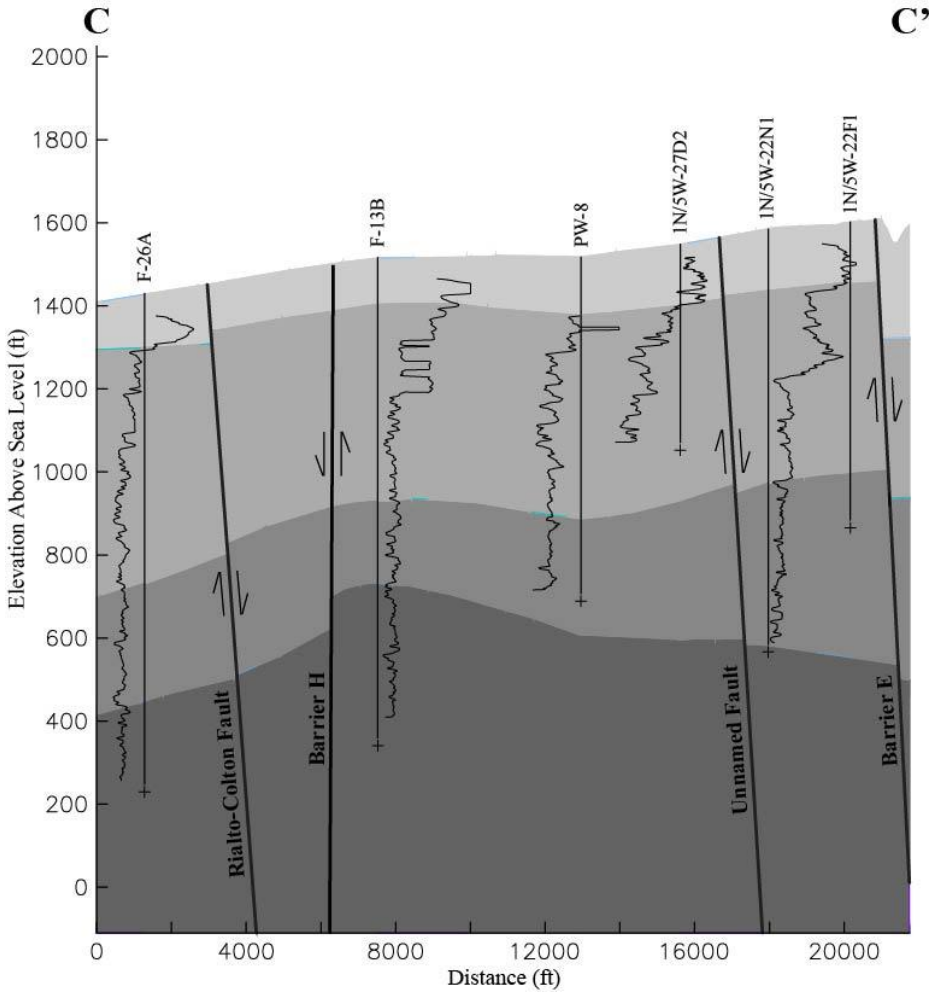

Figure 81: Cross Section C-C'.

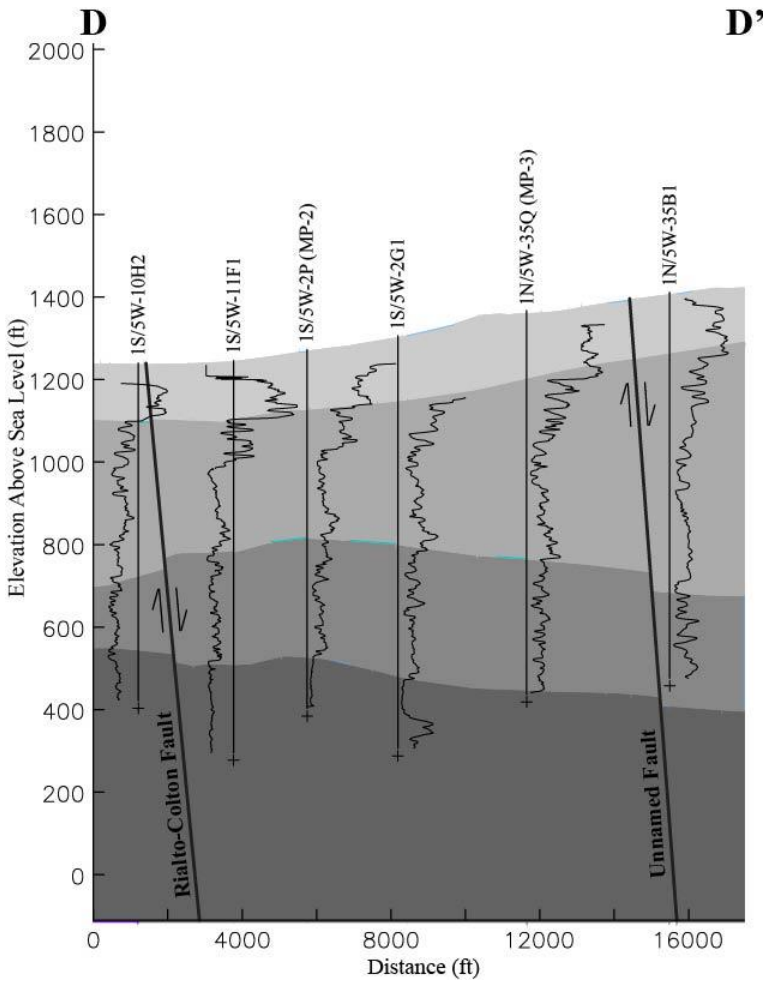

Figure 82: Cross Section D-D'.

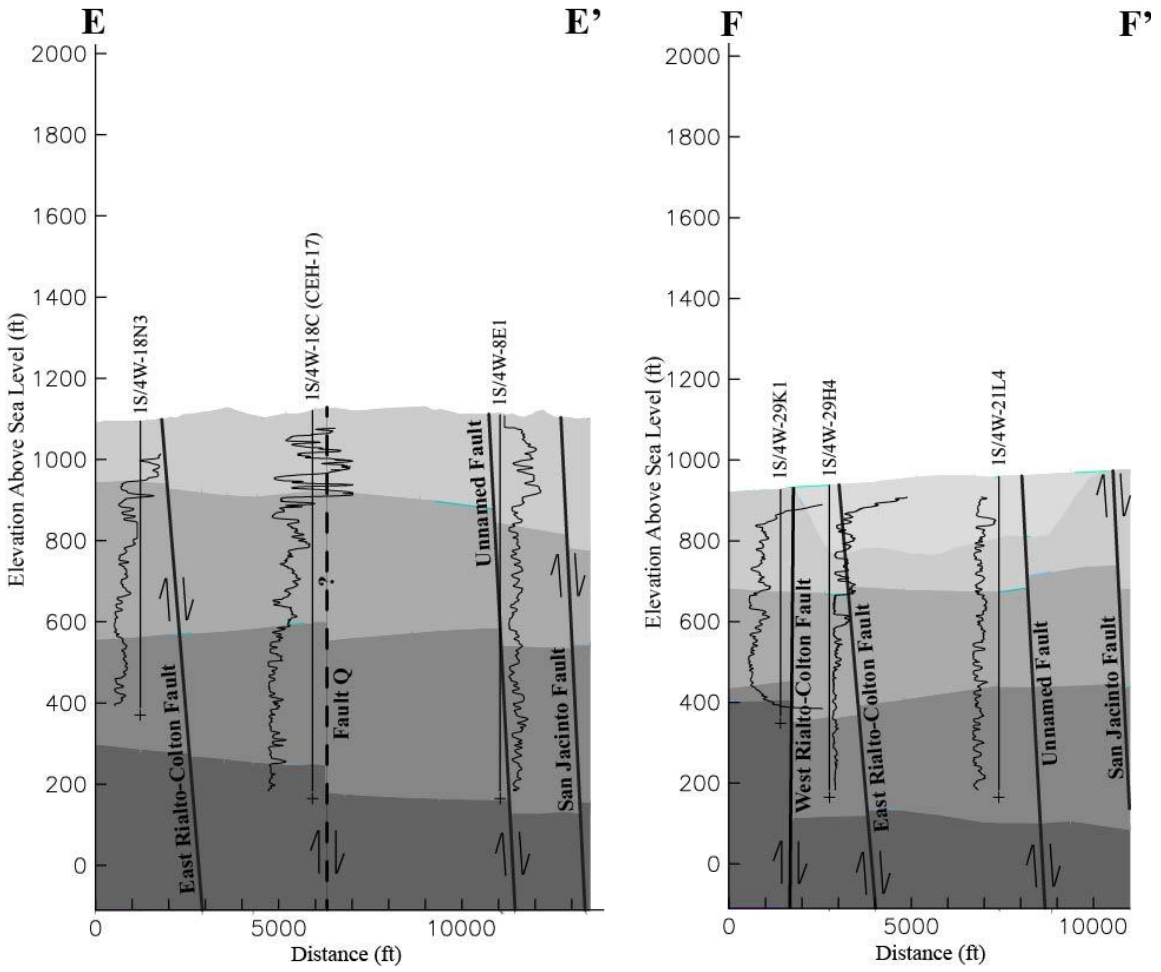

Figure 83: Cross Sections E-E' and F-F'.

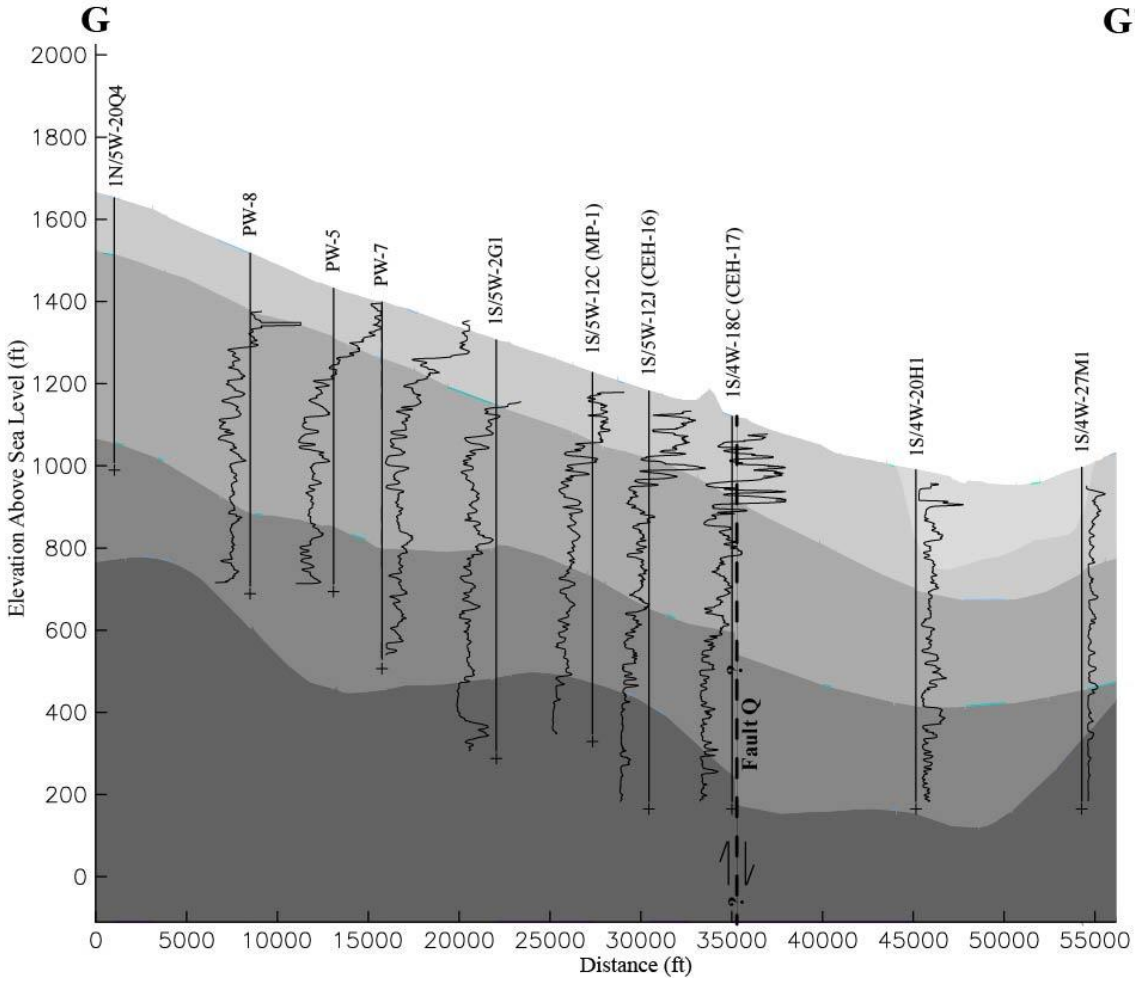

Figure 84: Cross Section G-G'.

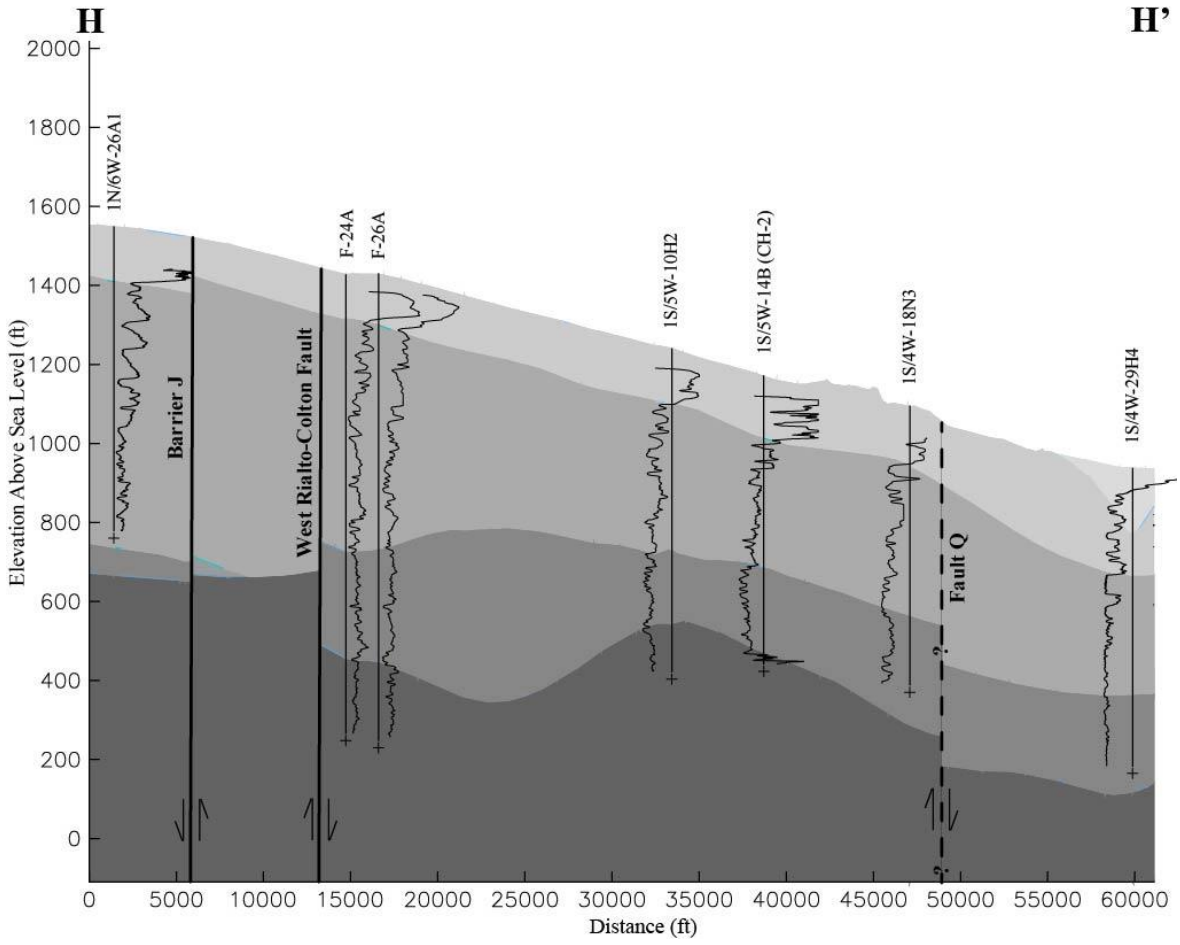

Figure 85: Cross Section H-H'.

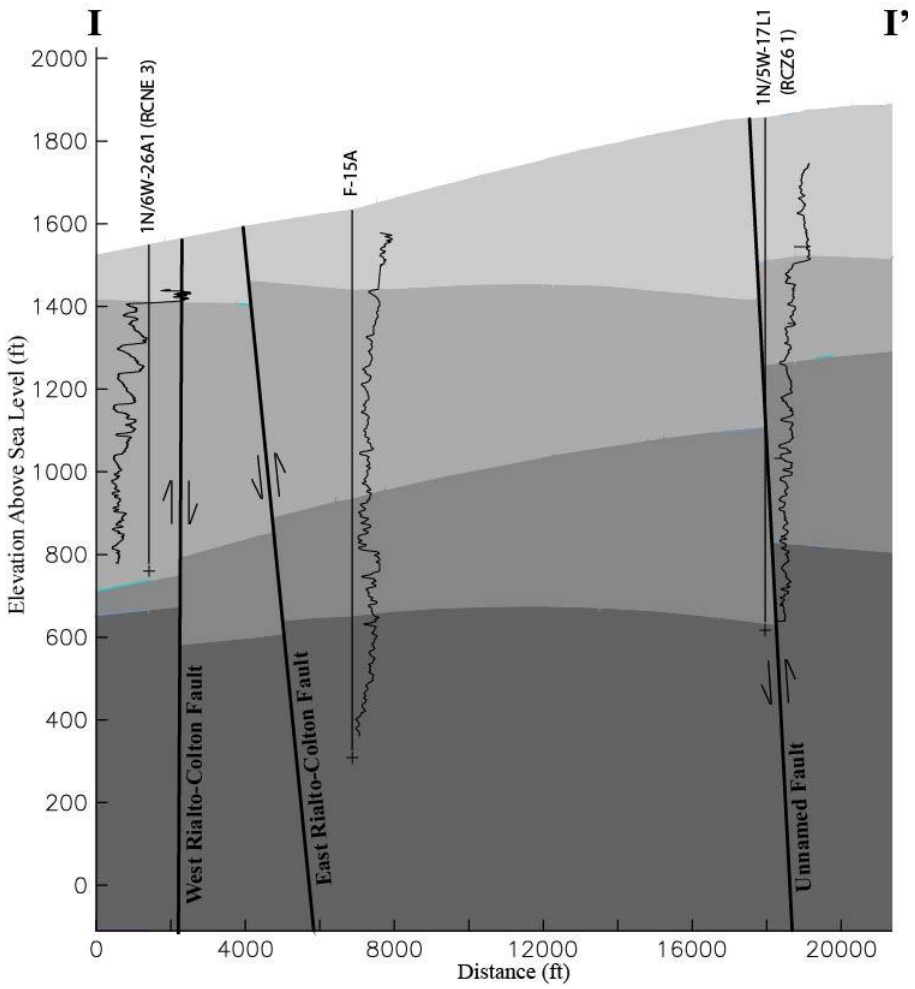

Figure 86: Cross Section I-I'.

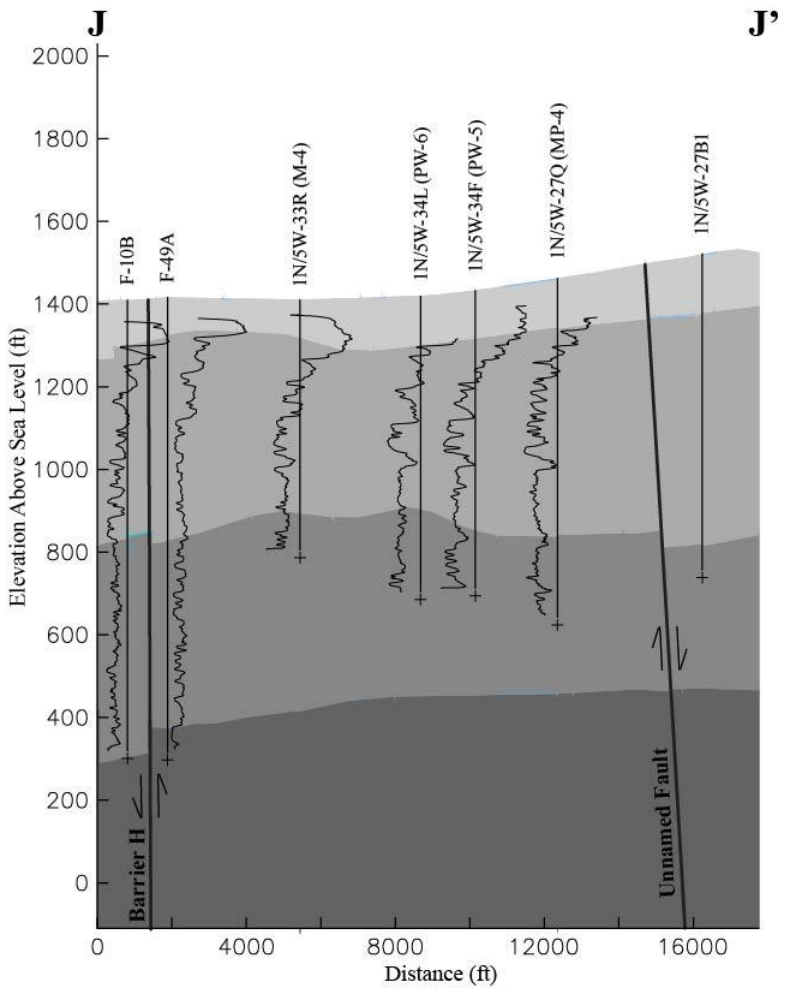

Figure 87: Cross Section J-J'.

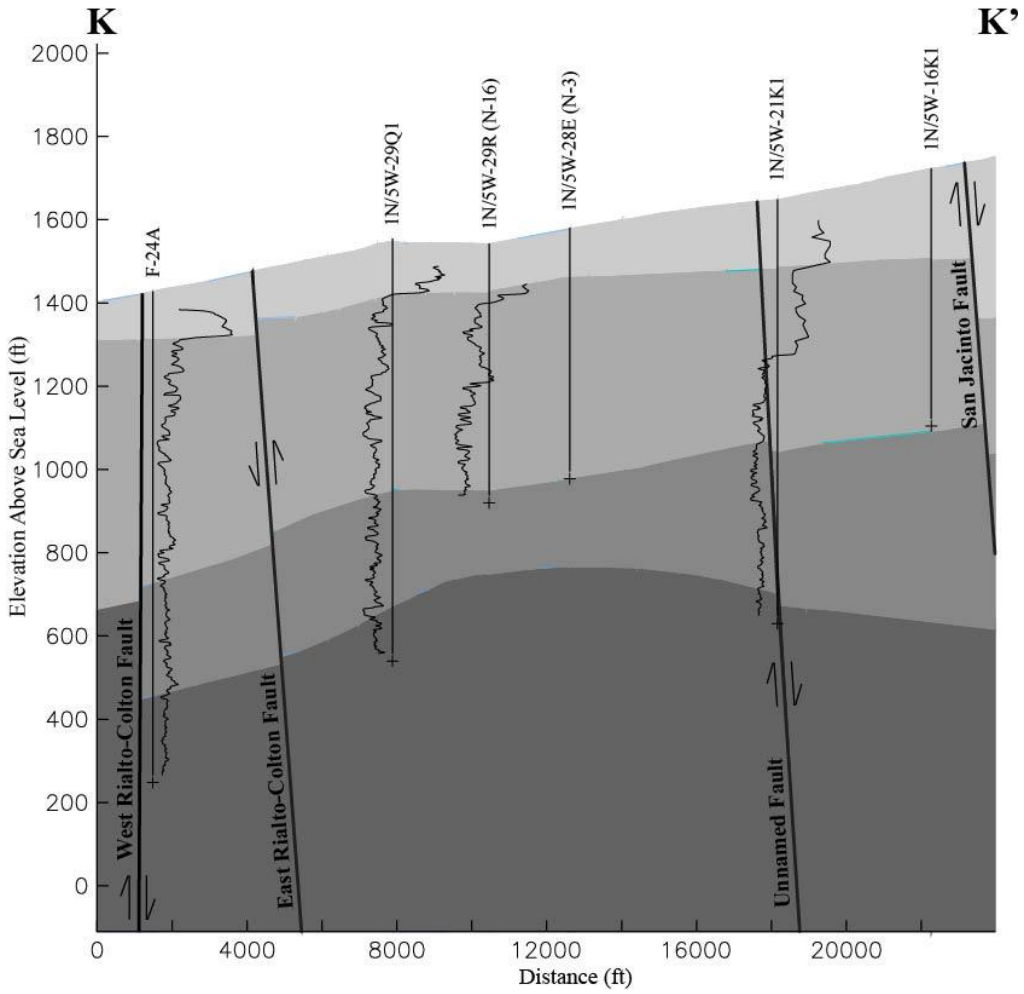

Figure 88: Cross Section K-K'.

References

Anderson, M., Matti, J., and Jachens, R., 2004, Structural Model of the San Bernardino basin, California, from analysis of gravity, aeromagnetic, and seismicity data, J. Geophys. Res., v. 109, B04404, p. 1-20.

Anderson, M., Roberts, C., and Jachens, R., 2000, Principal facts for gravity stations in the vicinity of San Bernardino, southern California, U.S. Geological Survey Open-File Report 00-193, 32 p.

Anderson, M, and Woessner, W, 1992, Applied Groundwater Modeling Simulation of Flow and Advective Transport, Academic Press, 381 p.

Boggs, S, 2006, Principles of Sedimentology and Stratigraphy, 4th ed., Merrill, 662 p.

California Department of Public Health, 2012, Perchlorate in Drinking Water, http://www.cdph.ca.gov/certlic/drinkingwater/pages/Perchlorate.aspx (accessed June 2012).

Catchings, R., Rymer, M., Goldman, M., Gandhok, G., and Steedman, C., 2008, Structure of the San Bernardino Basin along two seismic transects: Rialto-Colton fault to the San Andreas fault and along the I-215 Freeway (I-10 to SR30), U.S. Geological Survey Open-File Report 2008-1197, 70 p.

CH2MHILL, 2009, Groundwater Elevation Contours – Regional Aquifer, B.F. Goodrich Site, 1 sheet

CH2MHILL, 2010, Remedial Investigation/Feasibility Study Report B.F. Goodrich Superfund Site Rialto, California, Prepared for: U.S. Environmental Protection Agency Region 9, 272 p.

Cooke, M, and Dair, L, (2011), Simulating the recent evolution of the southern big bend of the San Andreas fault, Southern California, J. Geophys. Res., 116, B04405, 1-20

Dynamic Graphics, Inc., 2009, EarthVision 8.1 User Guide, p. 12, 32-34.

Dorsey, R, and Roering J, 2006, Quaternary landscape evolution in the San Jacinto fault zone, Peninsular Ranges of Southern California: Transient response to strike-slip fault initiation, Geomorphology, v. 73, p. 16-32.

Dutcher, L, and Garrett, A, 1963, Geologic and Hydrologic Features of the San Bernardino Area California—with special reference to underflow across the San Jacinto fault: U.S. Geological Survey Water-Supply Paper 1419, 114 p.

Environmental Protection Agency, 2011, Perchlorate in the Pacific Southwest, http://www.epa.gov/region9/toxic/perchlorate/per_ca.html#hill (accessed June 2012).

Faunt, C, Hanson R, and Belitz K, 2009, Groundwater Availability of the Central Aquifer, California: U.S. Geological Survey Professional Paper 1766, Chapter A, 57 p.

Fox, R, and Roberts, M, 1995, Hydrogeologic Features of the Rialto-Colton Fault and Associated Structures, Prepared for: West San Bernardino County Water District, 57 p.

GeoLogic Associates, 2007, Hydrogeologic Model of Perchlorate Transport Conditions in the Northern Rialto-Colton Basin, Prepared for: County of San Bernardino, 150 p.

Geophysics Unit of Menlo Park CA, 2012, U.S. Geological Survey – Western Region – Geology and Geophysics San Bernardino Basin, Southern Calif., http://geomaps.wr.usgs.gov/gump/people/jachens/rialto/rialto.html (accessed June 2012).

GeoSyntec Consultants, 2006, Additional Interim Remedial Investigation Report, Prepared for: Goodrich Corporation, 127 p.

Griffith, W, and Cooke, M, 2005, How sensitive are fault slip rates in the Los Angeles to tectonic boundary conditions?, Bulletin of the Seismological Society of America, v. 95, p. 1263 – 1275.

Hilchie D, 1978, Applied Openhole Log Interpretation for Geologists and Engineers, Douglas W. Hilchie Inc., 328 p.

Keys, S , and MacCary, L, 1971, Application of Borehole Geophysics to Water-Resources Investigations, Techniques of Water-Resources Investigations of the United States Geological Survey, Book 2, 126 p.

Lu, Z, and Danskin W, 2001, InSAR analysis of natural recharge to define structure of a ground-water basin, San Bernardino, California, Geophysical Research Letters, v. 28, p. 2661-2664

Scott, E., 2009, Statement of Support for H.R. 2316 Before The Natural Resources Subcommittee on Water and Power, http://naturalresources.house.gov/UploadedFiles/ScottTestimony09.22.09.pdf (accessed June 2012).

Stephenson, W, Odum, J, Williams, R, Anderson, M, 2002, Delineation of faulting and basin geometry beneath urbanized San Bernardino Valley California, Bulletin of the Seismological Society of America, v. 92, p. 2504-2520

U.S. Geological Survey (USGS), EROS Data Center, 1999, National Elevation Dataset for California, http://gisdata.usgs.net/ned/ (accessed May 2011)

Water Master Support Services For San Bernardino Valley Municipal Water District Western Municipal Water District, 2009, Water Extractions for Calendar Year 2008, 664 p.

Wildermuth Environmental, Inc., 2003, Chino Basin Dry-year Yield Program Modeling Report Volume III, 381 p.

Wisely, A, and Schmidt, D, 2010, Deciphering vertical deformation and poroelastic parameters in a tectonically active fault-bound aquifer using InSAR and well level data, San Bernardino basin, California, Geophysical Journal International, vol. 181, p. 1185-1200

Woolfenden, L, and Kadhim, D, 1997, Geohydrology and Water Chemistry in the Rialto-Colton Basin, San Bernardino County, California, U.S. Geological Survey Water-Resources Investigations Report 97-4012, 101 p.

Woolfenden, L, and Koczot, K, 2001, Numerical simulation of ground-water flow and assessment of the effects of artificial recharge in the Rialto-Colton Basin, San Bernardino County, California, U.S. Geological Survey Water-Resources Investigations Report 00-4243, 147 p.

Woolfenden, L., 2008, Aquifer susceptibility to perchlorate contamination in a highly urbanized environment, IAHS Publication 324, p. 156-1